INVESTIGATING MICROBIOLOGICALLY INFLUENCED CORROSION USING CO-CULTURE BIOFILMS

A Dissertation

by

SUSMITHA PURNIMA KOTU

Submitted to the Office of Graduate and Professional Studies of
Texas A&M University
in partial fulfillment of the requirements for the degree of

DOCTOR OF PHILOSOPHY

Chair of Committee,	Arul Jayaraman
Co-Chair of Committee,	M. Sam Mannan
Committee Members,	Chad Mashuga
	Arum Han
Head of Department,	M. Nazmul Karim

December 2018

Major Subject: Chemical Engineering

ABSTRACT

A holistic understanding of microbiologically influenced corrosion (MIC) requires investigation of the underlying microbiological, metallurgical and electrochemical mechanisms. MIC studies are typically conducted using batch reactors or large scale flow loops that are nutrient-limited and have buildup of waste products. To overcome these disadvantages, we developed a continuous-flow, microfluidic microbiologically influenced corrosion model, M-MIC-1, comprising of carbon steel coated glass slide bonded to a microchannel imprinted in a polymer. Using M-MIC1, we investigated the effect of two biocides on short-term and long-term, single-species and co-culture biofilms of *Shewanella oneidensis* and *Vibrio natriegens*. We found that biocide resistance was impacted by biofilm type, biofilm growth time and the type of biocide. These results show the importance of conducting biocide screening studies with process fluids for effective MIC mitigation. Our studies illustrate that M-MIC1 flow model provides an ideal platform.

To effectively comprehend MIC mechanisms, we developed M-MIC2 flow model that is amenable to dynamic and integrated measurements of biofilm dynamics and electrochemical impedance. M-MIC2 comprises of a two-metal electrode system with carbon steel and titanium bonded to a microchannel. Preliminary static and continuous-flow studies with single-species and co-culture biofilms of *S. oneidensis* and *V. natriegens* in M-MIC2 indicated some correlation of the variations in biofilm biomass to impedance spectra for *S. oneidensis* biofilms.

We also hypothesized that a systems-level understanding of the microbial community and their metabolism can enhance the understanding of underlying mechanisms. Produced water from a MIC-impacted oil field was exposed to carbon steel coupons to mimic the corrosion environment in the laboratory. We observed an increased abundance (using 16S rRNA sequencing) of the genera, *Nitratireductor* and *Desulfovibrio* and unclassified genera of *Rhodobacteraceae*, *Deltaproteobacteria*, and *Desulfobacteraceace*. Based on the metagenome, we predicted an increased abundance of several genes related to energy, carbohydrate, lipid, and xenobiotic metabolism. This correlated to the increased abundance of measured metabolites (using untargeted metabolomics analysis) such as carboxylic acids, fatty acids, and amino acids that were earlier associated with MIC. These analyses can be repeated for multiple MIC-impacted field locations to delineate common features and identify metabolite biomarkers for MIC detection.

DEDICATION

To Prof. Sam Mannan

and

To my parents, my husband, my brother and all my family and friends who helped me achieve everything I could and shaped me into who I am

ACKNOWLEDGEMENTS

I am enormously thankful to my committee chairs, Dr. Arul Jayaraman, and Dr. Sam Mannan for constantly supporting and guiding me throughout my graduate school both professionally and personally. I garnered scientific knowledge, critical thinking skills, and valuable soft skills from them over the past five years that will be very beneficial for my career. They serve as exceptional role models and incredible mentors.

I thank my committee member and collaborator, Dr. Arum Han for sharing his expertise whenever needed. I am also grateful to him for his critical feedback on my work. I thank my committee member, Dr. Chad Mashuga for his assistance and support throughout the duration of this research. I also thank Dr. Homero Castaneda who shared his timely expertise in electrochemical impedance spectroscopy and inputs on designing experiments.

Special thanks to Ms. Ashley Henley, Ms. Valerie Green, Ms. Alanna Scheinerman and Ms. Sheera Helms for their administrative support throughout the graduate program. I am thankful to the Department of Chemical Engineering faculty and other staff for the help whenever needed.

I am grateful to my mentors Dr. Dennis Enning (ExxonMobil Upstream Research Company) and Ms. Crystal Lee (Baker Hughes, a GE company) who helped me with career decisions when needed. They shared their valuable research and field knowledge in microbiologically influenced corrosion during my internships that shaped my perspectives.

I also thank my friends and colleagues for making my time at Texas A&M University a great experience. Special thanks to Dr. Nandita Kohli, Dr. Sneha Jani, Dr. Nitesh Sule, Dr. Sasi Pasupuleti, Daniel Penarete, Dr. Michelle Olson, Yufang Ding and Jingyun Yang for always supporting me with lab experiments. Thanks to Dr. Rani Menon for helping me tremendously with metagenomics and metabolomics. I also like to thank Dr. Cory Klemashevich for help with conducting LC-MS. Special thanks to Dr. Pranav Kannan for the technical discussions and brainstorming sessions in the area of microbial corrosion and electrochemical impedance spectroscopy. I also like to thank the students and post-docs at the Mary Kay O' Connor Process Safety Center and the members of the 5th floor in Jack E. Brown Building for their emotional support. I am grateful for my friends, Sravani Jaligama, Pavitra Murru, Abhijeet Shinde, Dr. Nirup Nagabandi, Srikanth Panyaram, Prashanth Potana who supported me as my family in College Station. I am glad our paths crossed and we got to share several amazing and fun memories.

Finally, thanks to my parents, Dr. Girija Mangatayaru Kotu and Mr. Madhusudhan Rao Kotu for their encouragement and support every single day of my life and to make me the person I am. I would never have joined the Ph.D. program nor sustained through the program if not for their support. They gave importance to my education and school more than their career. They taught me several qualities like honesty, discipline and commitment that helped me reach this position. I am incredibly lucky to have them as my parents. Thanks to my younger brother, Sai Chandan Kotu for being the go to person I can call anytime of the day for any support and advice. I can't thank my husband, Rama Srinath Kondaveeti, enough for his patience, love and support during the tough years of

my Ph.D. He taught me to be assertive and maintain my composure in difficult times. He ensured that I stayed motivated and stress-free so that I could focus my time and energy on my research. I am also grateful to my in-laws for being very caring about my health, encouraging about my career and calming me during stressful days.

CONTRIBUTORS AND FUNDING SOURCES

This work was supported by a dissertation committee consisting of committee chairs, Professor Arul Jayaraman and Professor Sam Mannan of the Department of Chemical Engineering and committee members, Professor Chad Mashuga of the Department of Chemical Engineering and Professor Arum Han of the Department of Electrical and Computer Engineering.

Aluminum coated glass slide microfluidic flow models used in Section 4 were fabricated by Dr. Celal Erbay. SEM micrographs presented in Section 4 were imaged by Dr. Nirup Nagabandi. All other work conducted for the dissertation was completed by the student independently.

This work was supported in part by Mary Kay O'Connor Process Safety Center at Texas A&M University and Ray Nesbitt Chair endowment to Professor Arul Jayaraman.

NOMENCLATURE

MIC	Microbiologically influenced corrosion
PCR	Polymerase chain reaction
M-MIC	Microfluidic microbiologically influenced corrosion
EPS	Exopolysaccharide
MPN	Most probable number
EIS	Electrochemical impedance spectroscopy
OCP	Open circuit potential
SRB	Sulfate reducing bacteria
OTU	Operational taxonomic unit
DNA	Deoxyribonucleic acid
RNA	Ribonucleic acid
PDMS	Polydimethylsiloxane
THPS	Tetrakis-hydroxymethyl-phosphonium-sulfate
LC-MS	Liquid chromatography-mass spectrometry
GC-MS	Gas chromatography-mass spectrometry
MPN	Most probable number
FISH	Fluorescence in situ hybridization
SEM	Scanning electron microscopy
TEM	Transmission electron microscopy

TABLE OF CONTENTS

Page

LIST OF FIGURES

Page

LIST OF TABLES

Page

1. INTRODUCTION

1.1 Background

Microbiologically influenced corrosion (MIC), also known as biocorrosion or microbial corrosion, is an electrochemical process in which microbial metabolism initiates, facilitates or accelerates the corrosion reactions (Videla, 1996). Microorganisms associated with MIC exist in complex communities with other species of microorganisms in structures called biofilms (Little et al., 1992). The microorganisms in biofilms are held together and protected from harsh external environments within a sticky matrix of extracellular polymeric substance (EPS) that is produced by the microorganisms (Costerton et al., 1995).

Sulfate reducing bacteria/archaea (SRB/SRA) are the most widely investigated class of microorganisms associated with MIC (Miller and Tieler, 1971b). In the last fifty years, several other classes of microorganisms with direct or indirect relation to corrosion like methanogens (Zhang et al., 2003), acetogens (Mand et al., 2014), iron reducing /oxidizing bacteria (Semple and Westlake, 1987), acid-producing bacteria (Sowards and Mansfield, 2014), sulfur-oxidizing bacteria (Okabe et al., 2007a), nitrate reducing bacteria (Xu et al., 2013), slime-producing bacteria (Gaylarde and Beech, 1988) and general heterotrophic bacteria (Geissler et al., 2014a), have also been identified to be associated with MIC (31205(NACE), 2006).

MIC is a surface phenomenon that manifests differently across MIC impacted field locations. The corroding metal, the microbial community composition, and the physical and chemical conditions of the surrounding environment influence the location-specific

characteristics of MIC (Skovhus and Eckert, 2014). Detection of MIC is conducted when unexplained higher corrosion rates of a system are observed along with the presence of microbial activity. Once the causes for corrosion are identified, mitigation treatments are selected based on the corrosion rates, corroding environment and cost. Typical mitigation strategies for eradicating biofilms are the use of chemical methods like the application of biocides (Javaherdashti, 2008a), or the use of physical methods like "cleaning pigs" (Quarini and Shire, 2007). Development of effective mitigation strategies for MIC requires a comprehensive understanding of mechanisms associated with interplay of metal, environment and microbiota.

1.2 Motivation

MIC is a significant problem that affects various process units and systems including cooling water systems (McLeod et al., 1998), oil and gas carrying pipelines (Rajasekar et al., 2010a), aviation fuel tanks (Edmonds and Cooney, 1967; Rauch et al., 2006), sewer systems (Okabe et al., 2007b; Satoh et al., 2009a), drinking water systems (Herb et al., 1995; Lin et al., 2013b), and production well heads (Voordouw et al., 1993; Zhou et al., 2013). According to a survey by the U.S. Federal Highway Administration (FHWA), the direct corrosion costs in the US from 1999 to 2001 amounted to $276 billion; and when indirect costs are conservatively considered, the costs are approximately six percent of the US GDP (Koch et al., 2002). Another study estimates that the activity of microorganisms is the reason for around twenty percent of pipeline corrosion (Flemming, 1994). Based on the global costs of corrosion estimated by National association of

corrosion engineers' (NACE) IMPACT study published in 2016 (Koch G, 2016) and the contribution of MIC to total corrosion (Flemming, 1994), MIC amounted to about $460 billion in 2013. The costs and wide prevalence of MIC is an indicator of the significance of this problem and highlights the importance of effectively mitigating MIC.

1.3 Research objectives and novelty

MIC has been extensively studied using batch systems or large scale continuous circulating loop systems. Both batch systems and recirculating systems can provide confounding results as the microorganisms face nutrient limitation which affects their growth and biofilm formation. In addition, organic compounds and waste products produced by the microorganisms, as well as corrosion products accumulate in the system when experiments are performed over extended periods of time. Microfluidics-based flow systems however are continuous once-flow-through units similar to pipelines where MIC is a major concern, and is a novel aspect of this work. In addition to the use of microfluidics-based flow system for corrosion studies, integrating readouts of the biofilm through confocal microscopy and surface mechanisms through electrochemical impedance spectroscopy (EIS) has not been previously reported. In this work, we developed two different microfluidics flow systems to investigate microbiological and electrochemical aspects of MIC using microorganisms that have been previously reported to be present in communities affected by MIC.

Metabolomics is emerging as a powerful approach for understanding microbial activity and metabolism of microbial communities in a diverse set of environments ranging

from human health (Sule et al., 2017) to environmental engineering (Lin et al., 2006), and microbial ecology (Tang, 2011). However, their application to investigate MIC has been limited. In this work, we have used metabolomics to generate a systems-level understanding of microbial communities in MIC. Thus the aims are novel and help further fundamental knowledge and understanding about MIC from both corrosion and microbial community perspectives. The specific objectives of this research were

1. Development and characterization a microfluidic flow system to investigate microbiologically influenced corrosion and determine biocide efficacy
2. Development and characterization of a microfluidic flow system for integrated measurement of corrosion and biofilm physiology
3. Investigating the metabolomic basis of MIC

1.4 Overview

Section 2 provides a comprehensive literature review and background of the characteristics of MIC and the specific research techniques used in this work. **Section 3** outlines the development and characterization of a microfluidic microbiologically influenced corrosion flow model (M-MIC1) for investigation of biocide efficacy comparing single culture and co-culture biofilms using a model system approach. **Section 4** outlines the development of the microfluidic microbiologically influenced corrosion flow model (M-MIC2) that integrate readouts for both electrochemical changes occurring due to corrosion reactions and the biofilm dynamics. The results obtained by using this model for investigating single and co-culture biofilms using a model system based approach have

been discussed. **Section 5** describes the use of an integrated metagenomic and metabolomics based approach for profiling changes in the community composition and metabolism using produced water samples. Finally, **Section 6** summarizes the key findings from this work and also outlines future directions of investigation.

2. BACKGROUND

2.1 Overview of MIC

MIC is a major problem in various chemical process, on-shore and off-shore oil and gas, pipeline, marine, and aviation industries (Iverson, 1987). Microorganisms present at the field locations impacted with MIC can oxidize metal either directly using metal as an electron donor or indirectly through organic electron donors in the environment (Enning and Garrelfs, 2014). MIC is characterized by interactions between the microorganisms, the corroding metal, and the surrounding environment (Videla, 2001). Therefore, understanding the mechanisms underlying MIC and developing effective mitigation strategies requires investigating all three facets of the problem (Eckert and Skovhus, 2018; Skovhus et al., 2017). While the environmental and electrochemical aspects have been relatively well studied (Eckert and Amend, 2017; Enning and Garrelfs, 2014; Javaherdashti, 2017), information on the mechanisms underlying the formation of microbial communities and the molecules through which they lead to MIC is only recently emerging.

This section details the important aspects for obtaining holistic understanding of MIC like MIC mechanisms, microbial communities, MIC detection methods, approaches for MIC mitigation, traditional approaches for laboratory investigation of MIC, proposed approaches for MIC investigation in this dissertation, and susceptibility of various materials to MIC.

2.2 MIC mechanisms

Corrosion of iron, or the loss of electrons of iron to form ferrous ion, is widely used to study MIC because of its widespread use in metal parts and process equipment. Iron corrosion is thermodynamically coupled to the reduction of oxygen in the air to form iron hydroxides, commonly called as rust (Evans, 1969). In the absence of oxygen (i.e., anoxic environments) and any microorganisms, protons from dissociated water molecules can accept the electrons that are lost by anodic dissolution of the metal, aiding in corrosion processes. While this process is thermodynamically feasible, it is nevertheless kinetically slow and thus, corrosion of iron is generally not seen in anoxic environments without microorganisms. In the presence of microorganisms, several mechanisms have been proposed to explain MIC. Some widely-accepted mechanisms among these are chemical MIC (CMIC) and electrical MIC (EMIC) mechanisms. In CMIC, sulfate reducing bacteria (SRB) present in sulfate-rich environments convert sulfate to hydrogen sulfide. This hydrogen sulfide then reacts with metallic iron and produces iron sulfide as a by-product. Iron sulfide forms a crust on the surface of corroding surfaces and is commonly observed to be associated with MIC locations (Enning et al., 2012).

$$SO_4^{-2} + H^+/\text{organic compounds} \rightarrow H_2S + CO_2$$

$$Fe + H_2S \rightarrow FeS + H_2$$

In EMIC, some SRB can directly obtain electrons from iron oxidation and convert sulfate to hydrogen sulfide (Enning and Garrelfs, 2014). As a result, hydrogen sulfide precipitates iron carbonate and iron sulfide. EMIC is characterized by crusts of iron

carbonate and sulfide that are electrically conductive and do not need the bacteria to be in direct contact with the corroding iron surface (Enning et al., 2012).

$$4Fe + SO_4^{-2} + 3HCO_3^- + 5H^+ \rightarrow FeS + 3\,FeCO_3 + 2\,H_2O$$

2.3 Microbial communities associated with MIC

Microorganisms that have been implicated in MIC are often found as biofilm communities attached to metal surfaces (Beech and Sunner, 2004). Such communities of attached bacteria also occur in aquatic natural environments (Costerton et al., 1987a), on biomedical implants (Hall-Stoodley et al., 2004), on tissues in the human body (Costerton et al., 1999), on filters in the wastewater treatment plants (Capdeville and Rols, 1992), on meat surfaces in the food processing industry (Kumar and Anand, 1998) etc. In biofilms, hundreds of organisms coexist with each other enmeshed in an extracellular polymeric substance (EPS) matrix with distinct channels for the transport of nutrients and waste (Costerton et al., 1995; De Beer et al., 1996). The EPS helps microorganisms adhere to surfaces to initiate biofilm formation, as well as helps the microorganisms adhere to each other. In addition, the EPS layer also protects the microbial consortia present inside the biofilm matrix from harsh external environments and makes it more resistant to biocides and disinfectants (Vert et al., 2012).

Several studies have shown that the structure, composition, and spatial distribution of cells in biofilms vary across different MIC impacted field locations (Geissler et al., 2014a; Sun et al., 2014; Teng et al., 2008), and even at different equipment in the same location (Gomez-Alvarez et al., 2012; Stevenson et al., 2011). Until the 1970s, sulfate-

reducing bacteria (SRB) were speculated to be the sole causers of MIC (Miller and Tieler, 1971a). It is now clear that several other classes of bacteria and archaea (such as methanogenic- and acid producing-bacteria) (Enning et al., 2012; Larsen et al., 2010; Okoro et al., 2014) that have been identified at MIC impacted field locations, are also important (Bryant and Laishley, 1990; Geissler et al., 2014a; Gerchakov et al., 1986; Miller and Tieler, 1971a; White et al., 1986). The microorganisms at these locations have been classified based on their metabolic role in the microbial community (**Table 1**). In addition to bacteria and archaea, algae (for example, *Navicula spp.*) and fungi (for example, *Hormoconis resinae*) have also been associated with MIC (Eashwar et al., 2009; Javaherdashti, 2008b; Landoulsi et al., 2011; Little and Lee, 2009; Myers, 1947; NACE, 2006).

Table 1: Classification of different groups of bacteria/archaea identified at MIC impacted field locations

Group of bacteria/archaea	Metabolic role	Reference
Sulfate-reducing bacteria/archaea	Reduce sulfate or sulfite ions through anaerobic respiration	(Lee et al., 1995)
Iron-oxidizing bacteria/archaea	Oxidize Fe^{+2} or Mn^{+2} to Fe^{+3} or Mn^{+3}	(Rao et al., 2000)
Acid-producing bacteria/archaea	Metabolically produce organic and inorganic acids	(Adams, 2010)
Sulfur-oxidizing bacteria/archaea	Oxidize inorganic sulfur compounds to sulfuric acid	(Little et al., 2000)
Slime-producing bacteria/archaea	Produce polymeric slime that aids in bacterial adhesion and prevents diffusion of oxygen	(Gaylarde and Beech, 1988)
Iron-reducing bacteria/archaea	Reduce insoluble Fe^{+3} compounds to soluble Fe^{+2}	(Herrera and Videla, 2009)
Methanogens	Produce methane from hydrogen ions from the corroding metal	(Mori et al., 2010)
General heterotrophic bacteria/archaea	Various direct and indirect roles ranging from biofilm formation to corrosion	(Geissler et al., 2014a)
Nitrate-reducing bacteria/archaea	Reduce nitrate to nitrite	(Xu et al., 2013)

Microbial communities are characterized by complex interactions between the community members, spatial and temporal dynamics of community assembly, and functional redundancy between different members of the community. Of these, the functional redundancy between members of the microbial community is the least understood. While different members of the microbial community can carry out a broad range of overlapping biochemical reactions and metabolic functions (Boschker et al., 1998), the absence of information on which of the community members are actively contributing to MIC is a major obstacle in deciphering the functional redundancy among members of the community. Understanding functional redundancy in a microbial community is important as investigating community composition, inter-species interactions, and functional diversity in the community can be comprehensively utilized to predict the behavior of the community as a whole under different scenarios.

MIC associated microbial communities are also characterized by coexistence of different microorganisms. For example, Duan et al. reported the co-existence of sulfate reducing bacteria (*Desulfovibrio caledoniensis*) and iron reducing bacteria (*Clostridium sp.*) on microbiologically corroded carbon steel coupons immersed in seawater under laboratory conditions (Duan et al., 2008). The composition of the microbial community is a key determinant of the interaction between the microorganisms and the metal surface, and therefore important to understand the mechanisms underlying MIC (Bonifay et al., 2017; Duncan et al., 2009). It has been proposed that the community composition and inter-species interactions can be used to predict the behavior of the community as a whole (Aziz et al., 2015; Zuñiga et al., 2017). For example, nitrate injection in Canadian oil fields has

been shown to temporarily shift the dominant microbial species in the community to a sulfide-oxidizing, nitrate reducing *Campylobacter sp.* (Telang et al., 1997).

When microorganisms are present in a community, multiple microorganisms in the community derive specific advantages that promote their growth and survival. The simplest form of such cooperation is through the generation of environmental niches that support the growth of other organisms. Anaerobic or micro-aerobic pockets can exist within a biofilm although the bulk fluid above the biofilm is aerobic or even saturated with oxygen (Borriello et al., 2004; de Beer et al., 1994), which can support the growth of anaerobic organisms. An example of such interactions is the anaerobic environment for *Desulfovibrio* sp. growth that is provided by biofilms of *Spbaerotilus* sp. (iron-oxidizing bacteria) (Xu et al., 2007).

An equally important cooperation between microorganisms is the use of metabolic intermediates produced by other species for growth by other members of the community. For example, some species of sulfate reducing bacteria like *Desulfovibrio desulfuricans* can grow faster in the presence of lactate and the absence of sulfate, as the acetate and hydrogen produced by *D. desulfuricans* help the growth of a methanogen, *Methanosarcina barkeri* (Hamilton, 1983). Hence, knowledge of the metabolite profile of the community is also important for determining microbial community composition and its role in MIC.

2.4 Detection of MIC

The detection of MIC in industrial systems is not direct and straightforward. The traditional presence of microorganisms and/or corrosion rates that are unexplained with

abiotic corrosion mechanisms has led to the formulation of extensive testing schemes for the presence of microorganisms and to evaluate if their presence results in MIC.

With recent advances in microbiology and molecular biology tools, microbial testing methods and the study of microbial communities in MIC have evolved significantly from macroscopic determination of culture counts (Hardy, 1981) to molecular analysis of DNA present in the community (McLeod et al., 1998; Price, 1993) to large scale sequencing to identify microbial community members (Leary et al., 2014). **Figure 1** shows the evolution of the various techniques used for investigating microbial communities in MIC. Current methods for detecting and investigating microbial communities at the field locations impacted by MIC can be broadly classified into culture-, sequencing-, polymerase chain reaction (PCR)-, and hybridization-based methods. Culture based methods have been used extensively to identify microorganisms in MIC communities (Chen and Chen, 1984; TM0194, 2014). However, with advances in molecular biology and recombinant DNA techniques, hybridization and sequencing have been increasingly used to obtain information on microbial communities causing MIC (TM0212, 2018; Whitby and Skovhus, 2011).

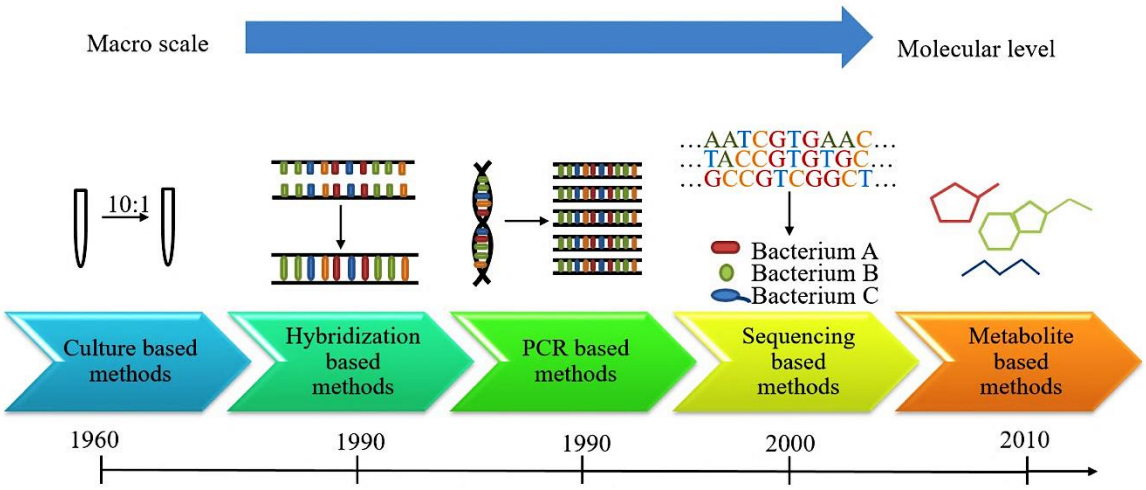

Figure 1: Emergence in the use of molecular techniques for investigation of MIC

While characterizing the microbial community composition at MIC impacted locations has proven to be informative and useful to predict the putative function of different organisms in the community (Gomez-Alvarez et al., 2012), it does not provide information on the actual functional activity of the microbial community. With the emergence of analytical methods for large scale analysis of metabolites and small molecules (Theodoridis et al., 2012), it is now possible to interrogate even the functional output of microbial communities in MIC using metabolomics methodologies.

Culture based methods

Culture-based methods are used to enumerate microorganisms in field systems prone to MIC for preliminary analysis of whether microorganisms are present in the sample. In this method, 10-fold dilutions of the sample are cultured in liquid broth and incubated for extended periods of time to grow the organisms of interest (Alexander, 1965).

The turbidity of the culture and/or changes in the media color are used as a semi quantitative measure of the microorganisms present. Though inexpensive and easy to carry out and interpret, culture based techniques do not offer a good representation of the community as only 0.1-1% of the total microorganisms can be cultured in the laboratory (Amann et al., 1995). Even if the microorganisms can be cultured, growth media are quite strain-specific and therefore not practical to use for enumerating several different species. Further, competitive growth of certain strains over others can result in shifts in the microbial community composition and lead to low or even no detection of specific members of the community. This is illustrated from a study by Zhu et al. where the number of sulfate reducers that were initially at very low abundance increased considerably when grown in SRB-specific media (Zhu et al., 2005). Under certain conditions, some of the viable microorganisms can go into uncultivable metabolic states (Kell and Young, 2000), which underestimates the microbial count in the samples. Due of these drawbacks, culture-based methods are often used with molecular approaches like PCR, sequencing, and metabolite profiling to confirm the results (Beale et al., 2014).

Hybridization based methods

Hybridization methods such as fluorescence in situ hybridization (FISH) and DNA microarrays use binding or hybridization of DNA probes to DNA or RNA extracted from the microbial community to identify the community members in MIC (Amann and Fuchs, 2008). FISH can also be used to obtain the spatial distribution of specific microorganisms in a biofilm without disrupting the biofilm structure. For example, Kolari et al. characterized the spatial distribution of α- and γ-*Proteobacteria* in the biofilms grown on

stainless steel coupons ennobled after laboratory incubation with Baltic sea water (Kolari et al., 1998). Although FISH is a powerful molecular method available to investigate microbial communities, it has not been used extensively in MIC studies primarily due to interference of particulates or oil droplets from field samples with fluorescence microscopy (Holmkvist et al., 2010; Muyzer and Marty, 2014). Moreover, FISH requires using organism-specific probes, and hence it can only provide information on the numbers of known species in the community (Lücker et al., 2007).

In DNA microarrays, DNA probes corresponding to multiple target genes are chemically bonded to a surface and used to hybridize RNA from the microbial community for identification of genes expressed in MIC communities (Zhang et al., 2007). The use of species specific probes in the array results in the identification of the species. Since the RNA present in the community is indicative of genes that are expressed (and hence, which metabolic functions are active), information from DNA microarrays can be used to determine the extent of cellular and metabolic processes related to MIC (e.g., sulfate reduction, hydrocarbon degradation, hydrogen sulfide production, and organic acid generation) that are present in a community (He et al., 2007; Wunch and Penkala, 2010). While DNA microarrays give quantitative information on the metabolic functions that are active in the microbial community, they also require prior knowledge about microorganisms for designing probes and arrays. A significant challenge that limits the use of DNA microarrays for analysis of MIC communities is the need for obtaining samples with sufficient amounts of nucleic acids and the detection of less abundant RNA molecules

primarily because RNA is extremely unstable and subject to rapid turnover (Bernstein et al., 2002; Kushner, 2002).

Polymerase chain reaction methods and sequencing

Polymerase chain reaction (PCR) and DNA sequencing have also been quite frequently used in the last two decades for microbial community composition analysis in MIC (Muyzer and Marty, 2014; van der Kraan et al., 2010). PCR is used to synthesize and amplify a specific section of the microorganism's DNA by designing short DNA fragments (primers) to bind DNA (Oliveira et al., 2011; Satoh et al., 2009) in genes such as the 16S ribosomal RNA (16S rRNA) gene that are ubiquitously present across organisms and have regions that are highly conserved across different species (Ludwig and Klenk, 2005). Following PCR, the amplified regions are sequenced and the data are used to identify the organisms present in the sample (Teng et al., 2008; Vincke et al., 2001). While this method provides important information on the microorganisms present and their relative abundances which can be useful for developing MIC treatment strategies, this approach cannot provide quantitative information on absolute numbers of the microorganisms, which might be important for designing biocide treatment strategies (Bryan et al., 1995). The issue of quantitative enumeration has been addressed using quantitative polymerase chain reaction (qPCR). This is evident in the study by Dang et al., who used qPCR to show that SRB were not the dominant species in short-term biofilms (1, 3 or 7 days) on the carbon steel coupons submerged in coastal seawaters in Qingdao, China; instead, sulfur-oxidizing bacteria and iron-oxidizing bacteria were the abundant species identified in short-term biofilms (Dang et al., 2011). However, PCR methods do not distinguish between live

and dead cells in a community, which can lead to errors in relative abundance (Sørensen et al., 2010). Though rare, PCR methods have been reported to result in amplification bias (i.e., some DNA sequences are amplified more than others) which can lead to less abundant microorganisms being missed (Baker et al., 2003). Another significant drawback of PCR-based detection is that it requires prior knowledge about the microorganisms present in the community (i.e., for designing primers) and hence the scope for discovery is limited.

DNA sequencing approaches (targeted sequencing and shotgun sequencing) are currently the state-of-the-art for investigating microbial communities associated with MIC. In targeted sequencing, primers for specific genes are first used to amplify and sequence specific genes, followed by identification of the microorganisms that have the target gene (Kuczynski et al., 2012) and investigation of different phenotypes related to MIC, such as biofilm formation (Elhariry et al., 2012). Such targeted sequencing can also help discover microorganisms that are not known to be associated with MIC. 16S rRNA gene sequencing of DNA extracted from microbial communities associated with MIC is routinely employed for targeted sequencing of specific regions of the 16S rRNA gene (Jan-Roblero et al., 2004). Using targeted sequencing along with other biochemical tests, McLeod et al. identified that *Aeromonas* and *Shewanella* (in addition to SRB) can produce hydrogen sulfide from sulfite and thus result in MIC in cooling water systems (McLeod et al., 1998). Because PCR amplification is done prior to targeted sequencing, even nanogram amounts of DNA is sufficient as starting material (Miller et al., 2009) and hence can be performed from samples with low amounts of DNA. However, the use of PCR methods for amplification of the target gene occasionally introduces amplification bias as discussed

earlier. In addition, no single variable region of 16SrRNA gene (amongst the 9 variable regions) can distinctly identify all the community members (Chakravorty et al., 2007).

To overcome these disadvantages, shotgun genomic sequencing has been proposed for sequencing the entire genomic DNA in the sample (i.e., DNA from all microorganisms). In this method, the genomic DNA is extracted, broken into smaller fragments, sequenced, and then computationally combined to obtain sequence information on the DNA fragment, which can then be used to identify the microorganisms in the community (Caffrey, 2010). While shotgun sequencing is an expensive and a resource-intensive method, the unbiased analysis facilitates the discovery of previously unknown community members. Shotgun sequencing can also provide information on functional genes in the sample such as those related to sulfate reduction and oxidation (Little and Lee, 2014). The use of multiple regions for sequencing and identification eliminates the problem of amplification bias associated with PCR amplification of a single DNA region as well as enabling accurate identification of microorganisms. However, as DNA amplification is not performed prior to sequencing, shotgun sequencing requires higher amounts of starting DNA (in the range of few micrograms) (White et al., 2009). In addition, using shotgun sequencing necessitates high sample purity as environmental DNA contamination in the sample can result in the detection of false positives (Biesbroek et al., 2012).

Employing DNA sequencing approaches provides valuable information on the composition of the microbial community that results in MIC. Based on this, the metagenome of the community and the functional potential of the community members in MIC mechanisms can then predicted using software packages such as PICRUSt (Langille

et al., 2013a) and Tax4Fun (Aßhauer et al., 2015). These software enable predictions of metabolic capabilities by comparing the predicted abundances of MIC relevant genes and pathways (e.g., dissimilatory sulfite reductase gene and sulfate reduction pathway). For example PICRUSt was employed to determine the impact of crude oil and dispersant exposure to carbon steel in seawaters on metabolic function of the community in addition to the standard procedures of determining corrosion using weight loss and microbial community composition using DNA sequencing (Salerno et al., 2018). This additional analyses determined a shift in the metabolic potential of communities (decrease in hydrocarbon degradation and increase in sulfur metabolism) in addition to increased corrosion rates. These observations assisted in concluding that oil spills and addition of dispersants could potentially increase the microbial degradation of shipwrecks.

Although these predictions of metabolic capabilities are valuable, these methods rely on the use of a single gene sequence data (16S rRNA) to predict the metagenome and the functional potential. In many cases, sequence information from the same species may be unavailable and therefore sequence information from related species are used for making predictions. As a result, the accuracy of the functional prediction can be unreliable (Langille et al., 2013a). Also, this predicted functional potential of the microorganisms need not directly correlate to the observed microbial activity in corrosion. For example, a higher abundance of microorganisms with a specific gene need not necessarily imply that the reactions catalyzed by the enzymes encoded by that specific gene indeed occurred. Consequently, there is a need for conducting metabolite analysis of the microbial

community to comprehend the functional importance and diversity of the community members that further enables effective understanding of MIC mechanisms.

Emerging molecular methods

An inherent characteristic of microbial corrosion is that the microbial community composition varies from equipment to equipment within the same field location, and even between two close positions within the same process equipment (Vincke et al., 2001). While metagenomics has been successfully used to identify different microorganisms in MIC and their relative abundance (Lanneluc et al., 2015), it is not possible to directly correlate relative abundance of microorganisms to a causative role in MIC. For example, while SRB are present in several MIC communities and widely acknowledged to be important in MIC (Beech and Sunner, 2007; Lee et al., 1995), they are not always the most abundant microorganism in the community to cause corrosion. MIC has been demonstrated in natural gas carrying pipelines across United States even when SRB were approximately only one percent of the microbial population and denitrifiers were about four percent and methanogens were thirteen percent of the microbial population at the location (Zhu et al., 2005). Given that different MIC impacted field systems are characterized by microbial communities of different composition that still exhibit relatively similar level of MIC, solely identifying the microorganisms present is unlikely to yield a comprehensive understanding of MIC occurring in that system. An emergent approach for understanding microbial communities and their interaction with the metal surfaces is not just to analyze the microbial community based on the microorganisms present in the community, but also in terms of the metabolic function of the microorganisms in the community.

Describing the function of the microbial community based on the products of metabolic reactions of the organisms present in the community is built on the postulate that a microbial community is formed and maintained based on metabolic interactions between the different members of the community (Wintermute and Silver, 2010). In this model, molecules made by one microorganism is assumed to be utilized by another, and such cooperation between different microorganisms underlies the formation and sustenance of the community. Since different microorganisms have the metabolic machinery to carry out the same biochemical and enzymatic reactions (Rowe et al., 2017), it is possible that communities can have different composition and yet are carrying out a similar set of reactions. Indeed, several recent MIC studies (Beale et al., 2013; Beale et al., 2012a; Beale et al., 2010; Beale et al., 2012b; Beale et al., 2014; Bonifay et al., 2017; Brauer et al., 2015; Duncan et al., 2009; Lenhart et al., 2014) point to the molecular footprint or metabolites produced by the microbial community as key factors in the onset and sustenance of MIC. In these studies, several carboxylic acids, amino acids, fatty acids, and fatty alcohols (Beale et al., 2013; Beale et al., 2012a; Beale et al., 2010; Beale et al., 2012b; Beale et al., 2014; Bonifay et al., 2017; Duncan et al., 2009) were identified as key metabolites associated with MIC. These studies suggest that the identification of the metabolites produced by the community in addition to the community structure could lead to a more comprehensive understanding of the complex microbiological and electrochemical interactions in MIC (Patti et al., 2012; Zhu et al., 2005).

Since metabolites represent the product(s) of different biochemical pathways present across the different members of the community, metabolomics provides more

information than the relative abundances of the microorganisms present in the community – i.e., on the biochemical reactions that were active in the community over the period of observation (Dettmer et al., 2007). While metabolomics has been extensively used in fundamental studies on microorganisms and communities (Sridharan et al., 2014; Sule et al., 2017; Tang, 2011), identifying biomarkers for early diagnosis of diseases (Gowda et al., 2008), in clinical chemistry (Becker et al., 2012), and in toxicology (Jin et al., 2014; Roux et al., 2011), it has been less frequently applied to the comprehensive study of microbial communities in MIC.

The significance of presence or absence of specific metabolites along with the composition of the associated microbial community can be understood analogous to how the presence or absence of certain microorganisms and microbial metabolites in the gastrointestinal tract is used to infer the source or a consequence of diseases in the human body (Sekirov et al., 2010). If a specific metabolite is detected at a MIC impacted field location, it could be indicative of metabolic reactions associated with either formation or consumption of that metabolite occurring in the microbial community at this locations. And if the same metabolite is also detected at multiple locations with MIC, it could suggest the importance of the metabolic reactions that lead to production of that metabolite as having an important role in MIC mechanisms. This information can also be used with the community composition to identify microorganisms that contribute to MIC at the different field locations. Thus, cataloguing the metabolite footprint of the microbial community has significant promise for answering several outstanding questions in MIC.

Metabolomics methodologies

The most common approaches for metabolite profiling couple chromatographic separations with mass spectrometry (MS). While the chromatographic method is used to separate the metabolites based on different biophysical properties (e.g., hydrophobicity, size, charge), MS is used to separate and/or identify various metabolites present in the samples based on their mass-to-charge (*m/z*) ratio. Both liquid chromatography (LC) and gas chromatography (GC) are used along with MS depending on the metabolites being analyzed. For example, GC is more effective for volatile and non-polar components such as short chain fatty acids (SCFA) (Schäfer, 1994), whereas less volatile and polar metabolites are separated using LC where the metabolites are in a mobile phase and separated based on their adsorption onto a stationary phase in a column (Dass, 2006). Once metabolites are separated either by GC or LC, they are injected into a MS where they are ionized, separated, and identified based on their mass-to-charge ratio under electromagnetic fields (De Hoffmann, 2000). To identify metabolite biomarker(s) from the data obtained using untargeted LC-MS/GC-MS or trends in metabolite changes from targeted LC-MS/GC-MS, multivariable statistical analysis of the concentration profiles of compounds is often utilized. Statistical tools like principal component analysis (Nyamundanda et al., 2010), discriminant analysis (Allen et al., 2003), and partial least-squares (Jonsson et al., 2004) have been used for data analysis and interpretation.

Metabolomics methods can be broadly classified into targeted or untargeted metabolomics based on the approach used for identifying metabolites (Patti et al., 2012). Targeted metabolomics is used to study alterations in a small panel of metabolites that are

selected *a priori* based on prior knowledge. Since these metabolites are known, pure standards are often available which are used to generate standard curves and quantify the concentration of metabolites in the different samples (Dudley et al., 2010). In the context of MIC, targeted metabolomics can be used to quantify the levels of metabolites known to be associated with microbial communities present at MIC impacted field sites, for example, alkylsuccinates and alkylbenzylsuccinates (Bonifay et al., 2017). If samples at multiple time points from the same microbial community are available, it is also possible to determine longitudinal or temporal changes in the levels of these putative biomarker metabolites present and use it to generate insights into the metabolic reactions and corrosion processes taking place in the microbial community.

In contrast to targeted metabolomics, untargeted metabolomics can be used to determine the relative abundance of a broad range of metabolites present in the sample (Patti et al., 2012). Untargeted metabolomics can be used in MIC to determine the levels of different metabolites present in a microbial community associated with MIC. Untargeted metabolomics analysis from microbial communities across different MIC locations could help identify aspects of microbial metabolism that are conserved across the different locations, as well as lead to identification of key metabolites correlated to MIC for different MIC locations. For example, Bonifay et al. identified succinic acids as metabolites unique to corroding pipelines in the Norwegian region (Bonifay et al., 2017).

The choice of using targeted or untargeted metabolomics in MIC depends on the scientific question that is being asked. While targeted metabolomics can provide quantitative information and more sensitive detection (Griffiths et al., 2010), a significant

limitation is that the target metabolites are selected by the user and requires *a priori* information on the metabolites of interest. While the issue of requiring *a priori* knowledge of the metabolites to be detected is addressed in untargeted metabolomics due to unbiased detection of metabolites, limitations with extraction of metabolites with specific solvents (Maharjan and Ferenci, 2003; Yanes et al., 2011), compatibility with orthogonal chromatographic separation techniques (Patti, 2011; Zhang and Watson, 2015) and limits of detection (Dunn and Ellis, 2005) all affect the breadth of the generated metabolite fingerprint. Also, a common problem with untargeted metabolomics is that only a small fraction of the identified features can be unequivocally identified as a specific compound (Dunn et al., 2013) due to limitations with the availability of extensive and standardized mass spectral libraries (Vinaixa et al., 2016). Moreover, the compounds identified using untargeted metabolomics are considered only putative unless the identities are confirmed with pure compounds that may not be commercially available or difficult to test due to their corrosiveness or hazardous characteristics.

Though metabolomics offers high potential for identifying biomarker metabolites and key microorganisms in MIC, few technical limitations need to be overcome to transform it from a research tool to standard practice in the industry. From a methodological perspective, a single analytical method cannot detect and identify all the metabolites in a sample due to the diversity in the properties of metabolites that can be produced by microorganisms (Wang et al., 2015). Thus, multiple methods may need to be used to increase metabolome coverage. Chemical derivatization is often required for non-volatile compounds to be compatible for GC-MS or to improve stability and binding to LC

columns for LC-MS. However, chemical derivatization has been shown to result in the formation of unexpected by-products that can result in misinterpretation of the concentration of the compounds (Little, 1999). Since metabolites can be rapidly degraded (Scalbert et al., 2009), it is also important that the right storage conditions and sample preservation techniques are used before metabolomics analysis of field samples. This is a non-trivial challenge as samples from MIC impacted field locations are often exposed to harsh environments (Alabbas, 2017; Duncan et al., 2009) and significant variability in the metabolite profile between different samples can arise just from sample handling. Thus, standardized protocols for sample collection and processing are required if multiple MIC impacted field locations are to be compared. A related consideration that limits the application of metabolomics to MIC is that information on the spatial distribution of metabolites is lost during sample collection and preparation. Lastly, databases used for identifying metabolites (e.g., Metlin (Guijas et al., 2018), Human metabolome database (Wishart et al., 2017)) often contain incomplete information on compounds; thus, the amount of information available can limit the ability to identify metabolites.

2.5 Traditional MIC studies

Most MIC studies in the laboratory are conducted using batch systems. In these batch reactors, metal pieces called coupons are immersed into bacterial cultures and incubated for extended periods of time (Castaneda and Benetton, 2008; Enning et al., 2012; Jayaraman et al., 1998). The difference in mass of the coupons due to exposure is used as the measure of corrosion. While these systems are simple to use, they have significant

disadvantages. First, static systems are not always representative of the environment where MIC occurs (i.e., pipelines where liquid is constantly flowing). Second, the metabolism of the bacterial suspension is also affected by nutrient limitation and accumulation of waste products. As an alternative, continuous flow systems (Jayaraman et al., 1997c), circulating flow loops (Enning et al., 2016b), modified continuous stirred tank reactor (Tidwell et al., 2016) have been developed. While these address some of the drawbacks of batch systems, they typically require large volumes of liquid.

These MIC reactors or flow systems are used to grow corrosive microorganisms to investigate their impact on corrosion. For example, inoculum from the field (liquid/biofilm scrapings from pipelines) with corrosive communities is grown in these systems to investigate their impact on metal coupons and corrosion (Stipanicev et al., 2014). In addition to field samples, several species' of SRB have been used to understand MIC corrosion mechanisms in the laboratory (Lopes et al., 2006b). In **Sections 3 and 4** of this dissertation, we demonstrate the development and application of the microfluidics-based flow models that overcome the drawbacks of both batch systems and recirculating systems by using minimal reagents as well as once-flow-through system conditions.

2.6 Mitigation of MIC

Prevention and mitigation of MIC can be achieved using physical methods such as "cleaning pigs", electrochemical methods such as cathodic protection, biological methods such as engineered biofilms, and chemical methods such as biocide and corrosion inhibitor application.

Physical methods

Mitigation of MIC in pipelines is typically done using tools such as cleaning pigs. Cleaning pigs improve flow efficiency, eliminate solid deposits, inspect the pipeline for the changes in the wall thickness, and collect samples for molecular and analytical testing (Quarini and Shire, 2007; Rajasekar et al., 2010b). In the context of MIC, frequent use of cleaning pigs removes biofilms and also reduces microbial attachment on the metal (Bhola et al., 2010b). However, the operation of cleaning pigs in pipelines can be challenging due to design and operational complications (Smart and Smith, 1992). In addition, cleaning pigs might not dislodge biofilms completely and hence MIC can persist (Eckert, 2015).

Electrochemical methods

Cathodic protection works by applying current to the corroding metal in the system by making it a cathode to prevent corrosion (Jones, 1996). However, the utility of cathodic protection for MIC inhibition is not clear (de Romero et al., 2009). Further, the use of cathodic protection can support the metabolism of certain microorganisms accepting electrons directly from metal or utilizing hydrogen produced by proton reduction or water from the metal surface (Wilson and Jack, 2017). Although this microbial growth is not alarming when the specific corrosion protection potentials are maintained, these elevated microbial populations can accelerate corrosion in downstream locations (Mand et al., 2014). Microbial activity can further increase the current required to maintain the protection potential because the conductive corrosion products can remove electrons from the metal (King, 2007).

Biological methods

While biofilms are generally considered deleterious in the context of MIC, several single and multi-species biofilms have been found to inhibit MIC (Pedersen and Hermansson, 1991). It is interesting to note that several single and multi-species biofilms have been engineered to be protective against MIC in model systems and laboratory environments on mild steel and carbon steel (Jayaraman et al., 1997b; Jayaraman et al., 1997d; Kip and van Veen, 2015). This inhibition of MIC occurs through removal of oxygen or other corrosive compounds by microbial metabolism, *in situ* antimicrobial generation to inhibit growth of corrosive microorganisms, and formation of corrosion protective EPS (Videla and Herrera, 2009; Zuo and Wood, 2004). However, Arps et al reported that these biological mitigation methods were not effective in industrial settings (Arps et al., 2003).

Chemical methods

Corrosion inhibitors and biocides are the commonly employed chemicals to prevent abiotic corrosion and MIC respectively. Corrosion inhibitors are organic compounds with properties of surfactants and form protective layers on metal surfaces (Papavinasam, 2011). On the other hand, biocides are organic or inorganic compounds that mitigate microorganisms and their proliferation by damaging the microbial cell wall or interfering with microbial metabolic processes or interrupting the ability of microorganisms to generate energy (Lee et al., 2010). Biocides are classified as oxidizing and non-oxidizing biocides based on their mode of action. Inorganic compounds such as chlorine, sodium hypochlorite, bromide, and peroxides fall under the class of oxidizing biocides. Due to their

highly corrosive nature, oxidizing biocides are not as widely used as non-oxidizing biocides (Morris and Van Der Kraan, 2017). Due to their lower reactivity, non-oxidizing biocides can also penetrate biofilms effectively improving their efficacy. The most common non-oxidizing biocides employed for MIC mitigation are aldehydes (e.g., glutaraldehyde, formaldehyde, acrolein), tetrakis-hydroxymethyl-phosphonium-sulfate (THPS), halogenated compounds (bronopol), and quaternary ammonium compounds (alkyl dimethyl benzyl ammonium chloride (ADBAC) (Javaherdashti, 2008b).

Mitigation strategies

Mitigating the deleterious effects of microorganisms and reducing the costs associated with MIC requires eliminating planktonic microorganisms present in the system as well as biofilms that are formed on the metal surfaces. MIC impacted field locations are commonly treated by applying different biocides or antimicrobial agents (Morris and Van Der Kraan, 2017; Park et al., 2011). However, the diffusion limitations associated with the EPS matrix in which biofilms are present (Stewart, 2003) often necessitates the use of high concentrations of biocides, typically in the range of 50-1000 ppm (Grobe et al., 2002), and poses environmental and cost concerns. Even with such high concentrations, complete eradication of biofilms is extremely difficult to achieve as biofilm microorganisms often exist in metabolically dormant states which makes them resistant to anti-microbial agents (Keren et al., 2004). To address these challenges, it has been recently proposed that biocide treatment regimens for pipelines be designed based on the composition of the community as well as the abundance of different microbial species present in the biofilm (de Paula et

al., 2014). However, this approach requires accurate determination of the microbial community composition and abundances at each MIC impacted field location.

2.7 Use of laboratory model systems for MIC studies

Laboratory MIC experiments have used various microbial cultures as inoculum such as single organisms (*Desulfovibrio vulgaris*), mock communities (*V. natriegens* and *D. vulgaris*), and process waters (Benbouzid-Rollet et al., 1991; Tidwell et al., 2016; Zhang et al., 2015). We employ an *in vitro* model in **Sections 3 and 4** to grow co-culture biofilms representative to MIC communities beyond focusing on the widely studied SRB. In this dissertation, two model microorganisms, *V. natriegens* and *S. oneidensis* were selected based on their metabolic capabilities distinctive to MIC communities to investigate biofilm growth dynamics. *V. natriegens* is a biofilm former identified to be present in process systems impacted with MIC (Benbouzid-Rollet et al., 1991; Cheng et al., 2009; Nivens et al., 1986; Yin et al., 2008b). *S. oneidensis* is an iron-reducing bacterium and a biofilm former that has been isolated from microbiologically corroding cooling water towers (McLeod et al., 2002). However, several studies reported that *S. oneidensis* inhibits corrosion in microbial communities indicating its dual role in MIC (De Windt et al., 2003; Herrera and Videla, 2009; Kotu et al., 2016).

2.8 Lab-on-a-chip devices for MIC

Miniaturization of several laboratory tasks onto a few millimeters to centimeters sized chip is referred to as the lab-on-a-chip technology (Dittrich and Manz, 2006). These

chips can be fabricated from various materials like silicon, glass, polyester, and polycarbonate. Lab-on-a-chip systems have widespread applications in biological and medical sciences, analytical chemistry, and sensors (Figeys and Pinto, 2000; Wang, 2000). Microfluidics is a subset of the lab-on-a-chip technology and refers to systems that have fluid flow in channels with dimensions lesser than a millimeter (Whitesides, 2006). Several studies outline the use of microfluidics to investigate biofilm growth dynamics for investigating quorum sensing, host-pathogen interactions, and biofilm-related infections (Hong et al., 2012b; Kim et al., 2010; Kim et al., 2012; Lee et al., 2008). However, the use of lab-on-a-chip technology for investigating biofilms and their impact on MIC has not been reported before.

In this dissertation, we used PDMS based microfluidics flow models for investigation of MIC. PDMS based microfluidics flow models are suitable for studies with biological species as PDMS is air-permeable and biocompatible (Mata et al., 2005). These flow models are fabricated by imprinting flow channels in PDMS polymer and bonding to glass slide. In addition to using flow conditions for simulating biofilm growth and MIC, microfluidic flow models have compact and micro-scale flow channels and require minimal reagents. In addition, the transparent PDMS polymer allows for imaging of fluorescently tagged biofilms over the metal surface. Further, microfluidic flow models are also amenable for high-throughput testing.

In **Section 3**, the development of a lab-on-a-chip model, microfluidic microbiologically influenced corrosion model (M-MIC1), to determine biocide treatment efficacy on laboratory grown biofilms was discussed (Kotu et al., 2018). In **Section 4**, the

development of a lab-on-a-chip model that integrates measurements of electrochemical impedance spectroscopy and confocal microscopy to investigate biofilm growth dynamics and MIC was presented (Kotu et al., 2016; Kotu et al., 2018).

2.9 Susceptibility of various materials to MIC

Various alloys such as steels, alloys of aluminum, titanium, nickel, and copper are the common materials of construction for equipment such as pipelines and tanks. These materials are briefly discussed for their susceptibility to MIC as the choice of material determines the degradation rate and hence the service life of the equipment. The trade-off between capital costs and operating costs plays a significant role in the material selection process.

Aluminum and its alloys

Upon exposure to air, aluminum forms an oxide layer on its surface that acts as a passive layer, preventing further corrosion. Because of this passive layer, aluminum and its alloys are fairly resistant to corrosion. However, aluminum is susceptible to localized corrosion and particularly susceptible to MIC. For example, MIC on aluminum was reported in aircrafts and in underground fuel tanks (Salvarezza and Videla, 1984).

Titanium and its alloys

Several studies conducted with titanium have concluded that it is resistant to MIC (Little et al., 1992; Schutz, 1991; Wagner and Little, 1993). Hence, titanium alloys are primarily used for construction of heat exchangers or in extremely corrosive environments. Because of its resistance to MIC, in **Section 4** of this dissertation, titanium was used as the

non-corroding counter electrode in the fabrication of M-MIC2.

Copper alloys

Though copper has been reported to exhibit antimicrobial properties (Faúndez et al., 2004), several copper alloys have been shown to be susceptible to MIC (Little and Lee, 2006). Copper alloys are also prone to erosion in high flow conditions further increasing their susceptibility to MIC (Eckert and Amend, 2017). Nonetheless, addition of nickel to copper alloys has been shown to increase corrosion resistance under such high flow conditions (Wagner and Little, 1993).

Nickel alloys

MIC has been reported in low-flow conditions with material of construction as nickel-copper alloys (Little et al., 1990). However, MIC was not observed with nickel-chromium and nickel-chromium-molybdenum alloys (Enos and Taylor, 1996). The use of nickel alloys because of their corrosion resistance (in liners, cladding, and welds between dissimilar metals like steels and other nickel alloys) should be coupled with appropriate and optimal fabrication methods to protect the corrosion resistance properties of nickel alloys (Eckert and Amend, 2017).

Steels

Steels are the most commonly used materials of construction and available as a wide variety of alloys based on their composition and heat treatment. The presence of chromium in stainless steels makes them fairly corrosion resistant compared to carbon steels (Gardner, 2005). Ferritic stainless steels that are commonly used in heat exchangers were reported to be susceptible to MIC around welds (Borenstein, 1991). Duplex stainless

steels consisting of a mix of austenite and ferrite stainless steels were also susceptible to MIC in SRB-mediated corrosion (Antony et al., 2007; de Romero et al., 2009). Though the addition of molybdenum increases corrosion resistance, super austenitic stainless steels that contain greater than 6% molybdenum are also susceptible to MIC (Scott et al., 1991).

Corrosion resistant alloys

Corrosion resistant alloys (CRA) that are manufactured using corrosion resistant elements (such as chromium, molybdenum, titanium, and zirconium) (Hashimoto, 2002) exhibit superior corrosion resistant properties than all the other materials. Their resistance to corrosion decreases the operating costs although they incur high capital investment (Eckert and Amend, 2017). Hence, selective application of CRA to the highly susceptible areas is an economical alternative.

2.10 Analysis of MIC

As MIC is a consequence of the interactions of the microbial community with the environment and the metal surface, analysis of MIC should also involve quantitatively or qualitatively assessing the impact of these factors. Typical MIC analysis includes assessment of corrosion rate directly from weight loss measurements, assessment of the electrochemical changes occurring by measuring electrochemical parameters like impedance, open circuit potential, and assessment of the microbial activity quantitatively using enzymatic assays or visualization the microbial community using microscopy techniques.

Corrosion rate assessment

Corrosion rate is defined as the rate at which a metal undergoing corrosion deteriorates in a specific environment. The rate of weight loss of a metal specimen placed in a corrosive environment can be used to directly calculate the corrosion rate (mm/y) of the metal specimen in the environment as

$$CR=\frac{87.6\times W}{D\times A\times T}$$

Where W is weight loss in milligrams, D is metal density in g/cm^3, A is area of metal exposed in cm^2 and T is the exposure time in h.

In the US, corrosion rates are commonly expressed as mils per year (mpy) that represents the corrosion penetration thousandths of an inch per year. In addition to the direct calculation of corrosion rate from weight loss, electrochemical methods like electrochemical impedance spectroscopy (EIS), Tafel plots, and linear polarization resistance (LPR) also allow for calculation of the corrosion rate indirectly.

Electrochemical assessment

Several direct current and alternating current methods are used to investigate the electrochemical changes to a corroding environment. The most commonly used techniques for electrochemical assessment are electrochemical impedance spectroscopy (EIS), open circuit potential (OCP), linear polarization resistance (LPR), Tafel plots, electrochemical noise, and cyclic voltammetry (Mansfeld and Little, 1991).

OCP is a commonly used electrochemical parameter to qualitatively measure the extent of corrosion. It is defined as the potential of the working electrode with respect to

the reference electrode when no external current or potential is applied (Perez, 2004). At OCP, both the anodic and cathodic reaction rates are at equilibrium. An increase in OCP could be interpreted as the result of the increase in corrosion activity while a decrease in OCP could be due to the formation of passivation layer of the working electrode.

In the context of MIC, the direct current methods have issues with accuracy of the data as the entire system is considered as purely resistive without considering the capacitive and inductive elements (Dexter et al., 1991). Biofilms typically have properties of a capacitor and hence the use of direct current methods are not effective. Thus, the changes in the impedance measurements using EIS, an alternating current technique, were utilized to comprehend the electrochemical changes associated with MIC processes in **Section 4**.

In potentiostatic EIS, alternating low voltage is applied to the system and the current is measured to give the impedance. Bode plots are used to represent the absolute impedance of the system along with the phase angle across the different frequencies swept. Increase in impedance values over time in Bode plot indicates the formation of corrosion product layer. Nyquist plots are used to represent the changes in imaginary impedance with the real impedance and an increase in Nyquist plot diameter correlates to formation of corrosion product layer. In a corroding system, the Nyquist plot diameter is expected to decrease and the impedance values are expected to increase (Kelly et al., 2002). Using the data from Bode and Nyquist plots, any electrochemical system can be fitted to an equivalent circuit of resistors and/or capacitors based on the nature of the system. These plots and equivalent circuit fitting can help obtain the polarization resistance that is related inversely to the corrosion current and the corrosion rate of the system (Perez, 2004).

Biological assessment

Several field and laboratory biological assessment methods are employed to determine the microbial activity resulting in corrosion. These methods vary in their ability to quantitatively measure the abundance of microorganisms, distinguish living and dead microorganisms, and their cost and complexity. The different molecular methods used for microbial assessment are described earlier in **Section 2.4**. Other commonly used methods for biological assessment of MIC are discussed here.

Energy storage molecules like adenosine triphosphate (ATP), adenosine monophosphate (AMP) are used to quantitatively estimate the microbial activity using enzymatic assays (Littmann, 1975). ATP tests are quick and simple to use methods that can be used effectively even by field operators (Lomans et al., 2016). One drawback with these tests is that they do not give exact numbers of active microorganisms.

Light microscopy methods like epi-fluorescence microscopy and confocal microscopy are also widely used to determine both qualitatively and quantitatively determine the living and dead microorganisms or total microbial count when used with appropriate DNA stains (Little et al., 2006). However, these methods require expensive equipment and rigorous equipment training. Epi-fluorescent microscopy can be used both for field and laboratory evaluations but confocal microscopy can only be used for laboratory evaluations because of the complexity of their setup and use of lasers. However, confocal microscopy enables visualization of thin optical slices within biofilms by eliminating out-of-focus signals resulting in valuable information (Lawrence et al., 1991). The images obtained from confocal microscopes can be used reliably for quantitative

estimation of living and dead microorganisms without misinterpretation to determine the effectiveness of MIC mitigation treatment (Tidwell et al., 2015). In **Sections 3 and 4**, confocal microscopy was used to quantitatively estimate the biofilm biomass of microorganisms causing MIC.

3. DEVELOPMENT AND CHARACTERIZATION OF A MICROFLUIDIC FLOW SYSTEM TO INVESTIGATE MICROBIOLOGICALLY INFLUENCED CORROSION AND DETERMINE BIOCIDE EFFICACY*

3.1 Introduction

MIC and biofilms

Microbiologically-influenced corrosion (MIC), commonly referred to as microbial corrosion or biocorrosion is an electrochemical process where the metabolic activity of microorganisms results in corrosion (Videla, 1996). Based on the global costs of corrosion estimated by the NACE IMPACT (Koch G, 2016) and the 10-20 % contribution of MIC to total corrosion, MIC amounted to about $250-500 billion in 2013. It is now widely accepted that surface attached biofilms of microbial communities, and not floating planktonic microorganisms, causes MIC on metal surfaces (Costerton et al., 1995).

Biofilms are microbial communities embedded in a matrix of extracellular polymeric substance (EPS) and have been associated with tissue surfaces, natural aquatic environments and industrial systems (Costerton et al., 1987b). Eradication of biofilms is a significant problem because the effective concentration of biocides needed for complete killing of biofilm microorganisms is orders of magnitude higher than that needed for planktonic microorganisms (Lock et al., 1984). An important characteristic of MIC is the

* Reprinted with permission from *Oilfield Microbiology*, "Lab-on-a-chip model for investigating the effect of biocides on co-culture biofilms" by Susmitha P. Kotu, Song-I Han, Arum Han, Sam Mannan, Arul Jayaraman,, CRC press. Copyright © 2020 by Taylor and Francis Group, LLC, a division of Informa plc.

difference in the composition of biofilms at different field locations impacted by MIC (Geissler et al., 2014b; Sun et al., 2014). Therefore, an effective microbial control program requires selecting the right type and dosage of biocide that can eradicate the specific MIC causing microorganisms present at the field locations. Identification of such a biocide (or combination of biocides) requires testing multiple experimental conditions (type of biocide, concentration, duration of exposure) before finalizing the biocide treatment strategy. Thus, there is a need for systems that can be effectively used for determining the appropriate biocide type and dosage for controlling MIC.

Flow systems to investigate biofilms and MIC

Most MIC studies in the laboratory are conducted using batch reactors, where metal coupons are immersed into bacterial cultures and incubated for extended periods of time (Castaneda and Benetton, 2008; Enning et al., 2012; Jayaraman et al., 1998). The difference in mass of the coupons due to exposure is used as the measure of corrosion. While these systems are simple to use, they have several disadvantages. First, static systems are not always representative of the environment where MIC occurs (i.e., pipelines where liquid is constantly flowing). Second, the metabolism of the bacterial suspension is also affected by nutrient limitation and accumulation of waste products. As an alternative, continuous flow systems (Jayaraman et al., 1997c), circulating flow loops (Enning et al., 2016a), modified continuous stirred tank reactor (Tidwell et al., 2016) have been developed. While these models address some of the drawbacks of batch systems, they typically require large volumes and are not amenable for testing where the amount of sample is limited. The model

described in this paper overcomes these drawbacks of both batch and recirculating systems by using minimal reagents and mimicking once-flow-through system conditions.

Lab-on-a-chip model to investigate biofilms and MIC

Lab-on-a-chip technology refers to the miniaturization of several laboratory tasks on to a chip that measures a few millimeters to few centimeters (Dittrich and Manz, 2006). Microfluidics is a subset of the lab-on-a-chip technology and has been used extensively for several applications like microarray analysis (Situma et al., 2006), genomics and sequencing (Williams, 2002), disease diagnostics (Chin et al., 2011) etc. Microfluidics has been used to investigate biofilm growth dynamics in several applications (Hong et al., 2012a; Kim et al., 2010; Kim et al., 2012; Lee et al., 2008). However, the use of lab-on-a-chip technology for investigating biofilms and MIC has not been reported before. We have previously developed a lab-on-a-chip model that integrated electrochemical impedance spectroscopy and confocal microscopy to investigate biofilm growth dynamics and MIC (Kotu et al., 2016). We recently modified this system and developed a lab-on-a-chip model using carbon steel as the corroding metal for investigating MIC using either corrosive process waters or laboratory grown biofilms (Kotu et al., 2018). This model is used in the current study to determine biocide treatment based on the laboratory grown biofilms. This model allows real-time monitoring of biofilm growth dynamics with microscopy, with less reagent usage, and can be further modified for simultaneous monitoring of biofilms and corrosion in a high-throughput manner.

Model system based approach for investigating single species and co-culture biofilms

Different types of microbial cultures, from single organisms to mock communities, have been used for laboratory MIC experiments. For example, inoculum from the field such as, liquid or biofilm scrapings from pipelines with MIC causing communities were grown in the different batch or continuous flow systems to investigate their impact on metal coupons and corrosion (Stipanicev et al., 2014). In addition to field samples, several sulfate-reducing bacteria (SRB) have been used to understand MIC mechanisms in the laboratory (Lopes et al., 2006a). In this study, two model microorganisms that have been detected at locations impacted with MIC, and representing metabolic functions characteristic to locations impacted with MIC, were selected. *V. natriegens* is a biofilm former identified to be present in the locations impacted with MIC (Benbouzid-Rollet et al., 1991; Cheng et al., 2009; Nivens et al., 1986; Yin et al., 2008c) while *S. oneidensis* is a marine biofilm forming iron-reducing bacterium, and has also been isolated from MIC impacted industrial locations like cooling water towers (McLeod et al., 2002). However, *S. oneidensis* has been found to inhibit corrosion in several microbial communities resulting in its dual role in MIC (De Windt et al., 2003; Herrera and Videla, 2009; Kotu et al., 2016).

Use of biocides for controlling MIC

Various physical, electrochemical, biological and chemical methods have been implemented for the prevention and mitigation of MIC. Cleaning pigs are typically employed to prevent solid accumulation in pipelines (Quarini and Shire, 2007). These cleaning pigs are also helpful to physically remove the surface attached biofilms and collect samples from pipelines. Frequent use of cleaning pigs can reduce microbial attachment and

further prevent the sustenance of MIC (Bhola et al., 2010a). Electrochemical methods like cathodic protection have been used in systems susceptible to MIC by using a sacrificial anode that provides electrons and hence prevents the metal from corroding (Wilson and Jack, 2017). However, this method is ineffective once a biofilm has been formed (de Romero et al., 2009). Corrosion inhibition by aerobic biofilms in the laboratory has been reported on various metals (Jayaraman et al., 1997a; Jayaraman et al., 1997c; Jayaraman et al., 1998). In addition, engineered biofilms were used to generate antimicrobials *in situ* and eliminate SRB from biofilms (Jayaraman et al., 1999). However, industrial applications of these biological methods have not been successful (Arps et al., 2003).

One of the most widely used MIC treatment methods is treating with different chemicals that show biocidal activity. Based on the physical conditions at the field locations impacted by MIC, oxidizing or non-oxidizing biocides are used to kill microorganisms and control MIC (Javaherdashti, 2008a). However, identification of the correct biocide for the microorganisms present and the appropriate dosage is important for maximum effectiveness. Laboratory methods for testing the performance of biocides include traditional bioassays and antimicrobial tests, while corrosion coupons are commonly used for field testing (Skovhus, 2014). The two most commonly used biocides for microbial control are glutaraldehyde and tetrakis-hydroxymethyl-phosphonium sulfate (THPS), as they are broad-spectrum biocides with quicker kill time compared to the other commonly used biocides such as 2-hydroxymethyl-2-nitropropane-1,3-diol (THNM), 1-(3-chloroallyl)-3,5,7-triaza-1-azoniaadamantane chloride (CTAC), and 4,4-dimethyl oxazolidine (DMO) (Williams and Schultz, 2015; Yin et al., 2018) in addition to being

biodegradable (Videla, 2002). The biocidal action of glutaraldehyde is due to the cross linking of the proteins in the cell wall disrupting routine functions (Maillard, 2002). The phosphine group in THPS reduces and disrupts the disulfide bonds to thiols in cell proteins and enzymes resulting in the death of cells (Ballantyne and Jordan, 2004). In this section, M-MIC1 (Kotu et al., 2018) was used to investigate the efficacy of short-term (4 h) glutaraldehyde and THPS treatment on laboratory grown single species biofilms and co-culture biofilms.

3.2 Materials and methods

Microfluidics flow model design and fabrication

Glass slides were acid-cleaned and then coated with 200 nm layer of carbon steel 1018 alloy using carbon steel 1018 target discs in a Lesker DC Sputter (Jefferson Hills, PA). The coated metal was then patterned into rectangular bands. The transparent polymer polydimethyl siloxane (PDMS) was poured into 3D printed molds to obtain rectangular micro channels. These channels measure 500 µm in height, 1000 µm in width, and 10000 µm in length. PDMS with rectangular micro channels is placed on top of the patterned rectangular metal band to obtain closed channels (**Figure 2**). Syringes connected to Tygon tubing were used to introduce fluids through the system. Flow was maintained in the micro channels by mounting syringes onto a Chemyx Fusion 200 syringe pump (Stafford, TX).

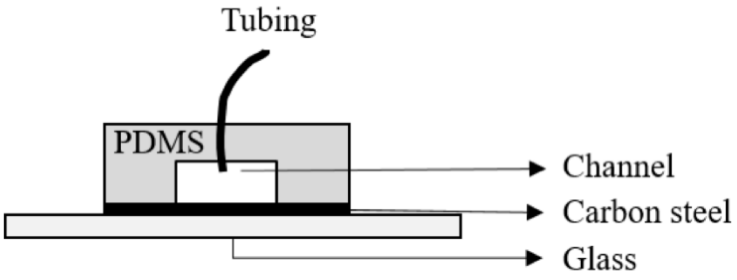

Figure 2: Side view of the microfluidic flow model M-MIC1

Biofilm culture in microfluidic devices

For single-species biofilms, overnight cultures of *V. natriegens* and *S. oneidensis* grown in LB media were diluted to an optical density of ~1.0 before seeding into the microfluidic flow cell. For co-culture biofilms, overnight cultures of *V. natriegens* and *S. oneidensis* diluted to an optical density of ~1.0 were mixed in equal ratio before seeding into the microfluidic channel. After seeding, these cultures were kept for 2 h without flow to initiate attachment to the metal. After 2 h, LB media was continuously flowed through the system at 0.25 ml/h to remove unattached cells as well as provide nutrients for the growth of biofilms throughout the duration of the experiment. Biofilms were grown under aerobic environment for either 12 h or 36 h at 30^{o}C prior to treatment with 400 ppm of glutaraldehyde or THPS for 4 h in batch mode (i.e., without flow). Staining of the live and dead cells in the biofilms was performed by diluting 3 μl of SYTO 9 and propidium iodide dyes from the Filmtracer biofilm Live/Dead stain kit (Carlsbad, CA) in 1 ml autoclaved DI water and flowing through the microfluidic device for 10 minutes at 0.25 ml/h, followed

by 15 minutes incubation before imaging. All experiments were done in triplicates with three independent cultures.

Confocal microscopy and image analysis

A Leica SP8 confocal laser scanning microscope (Wetzlar, Germany) was used to acquire z-stacks of the stained biofilms every 2.5 µm with a 20x objective. Z-stacks were acquired at five random locations in all of the devices. Argon (488 nm) and Helium-Neon lasers (561 nm) corresponding to excitation wavelengths of the dyes were used to image the biofilms over the metal surface. At the end of the experiment, the metal surface was also examined using a 20x objective for macroscopic indicators of corrosion after removing biofilm. Live dead staining was used to visualize as well as differentiate the living and dead biofilm biomass on the metal surface. Live cells stain green while dead cells stain red in this assay. The fold-changes in the percentage of dead cells before and after the biocide treatment was used as a measure of the effectiveness of the biocide. To account for variability in the percentage of dead biomass before the biocide treatment across different experiments, the dead cell percentage after the treatment was normalized to the percentage of dead cells before the biocide treatment.

3.3 Results and discussion

Treatment of short-term biofilms with glutaraldehyde and THPS

Single-species biofilms grown for 12 h and treated with 400 ppm of glutaraldehyde of *V. natriegens* showed 3.6-fold increase in the percentage of dead cells while single-species biofilms of *S. oneidensis* showed 2.7-fold increase in the percentage of dead cells

(**Figure 3**). For co-culture biofilms of *V. natriegens* and *S. oneidensis* grown for 12 h, 2.3-fold increase in dead cells was observed (**Figure 3**).

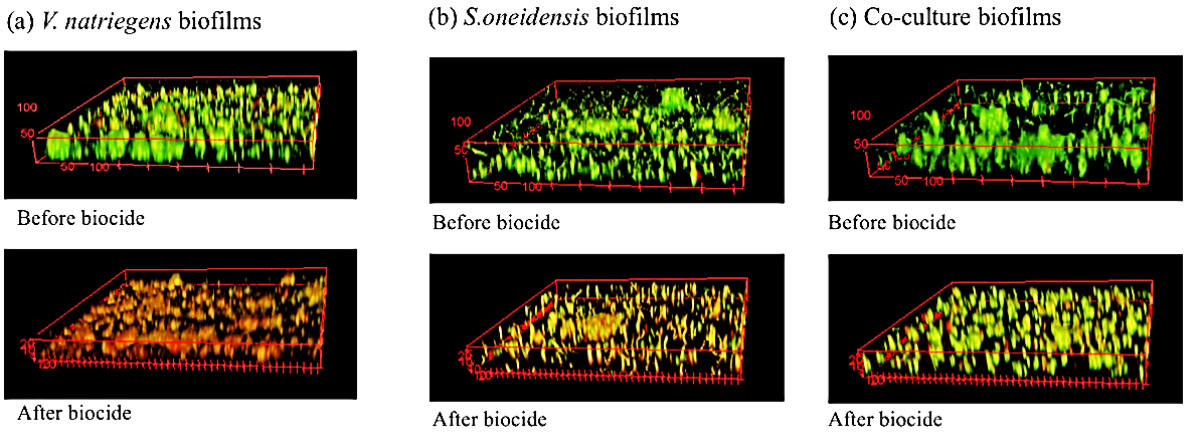

Figure 3: 3D view of *V. natriegens* biofilms (a), *S. oneidensis* biofilms (b), and co-culture biofilms (c) grown for 12 h before and after glutaraldehyde treatment

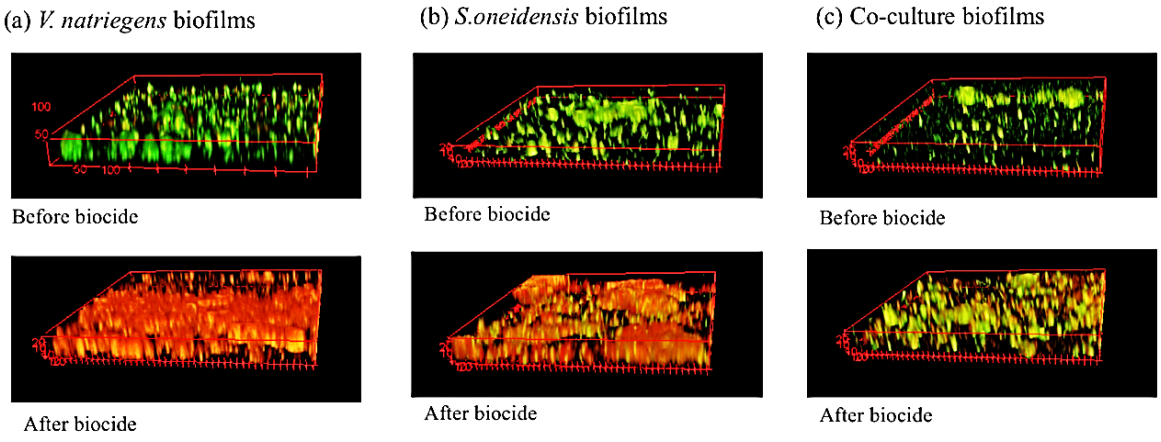

Figure 4: 3D view of *V. natriegens* biofilms (a), *S. oneidensis* biofilms (b), and co-culture biofilms (c) grown for 12 h before and after THPS treatment

Single-species biofilms of *V. natriegens* grown for 12 h and treated with 400 ppm of THPS showed 4.9-fold increase in the percentage of dead cells while *S. oneidensis* biofilms showed 3.1-fold increase in the percentage of dead dells (**Figure 4**). With co-culture biofilms of *V. natriegens* and *S. oneidensis* grown for 12 h, 2.9-fold increase in the percentage of dead cells was observed **(Figure 4**).

Treatment of long-term biofilms with glutaraldehyde and THPS

Single-species biofilms grown for 36 h and treated with 400 ppm of glutaraldehyde of *V. natriegens* showed 2.9-fold increase in the percentage of dead cells while single-species biofilms of *S. oneidensis* showed 2.0-fold increase in the percentage of dead cells (**Figure 5**). With 36 h co-culture biofilms of *V. natriegens* and *S. oneidensis*, 1.9-fold increase in the percentage of dead cells was observed (**Figure 5**).

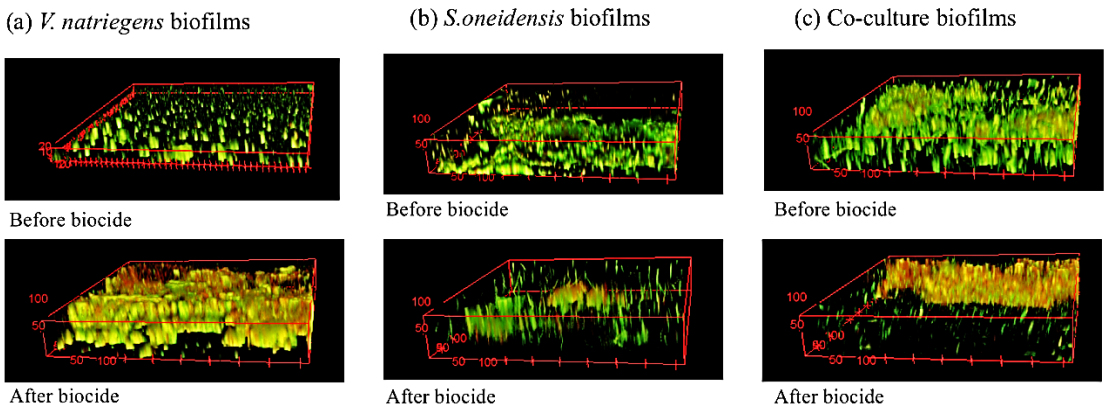

Figure 5: 3D view of *V. natriegens* biofilms (a), *S. oneidensis* biofilms (b), and co-culture biofilms (c) grown for 36 h before and after glutaraldehyde treatment

Single-species biofilms of *V. natriegens* grown for 36 h and treated with 400 ppm of THPS showed 3.0-fold increase in the percentage of dead cells while single-species biofilms of *S. oneidensis* showed 1.9-fold increase in the percentage of dead cells (**Figure 6**). With co-culture biofilms of *V. natriegens* and *S. oneidensis* grown for 36 h, 1.5-fold increase in the percentage of dead cells was observed (**Figure 6**).

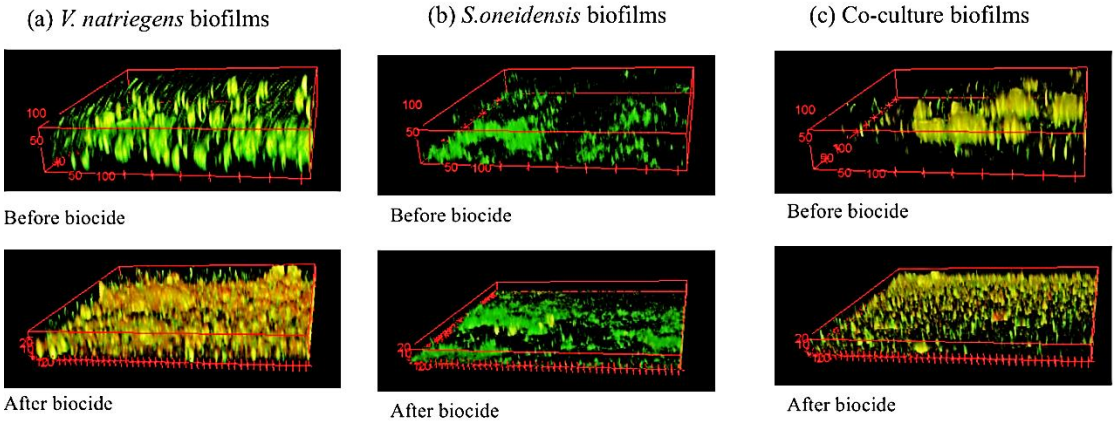

Figure 6: 3D view of *V. natriegens* biofilms (a), *S. oneidensis* biofilms (b), and co-culture biofilms (c) grown for 36 h before and after THPS treatment

Carbon steel corrosion

The metal surface in the lab-on-chip model did not show any indicators of corrosion after single-species biofilms or co-culture biofilms were cultured for 12 h or 36 h. Representative micrographs of metal surfaces are shown (**Figure 7**). Control experiments were conducted with LB growth media and no signs of corrosion was seen after 12 h and 36 h exposure.

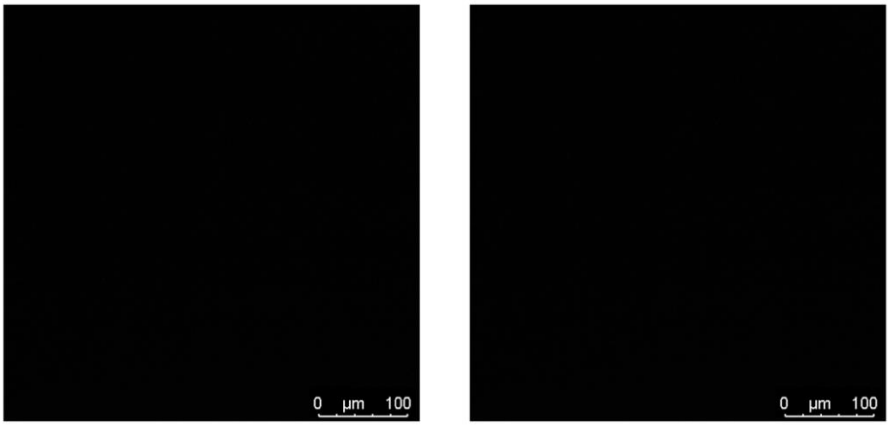

Figure 7: Images of the metal surface in the microfluidic flow system unexposed (left) and after growing single-species and multi-species biofilms for 12 h or 36 h (right)

Comparison of single-species biofilms to co-culture biofilms

Comparing the fold-changes in percentage of dead biomass in **Table 2, 3, 4, and 5**, showed that the susceptibility of biofilms to biocide treatment varied with the biofilm species. The highest susceptibility to biocide treatment was seen with *V. natriegens* biofilms, while *S. oneidensis* biofilms were ~1.5-fold more resistant to biocide treatment than *V. natriegens* biofilms. Co-culture biofilms and single-species biofilms of *S. oneidensis* were more resistant to biocide treatment (p-value < 0.05) than the single-species biofilms of *V. natriegens*. Previous work (Adam et al., 2002; Berry et al., 2006) comparing single-species biofilms to multi-species biofilms also reported multi-species biofilms to be more resistant to antimicrobial treatments than single species biofilms corroborating the results. The differences in the composition of extracellular polymeric substance (EPS) in

these biofilms was suggested as a reason to justify the increased resistance (Adam et al., 2002). However, the exact mechanisms behind the observed increased resistance of co-culture biofilms to biocides are unknown. Studying the complex biochemical interactions between *V. natriegens* and *S. oneidensis* with the extracellular polymeric substance in the co-culture biofilms is likely to provide insights on the increased resistance.

Table 2: Effect of glutaraldehyde treatment on percentage of dead biomass in single-species and co-culture biofilms grown for 12 h

Biofilms	**% dead biomass before biocide**	**% dead biomass after biocide**	**Fold-change in dead biomass**
V. natriegens	25.1±3.1	89.1±9.7	3.6
S. oneidensis	31.8±9.7	85.8±14.4	2.7
Co-culture	32.2±7.5	73.1±11.9	2.3

Table 3: Effect of THPS treatment on percentage of dead biomass in single-species and co-culture biofilms grown for 12 h

Biofilms	**% dead biomass before biocide**	**% dead biomass after biocide**	**Fold-change in dead biomass**
V. natriegens	18.1±0.6	88.7±3.3	4.9
S. oneidensis	27.5±5.3	86.0±3.8	3.1
Co-culture	24.4±2.3	70.0±12.0	2.9

Table 4: Effect of glutaraldehyde treatment on percentage of dead biomass in single-species and co-culture biofilms grown for 36 h

Biofilms	**% dead biomass before biocide**	**% dead biomass after biocide**	**Fold-change in dead biomass**
V. natriegens	26.5±1.4	76.8±8.9	2.9
S. oneidensis	26.7±6.2	53.7±10.7	2.0
Co-culture	33.1±5.6	63.6±5.9	1.9

Table 5: Effect of THPS treatment on percentage of dead biomass in single-species and co-culture biofilms grown for 36 h

Biofilms	**% dead biomass before biocide**	**% dead biomass after biocide**	**Fold-change in dead biomass**
V. natriegens	22.8±8.2	67.9±2.8	3.0
S. oneidensis	13.4±7.8	24.9±8.0	1.9
Co-culture	32.7±1.5	50.2±6.7	1.5

Comparison of biocide susceptibility of short-term and long-term biofilms

We compared biofilms grown for 12 h and 36 h (**Table 2, 3, 4, and 5**) and inferred that biofilms grown for 12 h were significantly more susceptible (p-value < 0.05) to biocide treatment than 36 h. This clearly points out the significance of selecting a representative

time for biofilm growth for determining the efficacy of biocide treatment. Further analysis was conducted to see if this difference was due to the difference in thickness of the biofilms or the biofilm biomass. No significant differences in terms of the biofilm thickness or biofilm biomass was seen for short-term biofilms compared to long-term biofilms (**Figure 8**). Hence, the difference in the susceptibility of short-term and long-term biofilms to the biocide treatment cannot be attributed to diffusion limitations. The observed differences in the susceptibility are likely due to the differences in the extracellular matrix composition or phenotypic mutations of the cells or persister cells or efflux pumps.

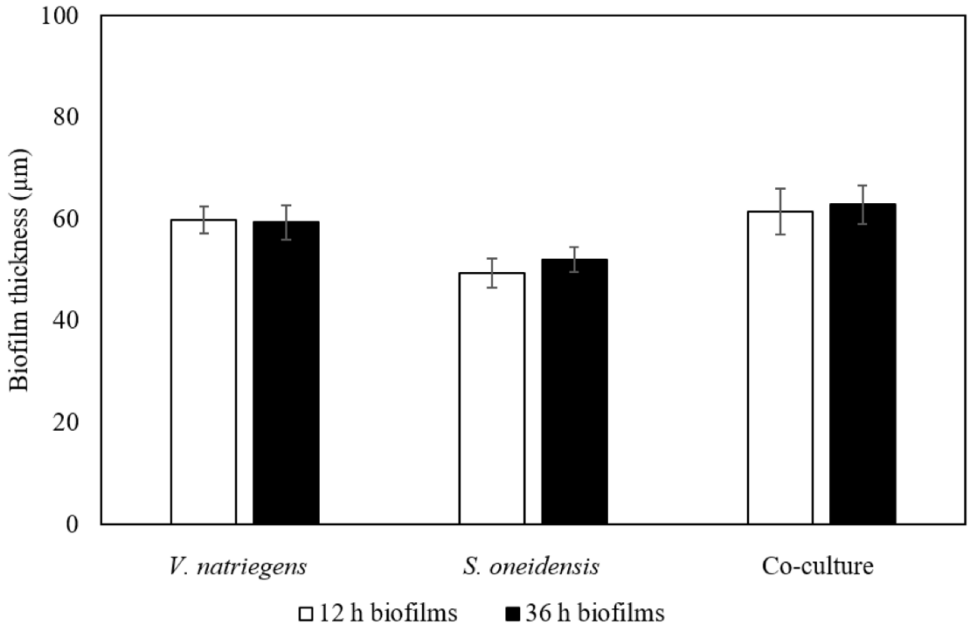

Figure 8: Comparison of the thickness of *V. natriegens*, *S. oneidensis* and co-culture biofilms grown for 12 h and 36 h

From biofilm susceptibility data, it was inferred that short-term biofilms of *V. natriegens* and co-culture biofilms were more susceptible to THPS than glutaraldehyde (p-value < 0.05) while with long-term biofilms the increased susceptibility to THPS treatment (p-value < 0.05) was observed only for co-culture biofilms. Since it is well established that biocides exhibit different degree of antimicrobial effects on different classes of microorganisms and are not as specific in their action as compared to antibiotics (Russell, 2003b; Williams, 1990), some variation in the susceptibility of microorganisms to biocides is expected. The difference in susceptibility to biocides can also be attributed to the differences in the composition of extracellular polymeric substance and/or the differences in the biocide adsorption mechanisms and subsequent uptake of biocides (Russell, 2003a). It is also possible that using Live/Dead staining underrepresents the biocidal effectiveness of glutaraldehyde as it is not clear if membranes that are cross-linked (upon glutaraldehyde exposure) are comparably permeable to the SYTO9 and propidium iodide dyes as normal (untreated) membranes.

3.4 Conclusions

This section demonstrates the application of a lab-on-a-chip flow system for screening biocides against MIC causing biofilms. This microfluidic system offers a platform for simulating pipeline flow conditions that overcomes the drawbacks of static systems and large-scale flow systems. Using minimal reagents for the establishment of biofilms and corrosive conditions in the system is advantageous particularly when using field waters to determine appropriate biocide type and dosage. While it is not possible to

replicate field conditions in the laboratory, this lab-on-a-chip model can be used to test a wide range of relevant process conditions (e.g. pressure, flowrate, temperature).

From the confocal microscopy images and quantitative analysis of the biofilm viability, it was concluded that co-culture biofilms were more resistant to biocide treatment than single-species biofilms. This reiterates the importance of investigating co-culture laboratory grown biofilms for understanding MIC mechanisms rather than solely investigating the obvious corroding species like sulfate reducers. Differences in the susceptibility to the biofilms to the two biocides was seen only for short-term biofilms, with THPS being more effective in killing biofilm bacteria than glutaraldehyde under these experimental conditions. Further, co-culture biofilms grown for longer time were more resistant to biocide treatment than single-species biofilms indicating the importance of biofilm growth time as an important parameter in biocide efficacy studies. Further investigation of the extracellular matrix composition, biocide adsorption, cellular uptake and efflux is essential for elucidating the differences in the biocide susceptibility of biofilms with species, time of growth and type of biocide.

The variability of biocide resistance seen across different biofilms highlights the importance of executing biocide efficacy screening and qualification studies for the specific microorganisms present in the locations impacted by MIC than performing a random selection of biocide. While the current work is limited to 36 h biofilm culture and no noticeable metal corrosion was observed, this lab-on-a-chip model can be adapted for longer term biocide efficacy studies to allow for metal corrosion and hence investigate MIC using model organisms or using inoculum from MIC impacted field locations.

4. DEVELOPMENT AND CHARACTERIZATION OF A MICROFLUIDIC FLOW SYSTEM FOR INTEGRATED MEASUREMENT OF CORROSION AND BIOFILM PHYSIOLOGY*

4.1 Introduction

MIC occurs when microorganisms utilize metal either directly or indirectly for their metabolism (Enning and Garrelfs, 2014). Investigating the interactions between the microorganisms in the biofilm and the microorganisms/biofilm with the metal surface are vital to effective understanding of MIC. Hence, characterization biofilm growth and their influence on corrosion processes is desirable.

MIC is a location-specific phenomenon, with significant spatial heterogeneity in the composition and abundance of microorganisms between different MIC-impacted locations, as well as within the same location. To effectively investigate MIC in the laboratory, it is important the microorganisms used for growing biofilms should be representative of those seen at the MIC-impacted field location. In addition, these organisms should also be amenable to cultivation, and potentially genetic manipulation, in the laboratory so that biofilm formation can be studied. For the current study, two model organisms that have been previously identified at MIC impacted field locations were selected. *V. natriegens* was chosen as a facultative anaerobic bacterium that helps in the

* Part of the chapter is reprinted with permission from NACE International, Houston, TX. All rights reserved. Susmitha Purnima Kotu, Celal Erbay, Nebras Sobahi, Arum Han, Sam Mannan, Arul Jayaraman, Paper 7793 presented at CORROSION 2016, Vancouver, British Columbia, Canada. © NACE International 2016

initial biofilm formation (Benbouzid-Rollet et al., 1991; Cheng et al., 2009; Nivens et al., 1986; Yin et al., 2008c). *S. oneidensis* was chosen as a marine biofilm forming facultative iron-reducing bacterium present at MIC impacted field locations (McLeod et al., 2002) also known to inhibit corrosion in certain cases (De Windt et al., 2003; Herrera and Videla, 2009; Kotu et al., 2016). Importantly, genetic manipulation tools are available to express fluorescent proteins and help visualize biofilm growth on metal surfaces.

Microfluidics-based flow systems have a micro flow channel inside a transparent polymer, polydimethyl siloxane (PDMS) bonded to a glass slide (**Figure 9**). Because of their advantages with minimal reagent usage, controlled environments, and real time measurements, microfluidic flow systems provide an excellent platform for investigating MIC if these flow systems incorporate both corrosion and biofilm growth measurements. The novel modified microfluidic system developed here helps visualize biofilms using confocal laser scanning microscopy (CLSM) as well as investigate the electrochemical changes occurring due to corrosion reactions using electrochemical impedance spectroscopy (EIS). To our knowledge, a device that can be used for integrated measurement of both corrosion and biofilm physiology has not been developed earlier. Different organisms chosen from the microbial communities identified across several MIC impacted field locations or field water samples can be used for establishment of biofilms in this model and the interplay of biofilm dynamics and electrochemical processes can be investigated to gain a fundamental understanding of MIC.

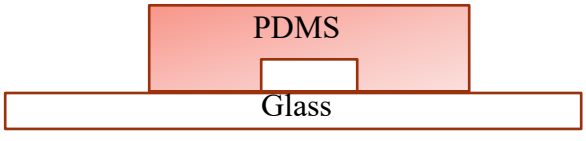

Figure 9: Side view of a microfluidic flow system consisting of a PDMS layer bonded to glass

4.2 Materials and methods

Bacterial strains and plasmids

V. natriegens was obtained from ATCC (ATCC 14048). *S. oneidensis* was obtained as a gift from Dr. Karim (Texas A&M University). *V. natriegens* and *S. oneidensis* were grown in LB media with 1.5% NaCl at 30ºC. Kanamycin (80 µg/ml) and chloramphenicol (20 µg/ml) were used to maintain the plasmids in the bacteria.

Engineering of fluorescent reporter bacterial strains

Green fluorescent protein (GFP) and red fluorescent protein (RFP) were introduced in to *V. natriegens* by using tri-parental mating (**Figure 10**). The helper strain used was *Escherichia coli* CC118λ*pir* with plasmid pEVS104 and the donor strain was DH5αλ*pir* with plasmids pVSV102 and pVSV208 containing *gfp* and *rfp* genes (Dunn et al., 2006; Sawabe et al., 2006), respectively. After triparental mating, *V. natriegens* strains with plasmids containing *gfp* and *rfp* genes were streaked on a plate to check for expression of fluorescence **(Figure 11**).

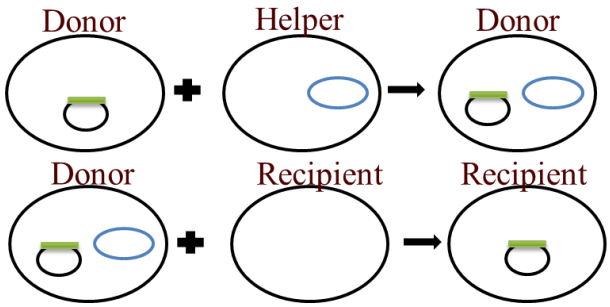

Figure 10: Schematic of tri-parental mating depicting the transfer of plasmid from donor to recipient with the help of a helper strain

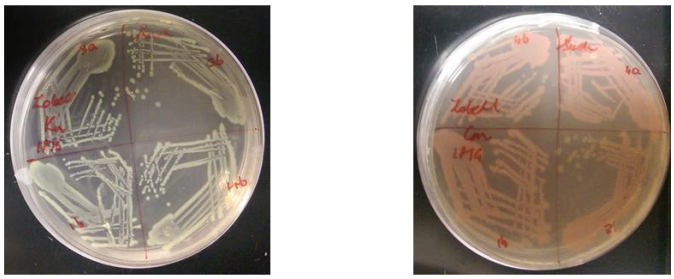

Figure 11: *V. natriegens* expressing green fluorescent protein (left) and *V. natriegens* expressing red fluorescent protein (right) after tri-parental mating

S. oneidensis with plasmid p519ngfp was obtained from Dr. El-Naggar (University of Southern California). A new plasmid, p519nrfp was constructed (**Figure 12**) by replacing the *gfp* gene in plasmid p519ngfp with the *mCherry* gene from plasmid pA13-RP4 oriT-Perm AM-mCherry-TpepN (kind gift from Dr. Katy Kao, Texas A&M University). Polymerase chain reaction (PCR) was performed to amplify the *mCherry* gene (forward primer as TAAGCATCTAGAGACTTAGAAATGGTGAGCAAGGGCGAG, reverse primer as TGCTTAGAATTCGTCGACCTACTTGTACAGCTCGTCCAT, and annealing temperature of 55^{o}C) for cloning and the amplified product was purified on a

1.3% agarose gel. Restriction digestion of the p519ngfp plasmid and the amplified *mCherry* gene was carried out using enzymes *XbaI* and *EcoRI*. The digested products were purified on a 0.7% agarose gel and further cleaned using the PCR Clean-Up System (Promega). Six independent restriction digestion reactions were purified and pooled. Instant sticky-end ligase master mix (New England Biolabs) was used for ligating the *mCherry* insert into p519ngfp plasmid backbone to obtain p519nrfp plasmid. The ligated p519rfp plasmid was transformed into NEB 10-beta Competent *E. coli* (New England Biolabs) and electroporated (550 V and 200 Ω) into *S. oneidensis* (Potter and Heller, 2003).

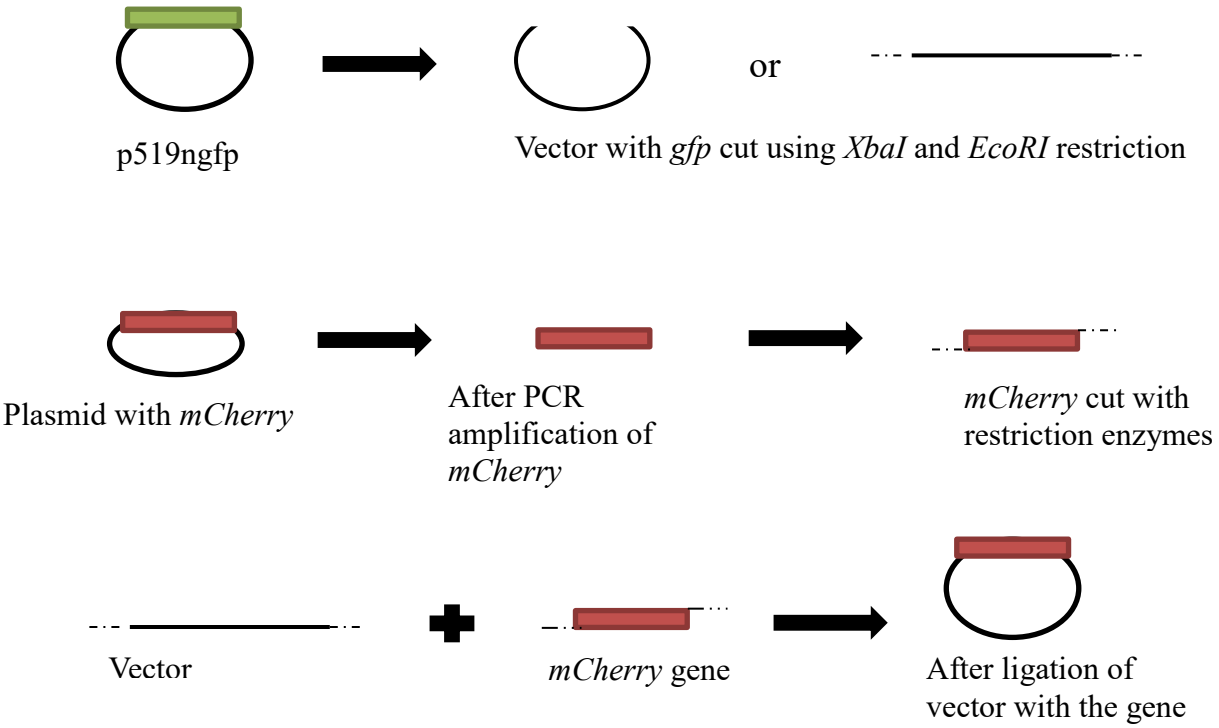

Figure 12: Cloning strategy for constructing plasmid p519nrfp using p519ngfp plasmid as vector and *mCherry* gene as insert

Glass-PDMS microfluidics device fabrication and biofilm studies

Polydimethylsiloxane (PDMS) microchannels were fabricated by mixing silicone elastomer and curing agent in a 10:1 ratio. The mixture was poured onto the silicon master that was patterned with SU-8 in the shape of rectangular lanes (200 µm wide and 100 µm tall). The silicon master with PDMS was cured at 80^{o}C for 2 h. The cured PDMS layer was peeled from the silicon master mold and then bonded directly to a clean glass slide (without any metal deposition) to obtain the first generation microfluidic device.

Overnight cultures of *S. oneidensis* and *V. natriegens* were grown in LB media with appropriate antibiotic (Kanamycin 80 µg/ml) were diluted to an OD ~1.0 and then introduced into the channel. The flow was stopped and bacteria were allowed to attach to the glass in the absence of flow. After 2 h, nutrient media was continuously flowed at different flow rates into the device to remove unattached bacteria and provide nutrients for growth of the attached bacteria. Biofilm images were acquired at 8 h, 16 h, and 24 h after starting the flow of nutrient media. All experiments were conducted in triplicates.

Biofilms were imaged using a Leica TCS SP5-RS Confocal Laser Scanning Microscope. A 488 nm argon laser was used for visualizing GFP (green fluorescent protein-expressing bacteria) and a 580 nm helium laser was used for visualizing red fluorescent protein-expressing bacteria. Images were captured at five randomly selected locations at different positions along the length of the channel. Z-stacks were constructed by acquiring 50 images at 2 µm resolution. The line accumulation was set to a value of 8 and an optical zoom of 10 was used for all the images. The values for gain and offset were adjusted for each individual experiment based on the background fluorescence. The image

files (.lif extension) were analyzed using COMSTAT image analysis software (http://www.comstat.dk/) (Heydorn et al., 2000; Vorregaard, 2008) with auto thresholding. The connected volume filtering feature that filters out pixels not attached either to the glass/metal substrate or to the biofilm in previous slices was used to eliminate any noise from pixels not attached to the substrate.

Microfluidic device for integrated measurements of corrosion and biofilm physiology using aluminum coated glass

Aluminum (~100 nm thickness) was deposited on glass slides using electron beam physical vapor deposition (LESKER PVD 75 Electron-Beam Evaporation). The aluminum was deposited as interdigitated fingers that were 135 µm long, 25 µm wide, and spaced 15 µm apart (**Figure 13**). The aluminum deposited glass slide was bonded to a PDMS channel (5 mm long, 200 µm wide, and 100 µm tall).

Figure 13: Top view of the coated aluminum on glass as interdigitated bands

Overnight grown *S. oneidensis* and *V. natriegens* cultures were diluted to OD of ~1.0 and used for seeding the microfluidic devices at a seeding ratio of 2:1 (*S. oneidensis*:*V. natriegens*). Nutrients were flowed at 0.02 ml/h as described above. As a control, sterile LB media was flowed through the device. Images were acquired every 8 h for 48 h.

VERSASTAT3 (Princeton Applied Research) was used for all EIS measurements. An input AC voltage signal of 10 mV was used over the frequency range of 100 kHz to 10 mHz to record the impedance. To analyze the amount of corrosion on the aluminum metal, scanning electron microscopy (SEM) was carried out after 24 h and 48 h of exposure. Prior to obtaining SEM images, the PDMS was peeled from the glass slide, and the biofilm and corrosion products were removed by dipping the slide in 2 M HCl for 15 minutes. A 10 nm layer of platinum metal was coated over the glass slide to make it conductive for SEM. SEM images were acquired using a FEI QUANTA 600 FE-SEM. A Leica TCS SP5-RS Confocal Laser Scanning Microscope was used for obtaining fluorescent biofilm images over metal.

Microfluidic device for integrated measurements of corrosion and biofilm physiology with two metal surfaces

To fabricate M-MIC2 (Kotu et al., 2018), glass slides were deposited and patterned such that two parallel rectangular bands of carbon steel and titanium are separated by a distance of 100 µm (**Figure 14**). First, titanium was deposited on the cleaned glass slides using electron beam physical vapor deposition (LESKER PVD 75 Electron-Beam Evaporation) and patterning of titanium was performed using photolithography such that the photoresist protects the desired titanium pattern (**Figure 15**). Positive photoresist S1818

(Dow) was spin coated for 30 s at 4000 rpm on the titanium deposited glass slides. The slides were then baked followed by exposed to UV along with a photomask for 20 s at a lamp intensity of 4 W/cm^2. The glass slides were then developed in AZ 726 MIF solution (Microchemicals) for 45-60 s. Etching of titanium was then carried out by dipping the slide in 2:100 solution of HF in DI water to remove undesired titanium. Photoresist was then removed by immersing the glass slides patterned with titanium in acetone for 5 minutes. Next, photolithography was used to pattern the titanium-patterned glass slide such that all regions of the glass slide except where carbon steel is to be patterned are protected with photoresist. Application of photoresist, baking of photoresist and patterning of photoresist was conducted as mentioned earlier. Carbon steel was then deposited using metal sputtering (LESKER PVD 75 DC Sputter) and finally acetone was used to etch carbon steel and photoresist from undesired regions.

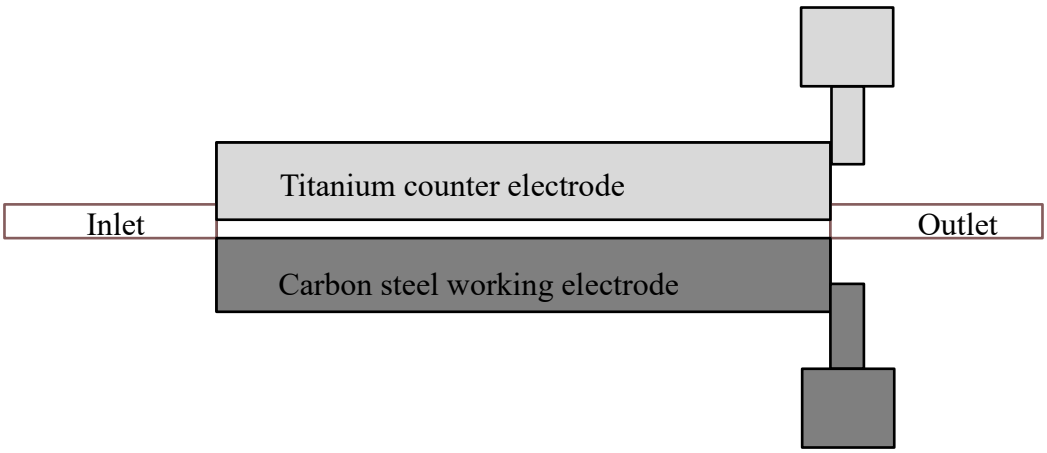

Figure 14: Top view of coated metal on glass in M-MIC2 with carbon steel and titanium as parallel rectangular bands

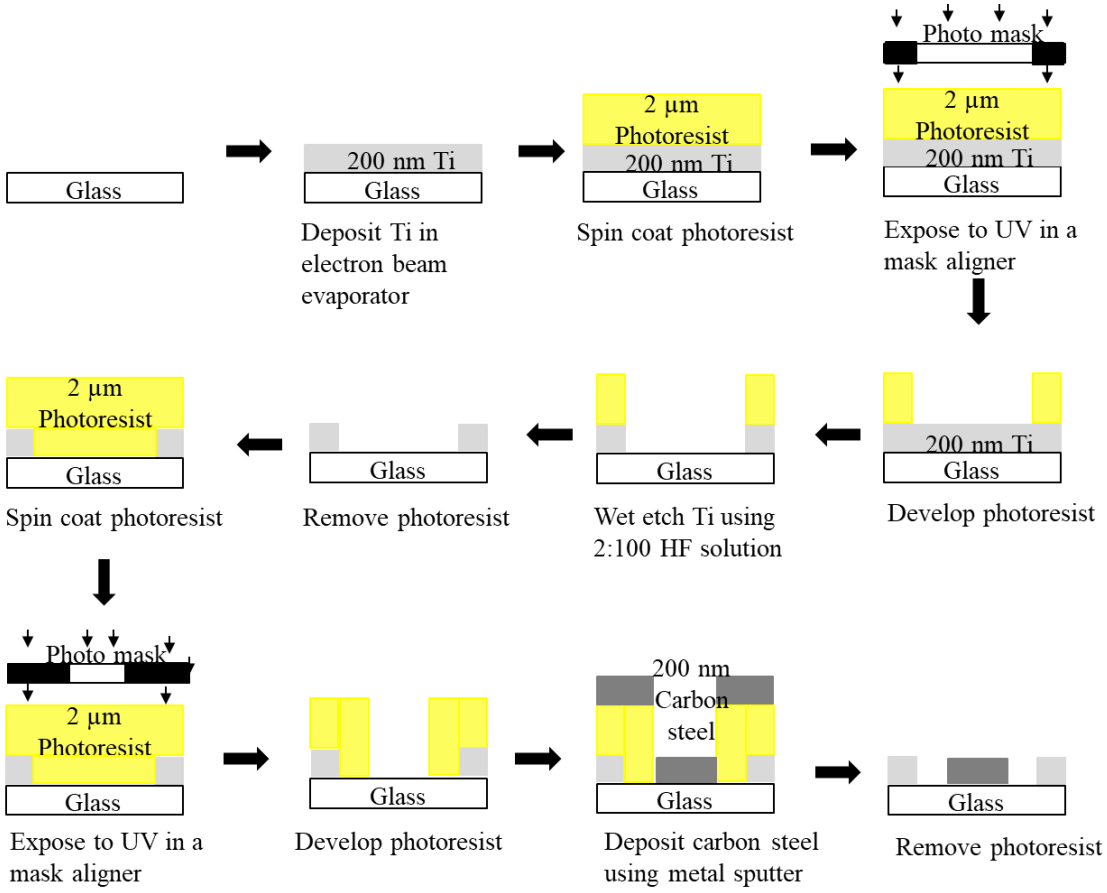

Figure 15: Schematic of the metal deposition and patterning process

Polydimethylsiloxane (PDMS) microchannels were fabricated as rectangular lanes 500 µm high and 1000 µm wide. Cleaned glass slides with metal pattern and PDMS layers were bonded together by oxygen plasma treatment. Tygon tubing of 0.01″ ID×0.03″ OD was used for making all fluidic inlet and outlet connections to the syringes. A syringe pump (Chemyx) was used to continuously perfuse growth medium. Copper wires (24 gauge) were attached to the electrode pads using silver paste and epoxy to prevent the wires from detaching.

Schematic of experimental setup for M-MIC2

Figure 16 depicts the schematic of the experimental setup for integrated measurements of corrosion and biofilm physiology using the M-MIC2 microfluidic model. The experimental device is placed on the stage of a confocal microscope placed inside a temperature controlled incubator. The metal wires from M-MIC2 were connected to the leads of the potentiostat placed next to the incubator and microscope.

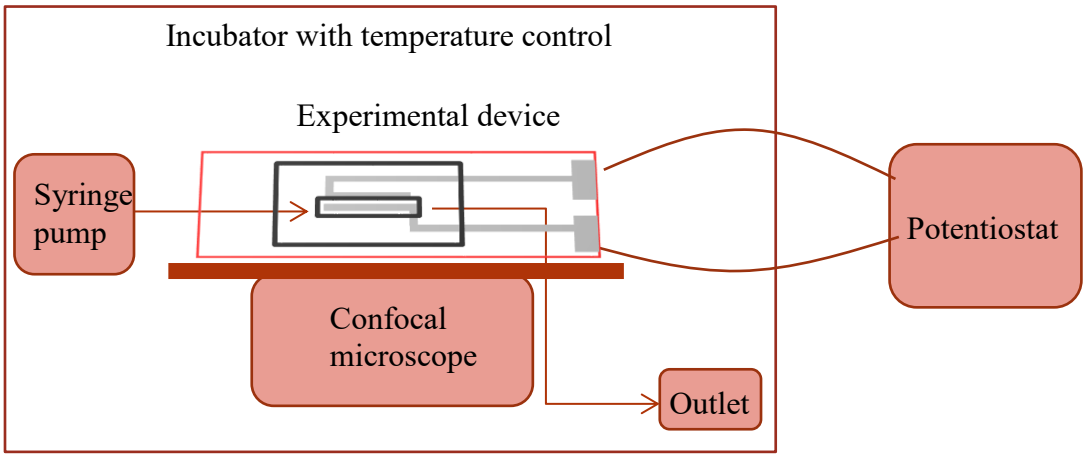

Figure 16: Schematic of the experimental setup for M-MIC2 using confocal microscope and potentiostat for biofilm growth and corrosion measurements

Control experiments were conducted by flowing LB media in the microfluidic device at a flow rate of 0.25 ml/h. *V. natriegens* strain expressing green fluorescent protein and *S. oneidensis* strain expressing red fluorescent protein were used for these experiments. Kanamycin (80 µg/ml) was used in the LB media to maintain the *gfp* and *rfp* plasmids in

the two strains. For single-species biofilms, overnight cultures of *V. natriegens* and *S. oneidensis* grown in LB media were diluted to an optical density of ~1.0 before seeding into the microfluidic flow cell. For co-culture biofilms, overnight cultures of *V. natriegens* and *S. oneidensis* diluted to an optical density of ~1.0 were mixed in equal ratio before seeding into the microfluidic channel. After seeding, these cultures were kept for 2 h without flow to initiate attachment to the metal. After 2 h, LB media was continuously flowed through the system at 0.25 ml/h to remove unattached cells as well as provide nutrients for the growth of biofilms throughout the duration of the experiment. Biofilms were grown under aerobic environment for 48 h at 30^{o}C. Control experiments without any seeded bacteria were also performed at 30^{o}C for 48 h. All experiments were done in triplicates with three independent cultures.

In addition to continuous flow experiments, preliminary batch/static experiments were conducted with *S. oneidensis*. Overnight culture of *S. oneidensis* was diluted to an optical density of ~ 0.2 before seeding into the microfluidic flow cell. After seeding, the system was kept static for 24 h. EIS was measured every 1 h until 24 h and biofilm imaging was executed every 4 h. Sterile LB growth media was used as the control. All batch culture experiments were done in duplicate.

A Leica SP8 confocal laser scanning microscope (Wetzlar, Germany) was used to acquire z-stacks of the stained biofilms every 2.5 µm with a 20x objective. Z-stacks were captured at five random locations in all of the devices. Argon (488 nm) and Helium-Neon lasers (561 nm), corresponding to excitation wavelengths of green and red fluorescent proteins, were used to image the biofilms over the metal surface every 12 h for continuous

flow experiments and every 4 h for static experiments. Line accumulation of 3 and frame average of 2 was used when obtaining z-stacks. The .lif extension files obtained were analyzed using COMSTAT2 image analysis software (http://www.comstat.dk/) (Heydorn et al., 2000; Vorregaard, 2008) with manual thresholding to quantify biofilm biomass. The connected volume filtering feature was used to eliminate any noise from pixels not attached to the substrate. Image J was used to obtain 3D biofilm structures.

VERSASTAT3 from Princeton Applied Research was used for EIS scans as mentioned earlier. For continuous flow experiments, potentiostatic EIS scans were recorded every 6 h with titanium as both reference and counter electrode and carbon steel as working and sense electrode. For static experiments, potentiostatic EIS scans were recorded every 1 h. The potential difference of carbon steel with respect to titanium electrode was also recorded every 20 seconds throughout the time of the experiment except when the EIS scans and confocal images were acquired.

4.3 Results and conclusions

Microfluidic device development for corrosion studies

The basic design of the microfluidic system consisted of a flow channel inside a block of transparent polymer polydimethyl siloxane (PDMS) that was bonded to a glass slide (**Figure 9**). To adapt this system for MIC studies, the glass substrate was modified by coating a thin layer of metal prior to bonding to the PDMS block (**Figure 17**). This modified microfluidic system can be used to both visualize biofilms using confocal laser

scanning microscopy (CLSM) as well as monitor the electrochemical changes occurring due to corrosion reactions on metal using electrochemical impedance spectroscopy (EIS).

Aluminum was initially used as the metal for investigating MIC as aluminum alloys are commonly used for fuel storage tanks and are susceptible to MIC (Iverson, 1987; Wagner and Little, 1993). Therefore, the susceptibility of aluminum to corrosion and the formation of co-culture biofilms on aluminum were simultaneously investigated using a microfluidic system. Since aluminum is prone to passivation due to the formation of the aluminum oxide layer, we concluded that aluminum was not an appropriate choice for corrosion studies in our microscale model. In all subsequent studies, carbon steel was used for patterning the glass slide, as it is well established that carbon steel corrodes more readily than aluminum.

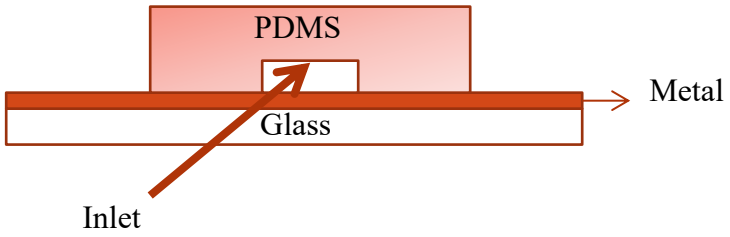

Figure 17: The side view of a modified microfluidic flow system with metal deposition

To further facilitate measurement of electrochemical changes in the microfluidic system, the device was further modified to deposit two different metals on the glass surface. One of the metals acts as a counter electrode while the other metal serves as the working

electrode that corrodes. In our work, we deposited titanium as the non-corroding counter electrode and pseudo reference electrode, while 1018 grade carbon steel was used as the working electrode. This microfluidic microbiologically influenced corrosion flow model, referred to as M-MIC2 was used subsequently (**Figure 14**).

Single and co-culture biofilm studies in Glass-PDMS microfluidic device

Four different flowrates between 0.02 ml/h and 0.14 ml/h were tested for their effect on biofilm formation by investigating the amount of biomass in the biofilm at 8 h, 16 h and 24 h. The biomass of *S. onediensis* for all flow rates except 0.06 ml/h increased from 8 h to 16 h (**Figure 18**). A further increase in biomass until 24 h was seen with only the lowest flowrate, 0.02 ml/h. A decrease in the biomass from 16 h to 24 h was seen with 0.06 ml/h and 0.14 ml/h (**Figure 18**). For *V. natriegens* biofilms, flow rate of 0.02 ml/h had the highest amount of biomass for all three time points (**Figure 19**). The biomass of *V. natriegens* decreased from 8 h to 24 h for 0.02 ml/h flow rate indicating removal of biofilms with time (**Figure 19**).

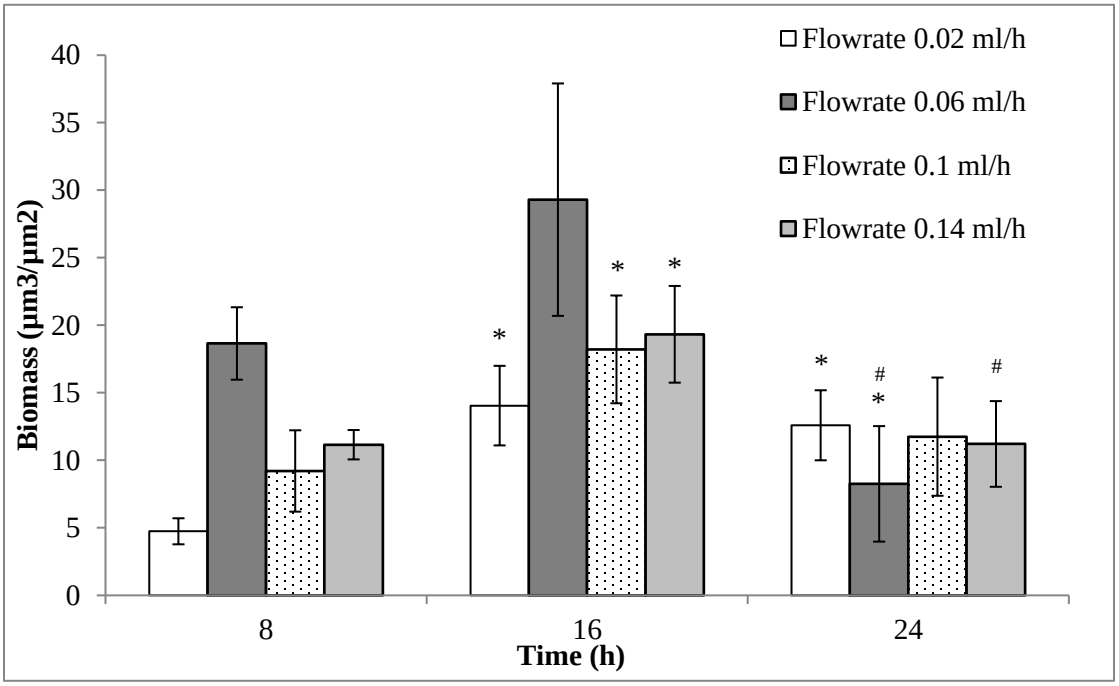

Figure 18: Effect of flowrate on biofilm formation of *S. oneidensis* (*: *p*-value < 0.05 with respect to 8 h time point; #: *p*-value < 0.05 with respect to 16 h time point)

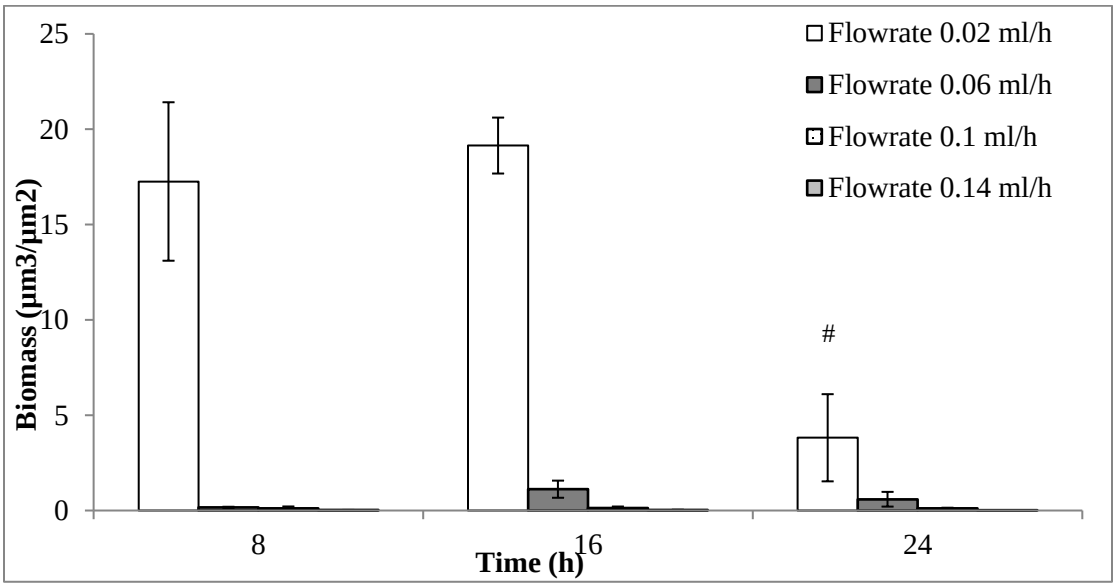

Figure 19: Effect of flowrate on biofilm formation of *V. natriegens* (*: *p*-value < 0.05 with respect to 8 h time point; #: *p*-value < 0.05 with respect to 16 h time point)

The optimal flowrate of 0.02 ml/h was used for co-culture biofilm experiments as both *S. oneidensis* and *V. natriegens* were able to form biofilms at this flowrate. When *S. oneidensis* and *V. natriegens* were seeded at a 1:1 (vol/vol) ratio for co-culture biofilm formation, the biomass of *S. oneidensis*, expressing red fluorescent protein, was about 50% to 75 % of the biomass of *V. natriegens*, expressing green fluorescent protein. When a 2:1 (vol/vol) initial seeding ratio of *S. oneidensis* and *V. natriegens* was used, the amount of *S. oneidensis* and *V. natriegens* biomass formed was equal (**Figure 20**). When co-culture biofilms were grown at 2:1 initial seeding ratio (**Figure 21**), the biofilm biomass of *S. oneidensis* increased from 8 h to 24 h while the increase with *V. natriegens* was insignificant.

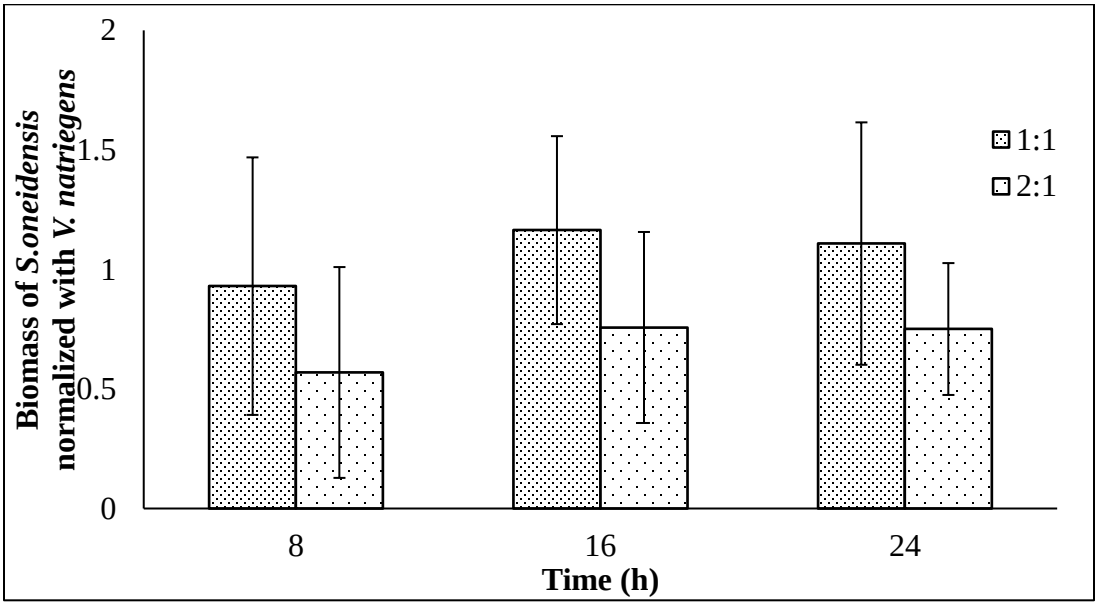

Figure 20: Effect of initial seeding ratios (vol/vol) of *S. oneidensis* and *V. natriegens* on the biofilm biomass of *S. oneidensis* normalized with *V. natriegens*

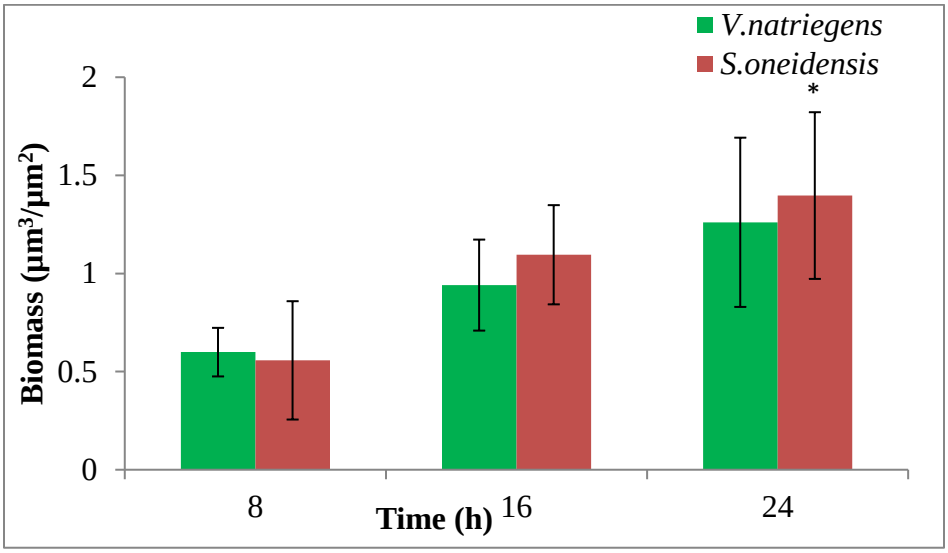

Figure 21: Biomass of co-culture biofilms of *S. oneidensis*, expressing red fluorescent protein and *V. natriegens*, expressing green fluorescent protein at different timepoints when seeded at 2:1 volumetric ratio (*: *p*-value < 0.05 with respect to 8 h time point)

Co-culture biofilm studies in the microfluidic device

When co-culture biofilms were grown on aluminum coated microfluidic devices, the biofilm biomass increased until 32 h and followed by a decrease in biofilm biomass. The impedance values based on EIS spectra of the co-culture biofilms increased from 8 h to 16 h and remained unchanged subsequently (**Figure 23**). From these changes in the impedance values, it can be concluded that the biofilms passivate the surface and prevent the occurrence of MIC over the duration of the experiment. Minimal signs of corrosion were observed on aluminum coated glass slides exposed to co-culture biofilms as compared to aluminum coated glass slides exposed to sterile media (**Figure 24**).

Use of the aluminum coated microfluidic devices led to several concerns including passivation of aluminum that prevented further corrosion, electrical shorting between the electrode fingers due to biofilm formation, and noise in the EIS measurements due to the absence of a counter electrode. To overcome the these concerns, a new microfluidic model, M-MIC2 with carbon steel as working electrode and titanium as counter electrode separated by 100 µm was developed.

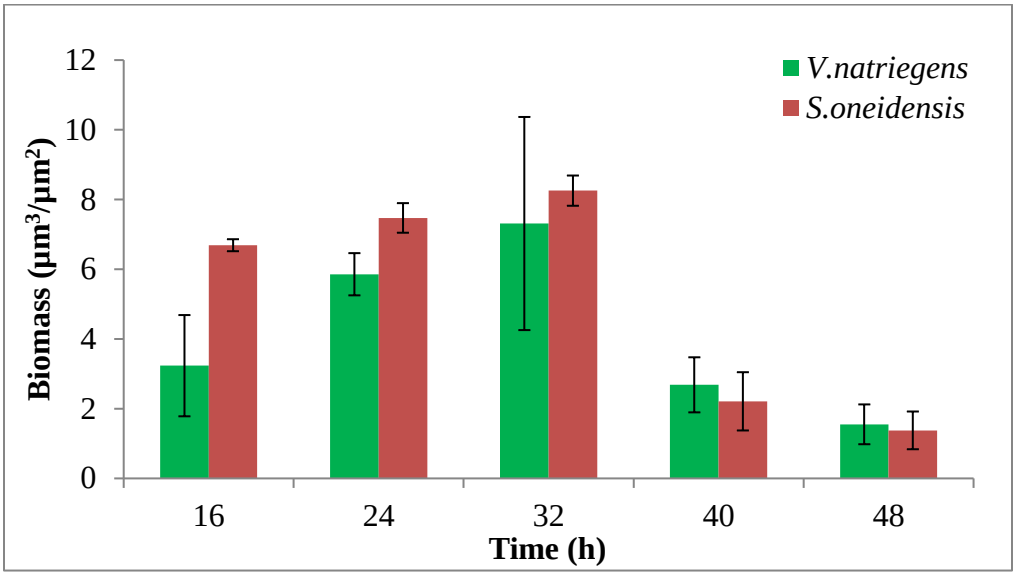

Figure 22: Biomass of co-culture biofilms on aluminum of *S. oneidensis expressing rfp* and *V. natriegens expressing gfp,* measured at different time points

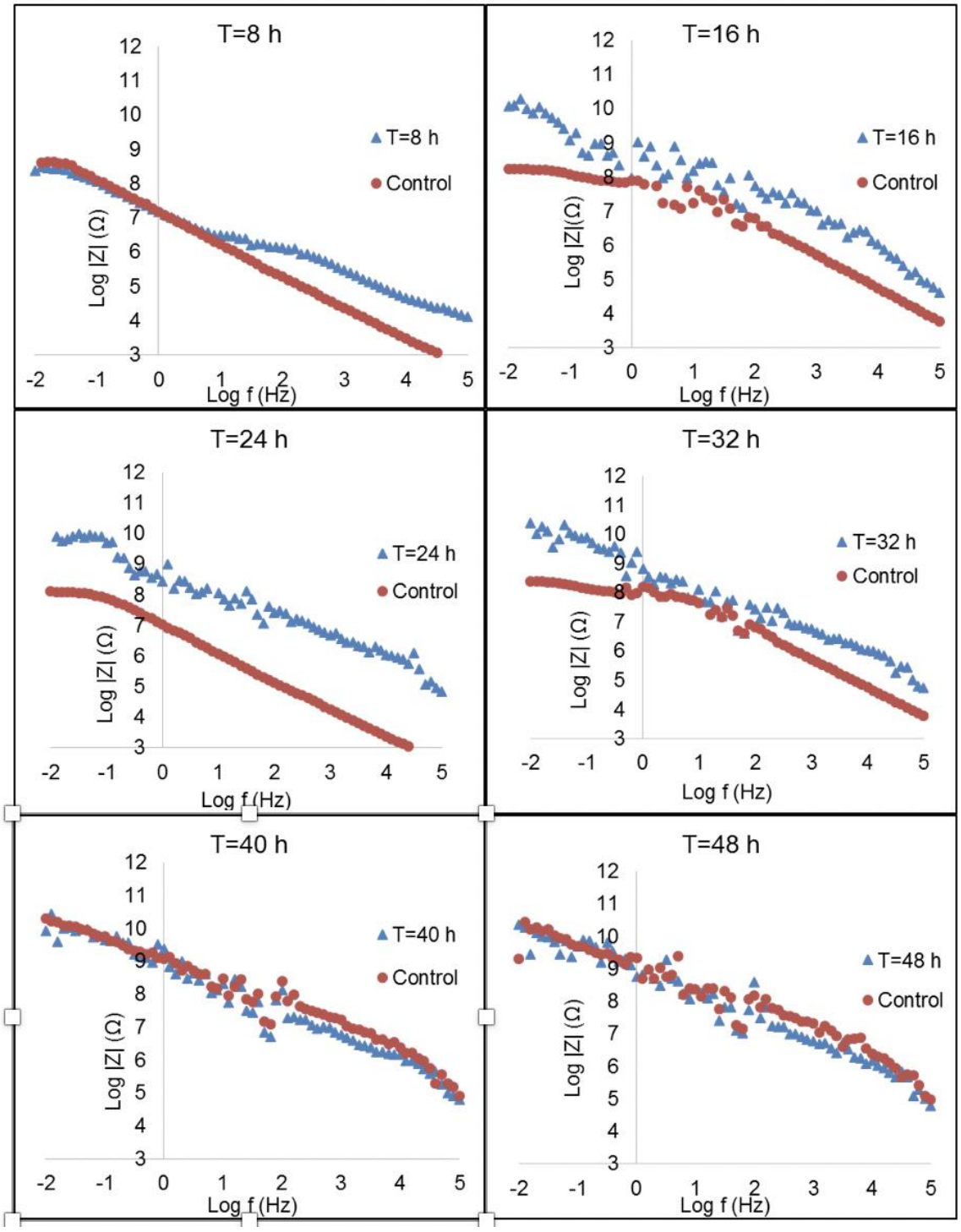

Figure 23: EIS spectra of co-culture biofilms on aluminum with respect to sterile LB control

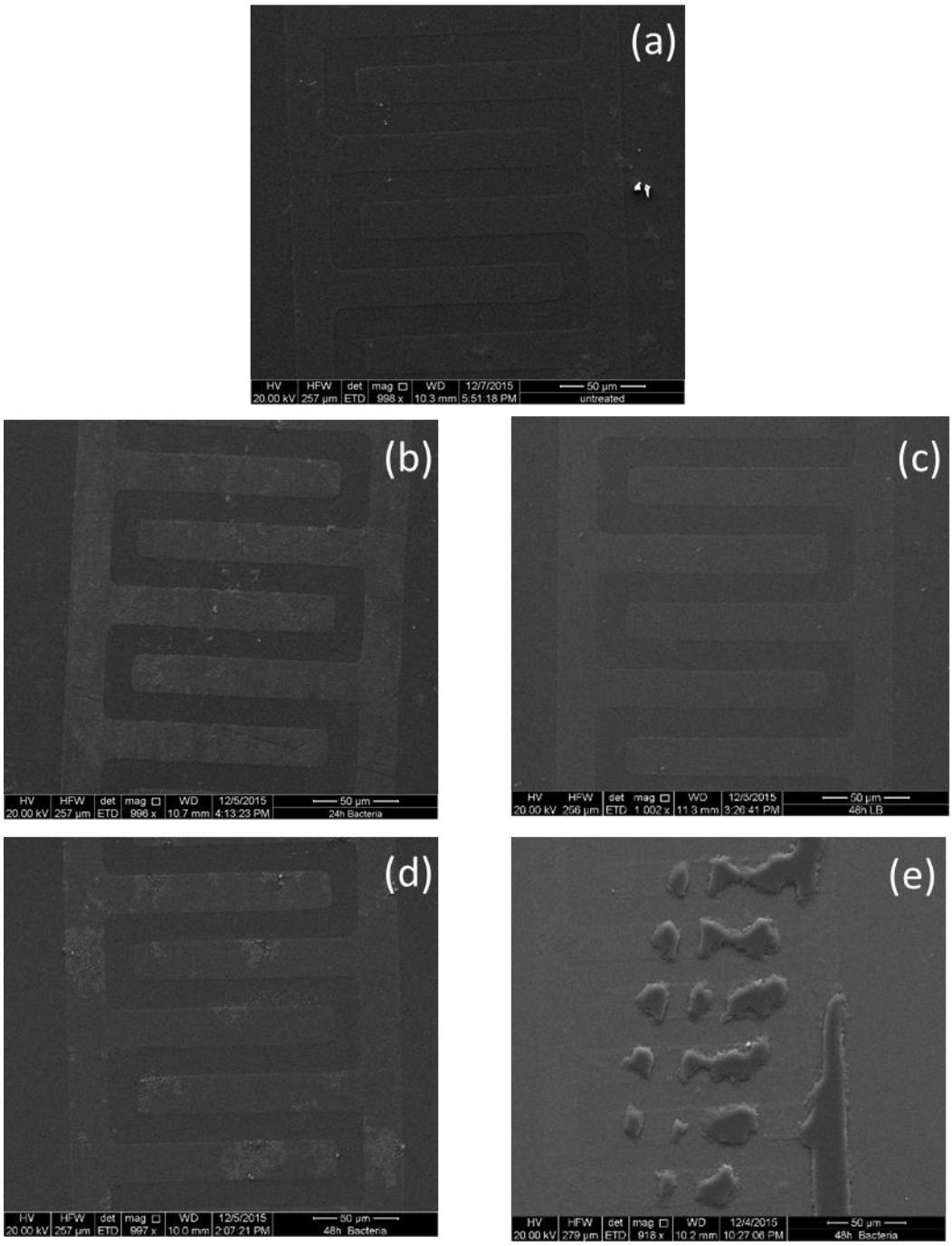

Figure 24: SEM images of glass slides with untreated aluminum (a); exposed to co-culture biofilms for 24 h (b) and 48 h (d); exposed to LB for 24 h (c) and 48 h (e)

Single and co-culture biofilm studies in M-MIC2

Control experiments with sterile LB media were conducted using the M-MIC2 device and the impedance spectra obtained. No significant differences were observed in impedance spectra for 48 h, as seen from the phase angle Bode plot (**Figure 25**).

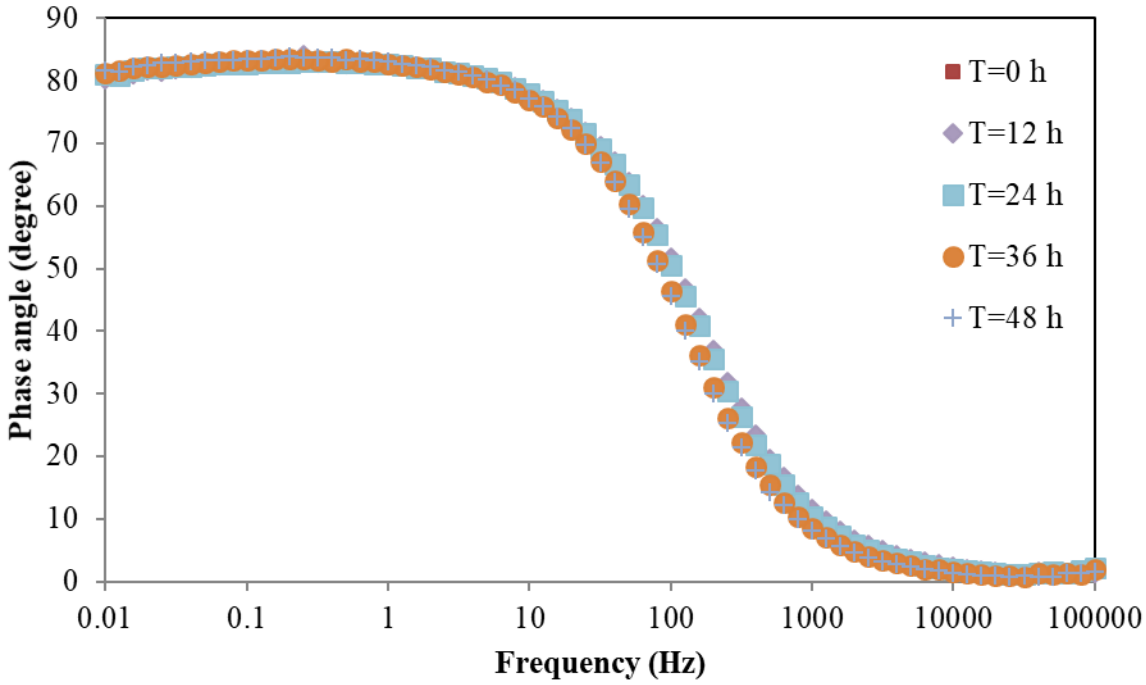

Figure 25: Bode plot of phase angle and frequency for sterile LB media in the M-MIC2 device

Single culture biofilms of *V. natriegens* expressing green fluorescent protein were cultured in the M-MIC2 device. No substantial variations in the EIS spectra were observed between 12 h, 24 h, and 36 h even when the biofilm biomass and biofilm thickness was considerably lower for 12 h compared to the later time points, 24 h and 36 h (**Figure 26**).

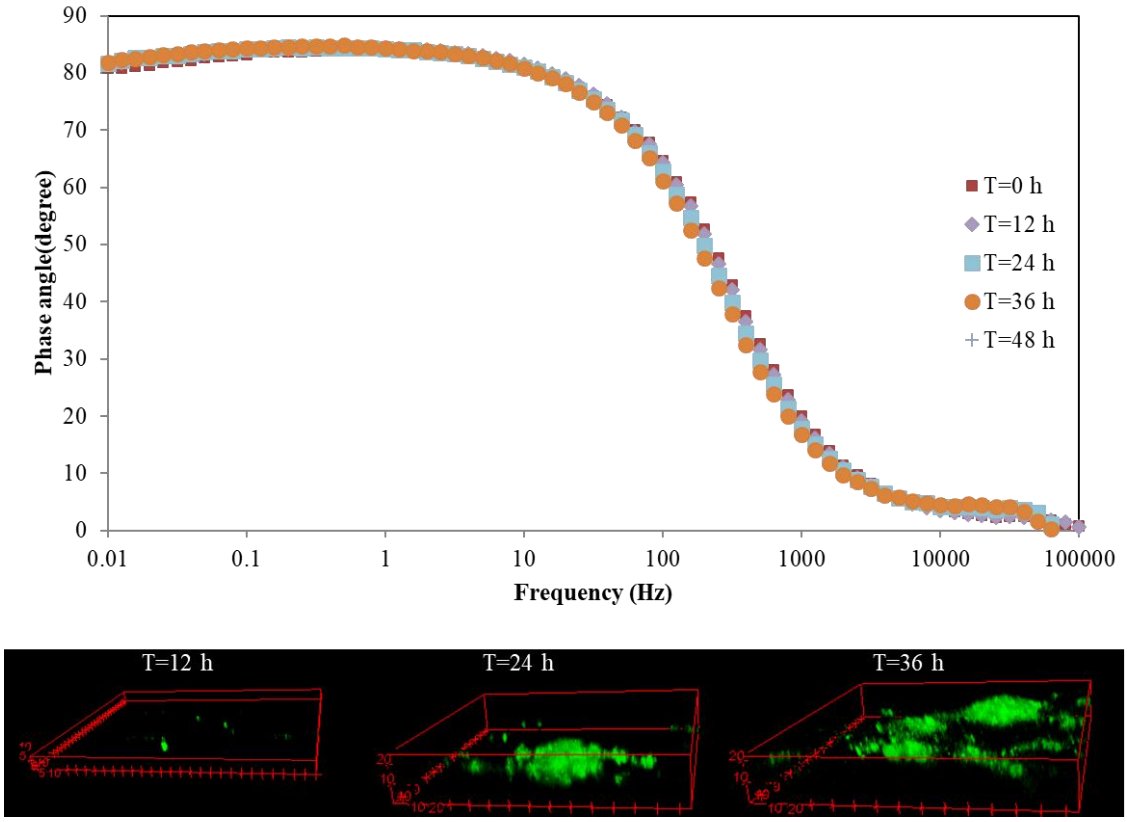

Figure 26: Bode plot of phase angle and frequency of *V. natriegens* biofilm (top). Representative 3 D biofilm images of *V. natriegens* (bottom).

Conversely, with single culture biofilms of *S. oneidensi*s expressing red fluorescent protein, a correlation was observed between the biofilm biomass and the mid-frequency region variations in Bode plot (**Figure 27, 28**). However, the time at which these changes in the biofilm biomass and EIS spectra was observed varied between the different experimental replicates (at 24 h for one replicate (**Figure 27**) and at 36 h for another replicate (**Figure 28**)).

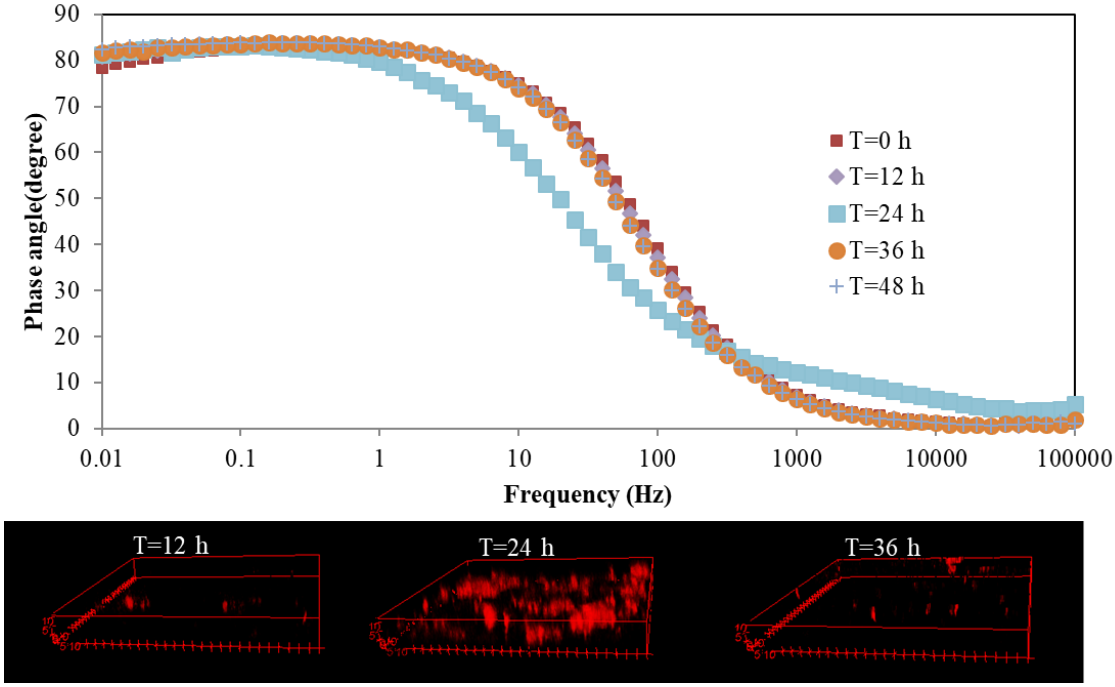

Figure 27: Bode plot of phase angle and frequency of a *S. oneidensis* biofilm experiment (top). Representative 3 D biofilm images of *S. oneidensis* (bottom).

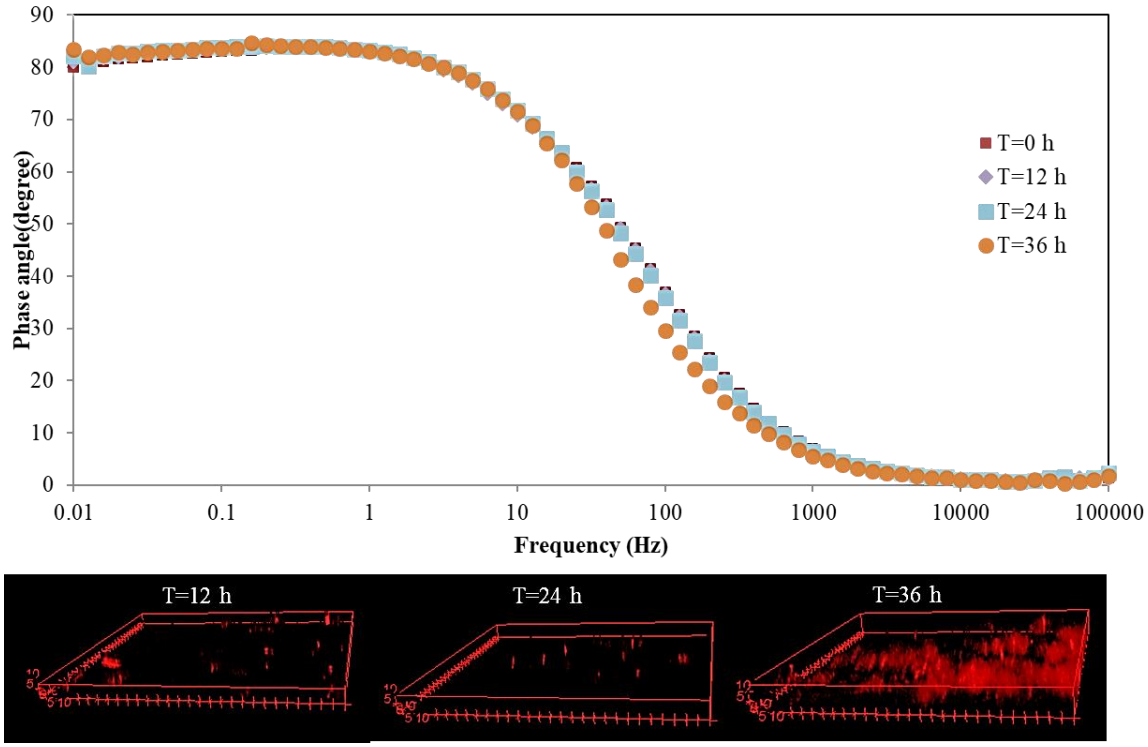

Figure 28: Bode plot of phase angle and frequency of another *S. oneidensis* biofilm experiment (top). Representative 3 D biofilm images of *S. oneidensis* (bottom).

The changes in EIS spectra with biofilm biomass as seen for *S. oneidensis* were not observed for co-culture biofilms of *V. natriegens* and *S. oneidensis*. The impedance spectra at all the time points for co-culture biofilms overlapped even though there were large differences in the biofilm biomass (**Figure 29**).

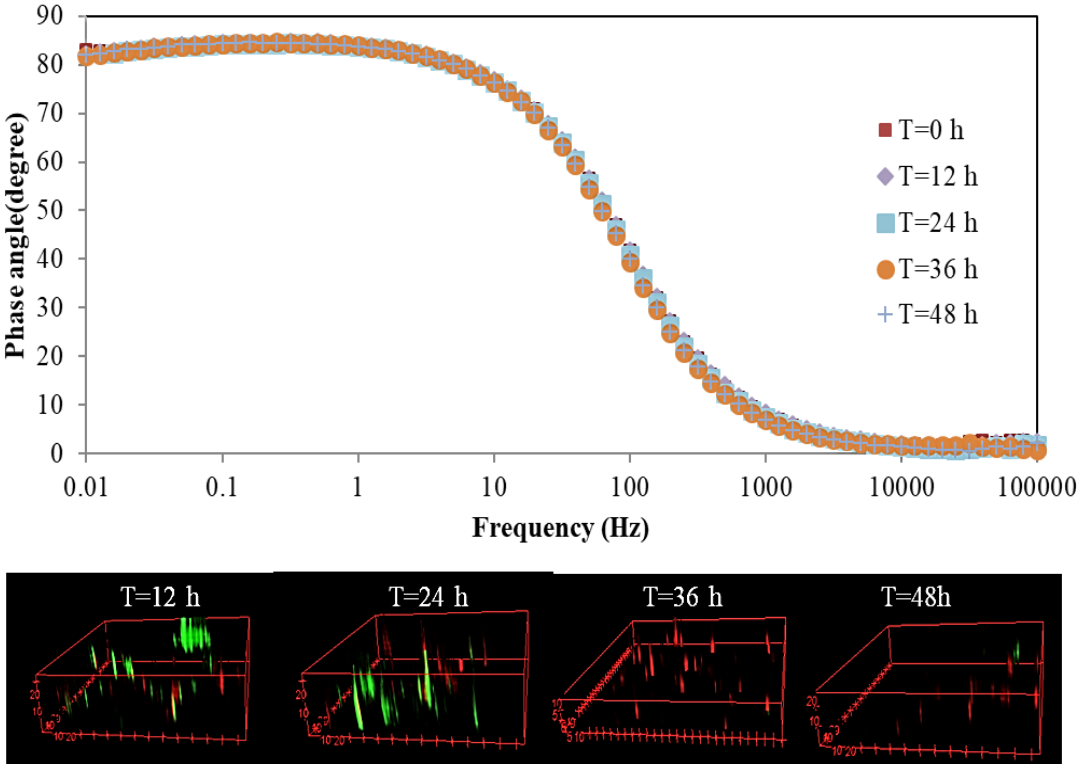

Figure 29: Bode plot of phase angle and frequency of co-culture biofilm of *V. natriegens* (expressing green fluorescent protein) and *S. oneidensis* (expressing red fluorescent protein) (top). Representative 3 D biofilm images of *V. natriegens* and *S. oneidensis* co-culture biofilms (bottom).

Static biofilm studies in M-MIC2

Because the experiments conducted under flow conditions did not reveal changes in EIS with time or exhibited inconsistent changes, we used a static (no-flow) model for correlating the electrochemical changes to biofilm formation. It is also possible that continuous flow in EIS systems results in fluctuations with the charge transfer resistance and the capacitive layers, which is absent in static systems and can lead to more easily

interpretable electrochemical changes. Therefore, static biofilm experiments were conducted with *S. oneidensis*, with sterile LB as the control. *S. oneidensis* was chosen as the biofilm forming strain as changes in impedance spectra were observed with it with higher biomass as compared to *V. natriegens* biofilms or *S. oneidensis* and *V. natriegens* co-culture biofilms.

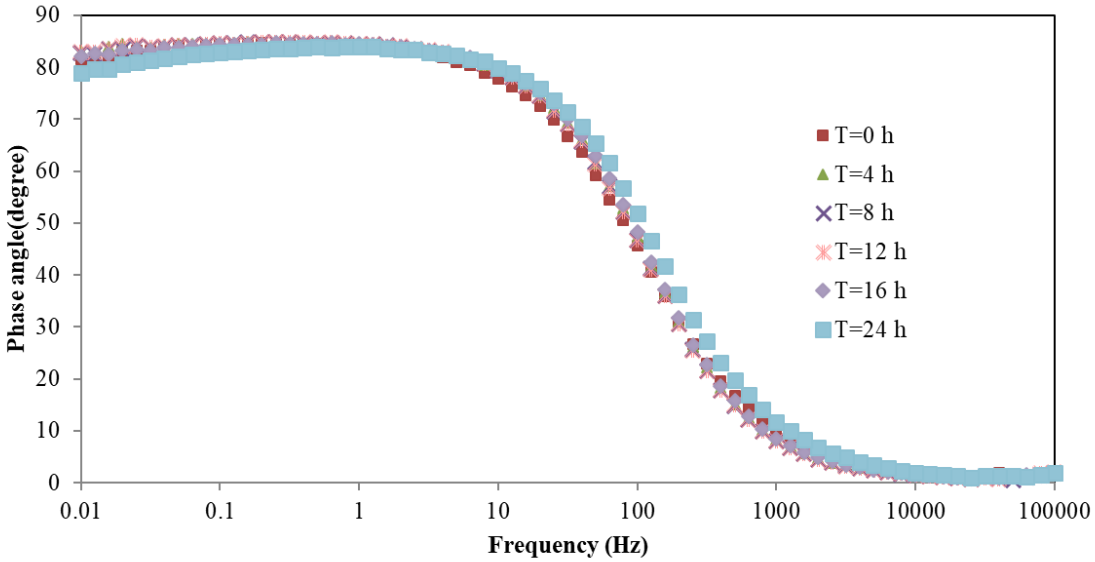

Figure 30: Bode plot of phase angle and frequency of sterile LB media under static conditions

Control experiments with LB media did not show significant variances in the impedance spectra even though minor differences were observed in the mid-frequency region of the Bode plot between 0 h and 24 h (**Figure 30**). When *S. oneidensis* biofilms were cultured under static conditions, significant changes were seen in the impedance

spectra at early time points (between 0 h and 4 h; **Figure 31**). However, the impedance spectra only showed minor changes from 8 h onward. Quantification of biofilm biomass and thickness revealed that the biomass values ranged 6-12 $\mu m^3/\mu m^2$ and the thickness values ranged between 35-50 µm between 4 h and 24 h.

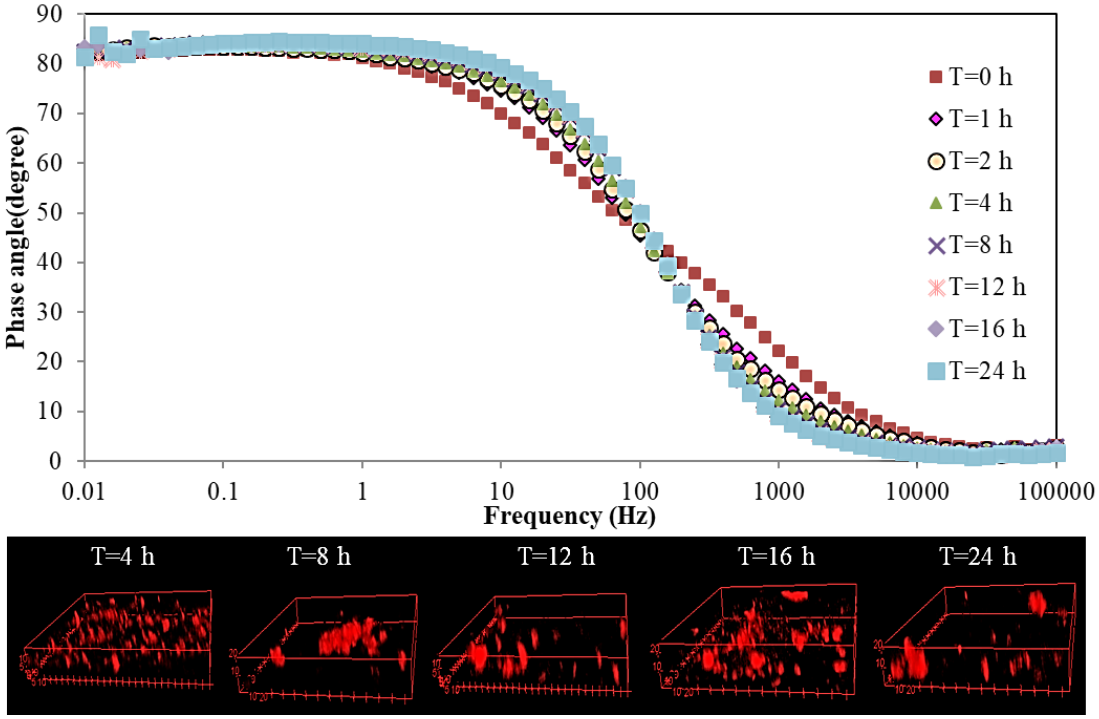

Figure 31: Bode plot of phase angle and frequency of *S. oneidensis* biofilm experiment under static conditions (top). Representative 3 D biofilm images of *S. oneidensis* (bottom).

While temporal correlations between biofilm biomass and thickness to the impedance spectra could be made with *S. oneidensis* biofilms, no changes in impedance

spectra were observed with the sterile LB control even under static conditions. The lack of detectable changes in the impedance spectra and temporal inconsistency can possibly be attributed to the differences in the metal surface roughness or variabilities in the thickness of the metal deposited.

4.4 Discussion

Biofilm growth and dynamics generally occurs in three stages: surface attachment of cells, formation of micro-colonies to form biofilm, and detachment of cells (Costerton et al., 1995). The first step occurs by reversible interactions of cells to the surface through pili or flagella or fimbria. The second step generally involves development of the extracellular polymeric matrix containing polysaccharides, proteins, nucleic acids, and lipids. This matrix has a wide range of functions from enhanced adhesion to the surface to protection of biofilm from harsh external environments. The final step is the biofilm dispersal process in which the detachment of the cells is seen. This detachment can be either active if the dispersal is initiated by the bacteria themselves or passive if external factors like flow and shear cause the detachment (Flemming and Wingender, 2010; Kaplan, 2010; Karatan and Watnick, 2009).

Both the bacteria picked for the investigation, *V. natriegens* and *S. oneidensis* were known for their biofilm forming abilities (Benbouzid-Rollet et al., 1991,; Thormann et al., 2004). This study showed that for single species biofilm formation with *V. natriegens* the optimal flowrate was 0.02 ml/h and for *S. oneidensis* it was 0.06 ml/h in a microfluidic flow channel. Further, both the single species biofilms were able to form mature biofilms

by 16 h. Active biofilm dispersal was seen by 24 h for both the strains when grown independently.

Since *V. natriegens* was reported to be a better biofilm forming strain, it was not surprising that it had higher biofilm biomass than *S. oneidensis* when initially seeded at equal volumetric ratios in co-culture biofilm studies. An initial seeding volume ratio of 2:1 of *S. oneidensis* to *V. natriegens* resulted in equal biofilm biomass for both the species. While monoculture biofilms detached within 24 h, co-culture biofilms did not detach significantly by 24 h, which indicates higher structural stability. From the changes in the impedance values of the co-culture biofilms, it can be concluded that the co-culture biofilm passivated the surface preventing corrosion. This result is also corroborated by the SEM images from 24 h and 48 h where metal surfaces with biofilms were similar to unexposed metal surfaces.

S. oneidensis has been shown to be protective against corrosion for various metals including an alloy of aluminum previously (Kus et al., 2006). *V. natriegens* corrodes metal surfaces when present as a monoculture (Cheng et al., 2009; Nivens et al., 1986; Yin et al., 2008a) or along with sulfate reducing bacteria (Benbouzid-Rollet et al., 1991). When both *S. oneidensis* and *V. natriegens* were present in the co-culture biofilm in a 2:1 (vol/vol) ratio, the role of *S. oneidensis* in protecting aluminum dominated over the corroding capabilities of *V. natriegens*. This study clearly illustrates the importance of investigating co-culture biofilms in evaluating their interaction with metal surfaces.

Experiments with M-MIC2 did not reveal any changes in the impedance spectra with sterile LB media or with *V. natriegens* until 48 h, although there was an increase in

the biofilm biomass. On the other hand, *S. oneidensis* biofilms showed correlation between impedance spectra and biofilm biomass. However, this variation in EIS observed was not temporally consistent across replicates. Co-culture biofilms of *V. natriegens* and *S. oneidensis* also did not indicate variations in impedance spectra although significant changes to biofilm biomass were observed.

Preliminary static control experiments with sterile LB media in M-MIC2 showed only minor variations with time in the impedance spectra. Bode plots of the *S. oneidensis* biofilms indicated a gradual change in the mid-frequency and high-frequency regions with increasing biofilm biomass and thickness in static system. However, to observe consistencies in impedance with continuous flow experiments in M-MIC2, increasing the metal deposition thickness is proposed in addition to performing surface characterization to measure the surface roughness and uniformity. Surface characterization of the metal surface (using techniques like optical profilometry, SEM, TEM) after metal deposition and patterning, before conducting experiments can aid in the investigation of electrochemical changes and associated corrosion and biofilm processes. In addition to these, the thickness of the biofilm is typically two orders of magnitude (~20-60 µm) higher than the metal layer thickness (200 nm) which could obstruct the detection of the subtle changes in the metal layer and may also lead to saturation of electrochemical signals. In the future, depositing metal layers at larger thickness (500 nm-50 µm) might provide better detection of electrochemical changes.

5. INVESTIGATING THE METABOLOMIC BASIS OF MIC

5.1 Introduction

Microbial communities can be characterized based on information obtained from different biological macromolecules such as DNA, RNA, proteins, and metabolites (Patti et al., 2012). Metagenomic strategies for analyzing the DNA extracted from microbial communities provide data on the information encoded in the community (*i.e.*, the genes that are present in the community and the potential biochemical reactions that can be carried out), whereas metabolomics strategies for analyzing the metabolites extracted from microbial communities provide information on the level of activity of the different biochemical reactions in the microbial community (*i.e.*, the products of biochemical reactions carried out) (Abram, 2015). Understanding the extent and scope of biochemical reactions is important for understanding the dynamics of different members of the community as well as for the interaction of the community with external substrates, such as the interaction of biofilms with metal surfaces in the case of MIC. Identifying the metabolome of microbial communities has facilitated the discovery of biomarkers for disease diagnostics (Mamas et al., 2011). In this Section, we explore the possibility of using metabolomics to identify biomarkers for detecting MIC in process systems.

In field MIC systems, several abiotic corrosive agents such as carbon dioxide, hydrogen sulfide, and oxygen usually co-exist with microorganisms, corroding metal, water, and electron acceptors/electron donors (Beech and Sunner, 2004; Li et al., 2013). Since interactions among metal, microorganisms, and these compounds defines MIC,

cataloguing these compounds and ascribing them to different sources is important to understand MIC mechanisms. Further, it is critical to examine the activity of microorganisms to specifically understand the contribution of MIC to the observed total corrosion.

Tools used for characterizing microbial communities in MIC have focused primarily on using DNA-based methods such as culturing, PCR/qPCR, 16S rRNA sequencing, and FISH (Muyzer and Marty, 2014). While these methods provide information on the microbial community composition and relative abundances of different microbes, they do not provide any information on the specific reactions occurring in the community. Furthermore, several studies that employed DNA-based methods indicated that the microbial communities associated with MIC vary in composition extensively (Vincke et al., 2001). These observations lead to the hypothesis that MIC is influenced by factors beyond the community composition. On the other hand, metabolomics-based approaches provide information on the end products of the reactions that have occurred in the community. However, information only on the metabolic reactions without the community composition is inadequate. As an alternative, utilizing metabolomics-based methods in combination with metagenomics-based approaches to establish underlying MIC mechanisms is proposed. Recently, some studies employed both metagenomics- and metabolomics-based approaches to identify the metabolome associated with microorganisms in pipelines transporting drinking water and produced water (Beale et al., 2013; Bonifay et al., 2017).

In this Section, we characterized the microbial community and metabolites present in produced water collected from West Texas pipeline systems. The microbial community and the metabolome were characterized using 16S rRNA sequencing and untargeted LC-MS/MS, respectively. The functional potential of microbial community was correlated to the putatively identified metabolites to establish the specific molecules that mediate MIC in this pipeline system.

5.2 Materials and methods

In vitro *MIC experiment*

Produced water (one gallon) collected from an oil well in the Permian basin of west Texas was obtained from Mr. Timothy Tidwell in Nalco Champion, an Ecolab company (Houston, TX). The container was transferred immediately upon delivery to an anaerobic chamber and maintained in a 90% nitrogen, 5% hydrogen, and 5% carbon dioxide environment. Eighty ml of produced or autoclaved produced water were collected in three 100 ml glass bottles (**Figure 32**). The autoclaved produced water (i.e., without any live microorganisms) was used as a control to account for abiotic corrosion. The produced and autoclaved produced water stocks were supplemented with 500 ppm sodium sulfate, 500 ppm sodium acetate, 200 ppm sodium propionate, and 10000 ppm vitamin supplement (ATCC MD-VS) to support microbial growth. To maintain anoxic conditions, 1 ppm of resazurin was added to all bottles.

Carbon steel 1018 grade rectangular coupons (Metal Company, Alabama) with dimensions of 3” length x 0.5” width x 0.0625” thickness were polished using 350 grit

sandpaper and cleaned by sequentially sonicating in acetone and methanol for 5 min prior to the experiment. These coupons were weighed to record their weight and then transferred to either produced water or autoclaved produced water bottles. All bottles were incubated at 37^{o}C in the anaerobic chamber for 7 weeks.

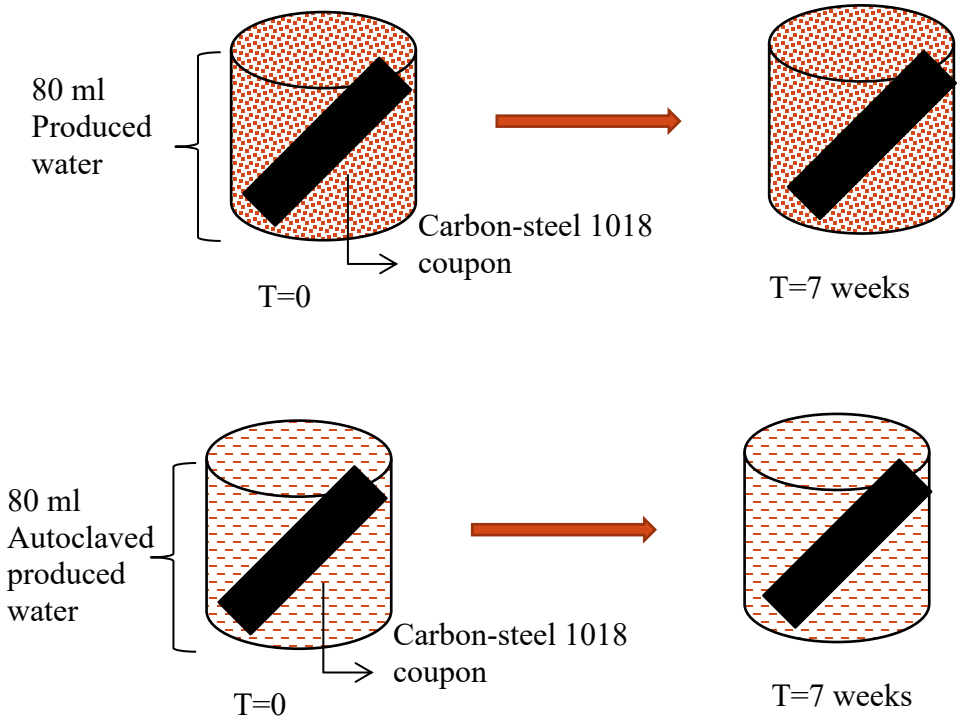

Figure 32: Schematic of the experiment setup

DNA extraction

DNA was extracted from produced water before and after exposure to carbon steel coupons using the DNeasy PowerSoil kit (Qiagen). Samples of 10 ml volume were

centrifuged at 3000 x *g* (4 ^{o}C), the pellet was resuspended in 1 ml of the supernatant, and DNA was extracted using the manufacturer recommended protocol. The DNA was eluted in 100 µl of elution buffer (10 mM Tris-Cl, pH 8.5). The extracted DNA was cleaned using the DNeasy PowerClean clean up kit (Qiagen) and resuspended in 30 µl of elution buffer. The concentration of DNA in the produced water samples before exposure to carbon steel coupons were 4.3 ng/µl, 4.1 ng/µl, and 4.5 ng/µl, while the concentrations after exposure to carbon steel coupons were 9.1 ng/µl, 4.3 ng/µl, and 7.5 ng/µl.

16S rRNA analysis

The V4 region of the 16SrRNA gene was sequenced on a 2x250 bp cycle using the MiSeq platform (Illumina) at Microbial Analysis, Resources, and Services, University of Connecticut. The reads were then processed by trimming, screening and alignment using mothur pipeline (Schloss et al., 2009). SILVA database v128 was used to align the reads and Greengenes database were used for taxonomical classification. Mothur outputs were then imported into MicrobiomeAnalyst (Dhariwal et al., 2017) for community profiling (using Chao's alpha diversity index and beta diversity analysis using principal coordinate analysis), clustering analysis (heat map and dendrogram analysis), and differential abundance analysis (DESeq2 method). PICRUSt was then used to predict the functional potential (gene abundance) using 16S rRNA gene sequences (Langille et al., 2013b). Fold-changes of genes belonging to pathways reported to be involved in MIC pathways (Nitrogen metabolism, methane metabolism, sulfur metabolism, propanoate metabolism, pyruvate metabolism, glycoxylate and dicarboxylate metabolism, butanoate metabolism, glycolysis degradation, toluene degradation, xylene degradation, benzoate degradation,

naphthalene degradation, styrene degradation, fatty acid biosynthesis, and biosynthesis of unsaturated fatty acids) were determined using the output from PICRUSt. The workflow used for data processing and analysis is shown in **Figure 33**.

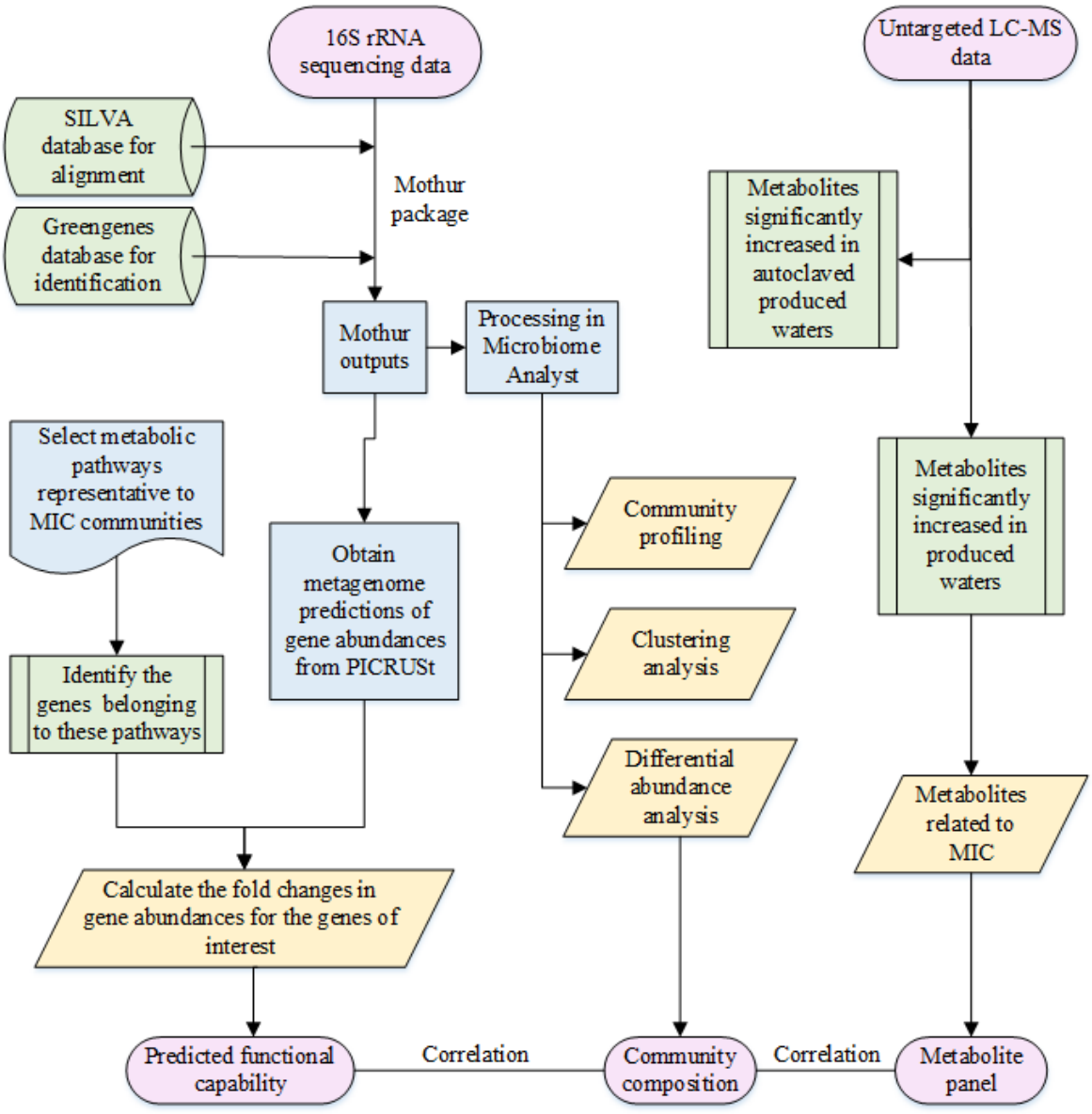

Figure 33: Workflow for analysis of metagenomic and metabolomic data from produced water cultures

Metabolite extraction

Metabolites were extracted from produced and autoclaved produced water before and after exposure to carbon steel coupons. In addition, metabolites were extracted from the surfaces of the coupons immersed in produced and autoclaved produced water at the end of the experiment. Metabolite extraction from produced water was carried out by solvent extraction (Sridharan et al., 2014). Briefly, 30 ml of methanol and 7.5 ml of chloroform was added to 15 ml of the cultures, vortexed briefly, incubated on ice for 5 minutes, followed by centrifugation at 4000 x *g* for 10 minutes. The upper phase (~ 48 ml) from each tube was collected and 1.5 ml of water was added. The contents were mixed vigorously and centrifuged again at 4000 x *g* for 5 minutes. The two phases were separately collected in fresh tubes and at stored at -80^{o}C until further processing. The upper phase (~48 ml) was freeze-dried (-120^{o}C and 0.01 mbar) using a lyophilizer (Labconco). The dried material was resuspended by sonication in 1 ml of 1:1 (vol/vol) methanol-water solution. The solution was then transferred to a spin column and centrifuged at 11000 x *g* (4^{o}C) for 1 minute and the supernatant stored at -80^{o}C.

Microbial communities and the metabolites on the coupon surfaces were collected by swabbing the coupons with a cotton swab and then homogenizing the swab in a bead beater with 300 µl lysis buffer (provided with DNeasy PowerSoil kit, Qiagen). The protocol described above for produced water was followed for metabolite extraction except that 600 µl of methanol and 150 µl of chloroform were initially added to the solution, and 600 µl of water was added to the upper phase collected from each tube. Lyophilized metabolites were resuspended in 200 µl of 1:1 (vol/vol) of methanol-water.

Metabolomic analysis

Untargeted LC-MS/MS metabolite analysis was carried on a Q-Exactive Plus Orbitrap (Thermo Scientific) coupled to a Dionex Ultimate 200 UHPLC at Integrated Metabolomics Analysis Core, Texas A&M University. Metabolite samples from produced water and coupon surfaces were diluted 5-fold and 2-fold respectively, prior to MS analysis. All samples were run on two different LC methods to maximize identification of metabolites. A hydrophilic interaction column (HILIC; SeQuant ZIC-pHILIC 5um polymeric, EMD Millipore) was used to detect polar metabolites and a reverse-phase column (Synergi 4um Fusion-RP 80A, Phenomenex) was used to separate a broad range of hydrophobic and polar metabolites. HILIC column was used with negative ion mode in MS and reverse-phase column as used with positive ion mode in MS. MS analysis was carried out at a resolution of 70,000 for MS1 and a resolution of 17,500 for MS2 analysis. Compound Discoverer 2.1 (ThermoFisher) was used to process the MS spectra and for metabolite identification using the mzCloud and ChemSpider databases.

The metabolomic data analysis workflow is shown in **Figure 33**. The metabolites identified from Compound Discoverer analysis were used to evaluate differentially abundant metabolites. The metabolites identified from produced water after exposure to carbon steel coupons were compared to that present in the produced water before exposure to the coupons. Similarly, supernatants from autoclaved produced water at after exposure to the coupons were compared to autoclaved produced water before exposure. Principal component analysis plots were generated using Compound Discoverer.

Corrosion rate measurements

Weight loss measurements were carried out after the coupons were swabbed for metabolite analysis. Carbon steel coupons were sequentially sonicated in DI water for 15 minutes, followed by sonication for 15 minutes in a solution of 2% antimony trioxide and 5% stannous chloride in hydrochloric acid according to ASTM standard G1-03 (Standard, 2017). The coupons were then mechanically brushed while immersed in this solution to remove any remaining corrosion products. All coupons were air dried with nitrogen gas and their weights were recorded. The difference in the weight loss of the coupons during the experiment was used to calculate the corrosion rate.

5.3 Results and discussion

Corrosion rate

The corrosion rate of the carbon steel coupons in produced water was nearly 5-fold higher compared to autoclaved controls (2.6 ± 0.6 mils per year for produced water compared to 0.5 ± 0.1 mils per year for autoclaved produced water; **Figure 34**). The higher rate of corrosion with produced water is likely due to the microbial metabolic activity in these samples which was absent in the autoclaved produced water controls. In addition, these observations also suggest that the rate of MIC was significantly higher than the abiotic corrosion rate under these experimental conditions.

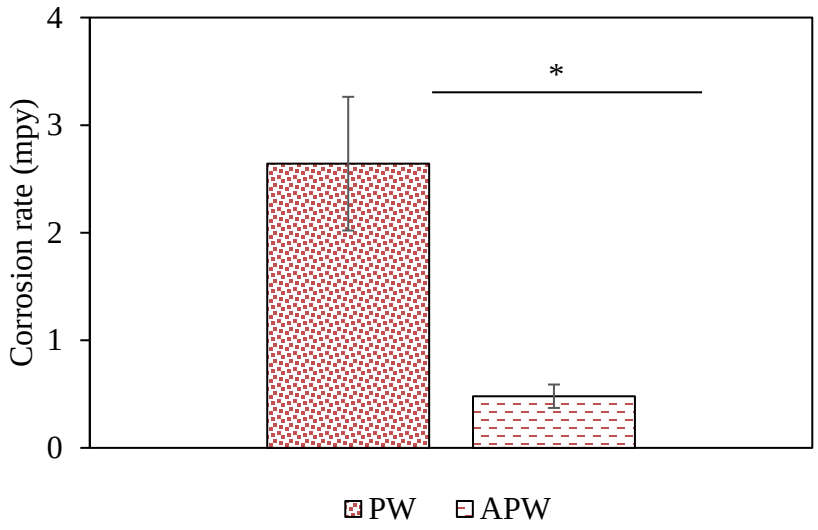

Figure 34: Corrosion rate of carbon steel coupons immersed in produced water and autoclaved produced water. * indicates statistical significance at a level of *p*-value < 0.05 using the Student t-test

Microbial community analysis

The OTUs (Operational taxonomic units) corresponding to the microbial communities were identified using Mothur (Schloss et al., 2009) and analyzed using MicrobiomeAnalyst (Dhariwal et al., 2017). Chao's alpha diversity index was computed for all samples to determine the diversity of the microbial community characterized by richness (number of distinct OTUs) and evenness (domination of some OTUs over the rest). **Figure 35** shows that no significant differences in the alpha diversity index were observed in the produced water before and after incubation with carbon steel coupon. Next, the differences of the microbial community in the produced water before and after

incubation with carbon steel coupon were determined using the principal coordinate analysis (PCoA) ordination method with weighted UniFrac distances. Significant compositional variation was observed in the microbial community of produced water during the 7-week experiment (**Figure 36**). The clear separation of the produced water before and after incubation strongly suggests a role for the incubation of the produced water with carbon steel for these changes. However, it is not possible to ascribe these changes exclusively to MIC as variations in the microbial community with time can also occur (e.g., due to microbial growth) even in the absence of carbon steel. Since the objective of our study was to investigate the role of the microbial community in MIC, our study design did not consider temporal changes in the composition of the microbial community in produced water.

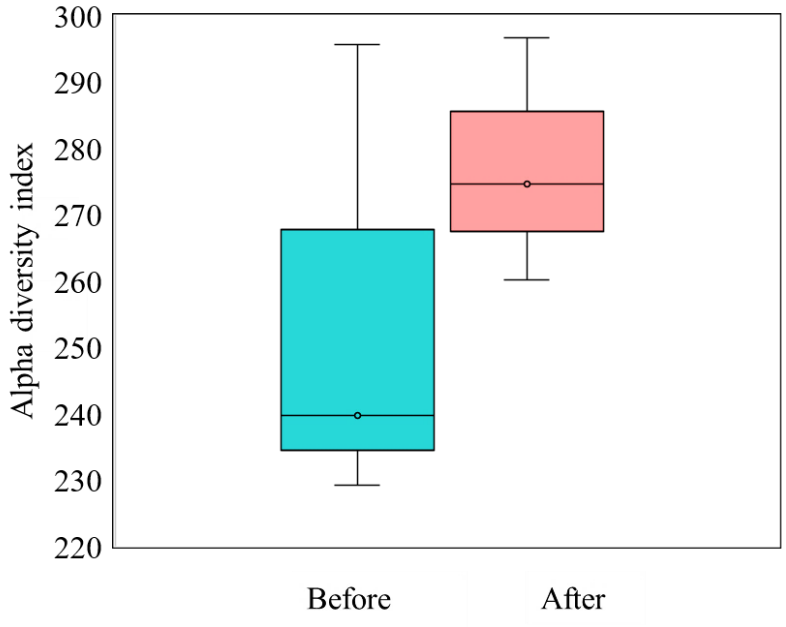

Figure 35: Chao's alpha diversity index of microbial communities in produced water before and after incubation with carbon steel coupons

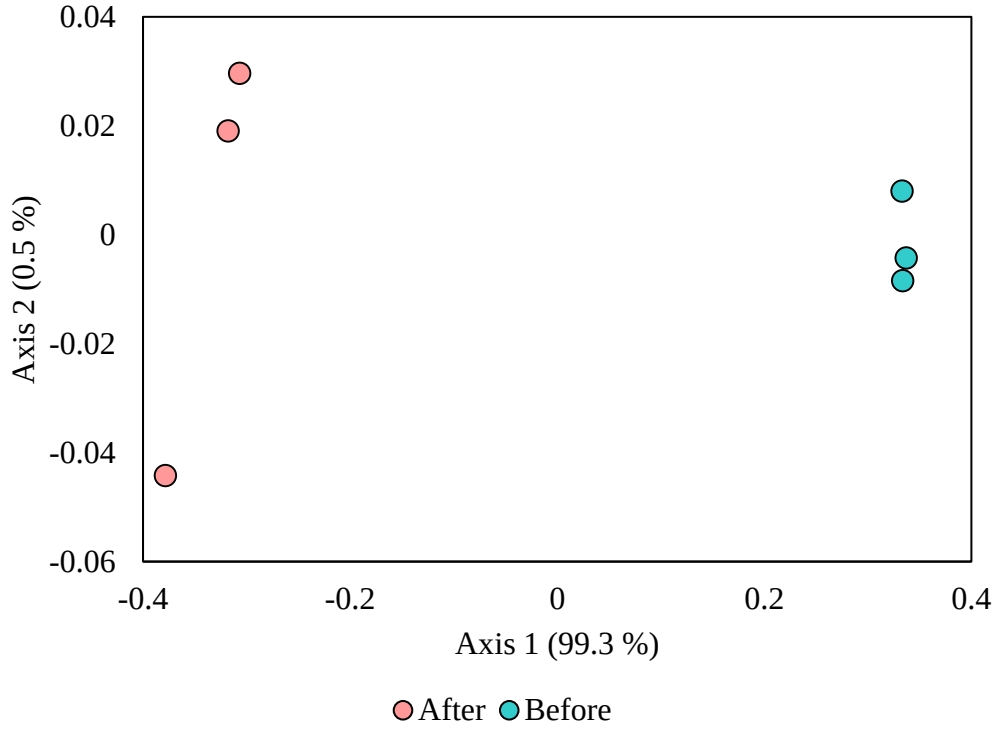

Figure 36: Principal coordinate analysis (PCoA) of microbial communities before and after incubation with steel coupons computed using the weighted UniFrac distance method

Hierarchical clustering of samples at the OTU-level showed that produced water before and after incubation with carbon steel clustered together with their respective groups **(Figure 37**). The OTU-level abundance was also visualized using heat maps **(Figure 38**) and shows that a majority of the OTU's decreased in abundance and only a few OTUs increased in abundance. Interestingly, some of the OTU's remained unchanged in abundance.

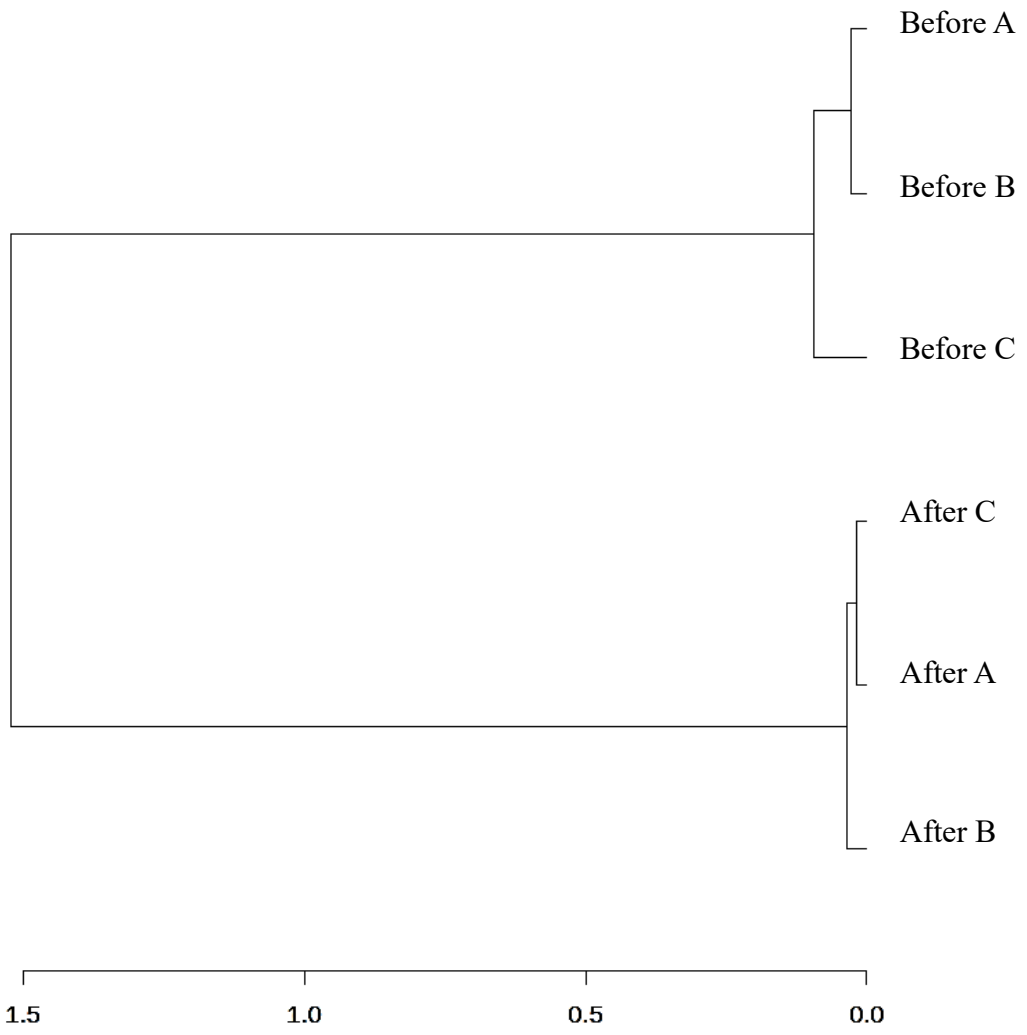

Figure 37: Hierarchial clustering of the microbial communities at OTU-level before and after incubation with carbon steel coupons using the weighted UniFrac distance method and Ward clustering algorithm

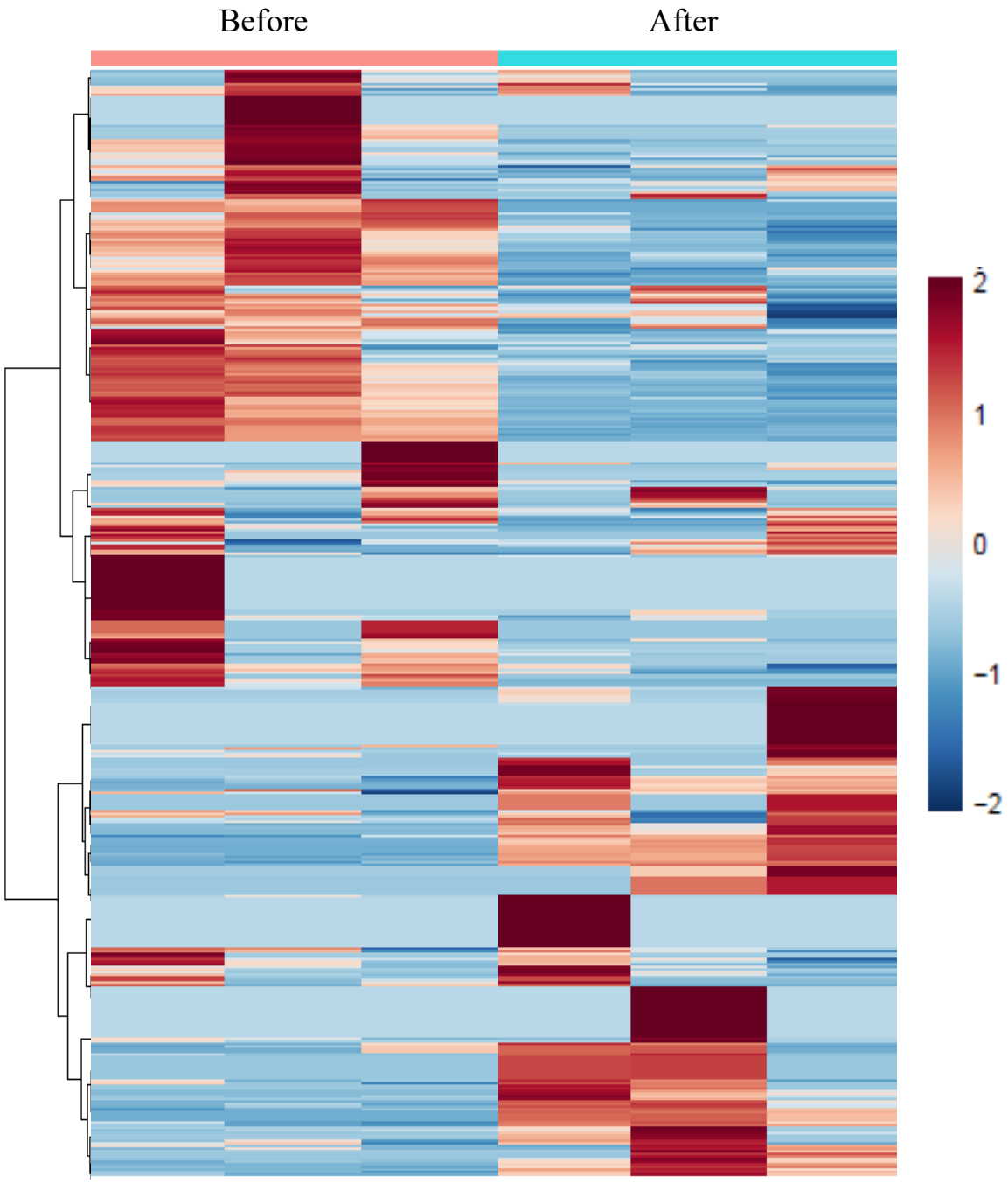

Figure 38: Heat map visualization of the microbial communities at OTU-level before and after incubation using the Euclidean distance method and Ward clustering algorithm

Taxonomic abundance in the produced water before and after incubation with carbon steel coupons was compared at the genus level. Using a statistical significance of *p*-value < 0.05 and a fold-change > 2.0 as the threshold, 14 genera showed a statistically significant increase in abundance after exposure to carbon steel coupons relative to abundance prior to exposure. The fold-changes of these genera are shown in **Table 6** and the comparison of the abundances of these genera before and after incubation is shown in **Figure 39**. Among these genera, HB2_32_21 and ecb11 have not been identified to be present in MIC communities. All the other genera, *Rhodobacteraceae_unclassified* (Elifantz et al., 2013), NP25 (Wuchter et al., 2013), *Deltaproteobacteria_unclassified* (Li et al., 2017), *Nitratireductor* (Liu et al., 2014), *Proteobacteria_unclassified* (Pournia et al., 2018), *Martelella* (Lin et al., 2013a), *Synergistales_unclassified* (Duncan et al., 2009), *Desulfobacteraceace_unclassified* (Almstrand et al., 2016), *Halomonas* (Okoro et al., 2016), *Rhizobiales_unclassified* (Huttunen-Saarivirta et al., 2017), *Thalassospira* (Dang and Lovell, 2016), *Desulfovibrio* (Ilhan-Sungur et al., 2007) have been previously reported to be identified in MIC impacted field locations. Among these, species belonging to *Rhodobacteraceae*, *Deltaproteobacteria*, *Nitratireductor*, *Desulfobacteraceace*, and *Desulfovibrio* are the most commonly associated microorganisms to MIC (Liu et al., 2014; Salerno et al., 2018; Suflita et al., 2012). The increase in the abundance of species belonging to these genera in the current study suggests an increase in MIC reactions and processes.

Table 6: Genera showing a statistically significant increase in abundance (*p*-value < 0.05 and fold-change > 2) after exposure to carbon steel relative to abundance prior to exposure

Genera	Fold-change in abundance after exposure to before exposure
Rhodobacteraceae_unclassified	514.06
NP25	15.25
Deltaproteobacteria_unclassified	10.35
Nitratireductor	9.07
Proteobacteria_unclassified	6.64
Martelella	6.62
HB2_32_21	6.08
ecb11	5.29
Synergistales_unclassified	4.18
Desulfobacteraceace_unclassified	3.96
Halomonas	2.53
Rhizobiales_unclassified	2.51
Thalassospira	2.05
Desulfovibrio	2.00

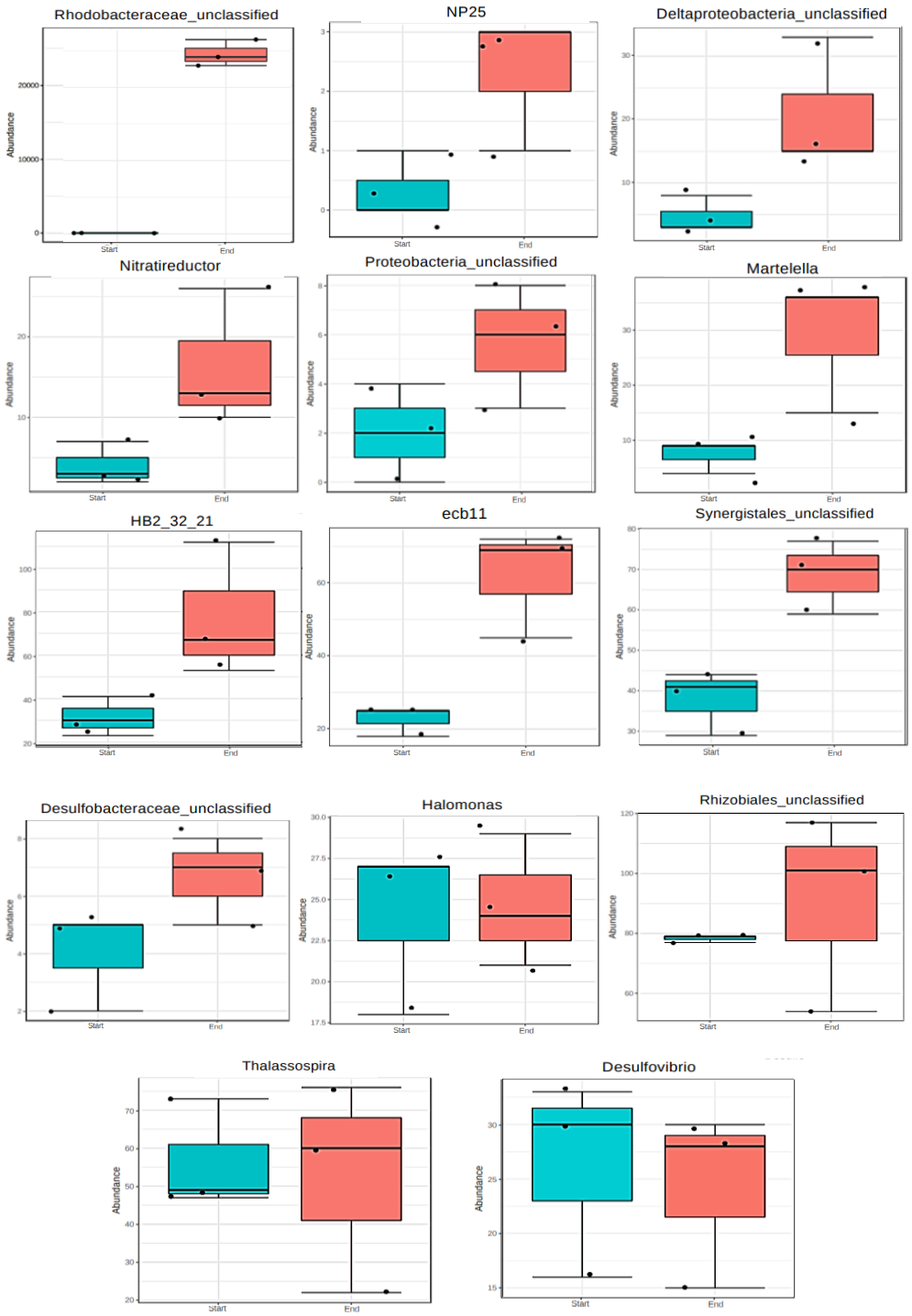

Figure 39: Genera showing statistically significant increase in abundance (*p*-value < 0.05 and fold-change > 2) after exposure to carbon steel relative to abundance prior to exposure

Using a statistical significance of *p*-value < 0.05 and a fold-change < 2.0 as the threshold, 11 genera showed a statistically significant decrease in abundance after exposure to carbon steel coupons relative to abundance prior to exposure. The fold-changes of these genera are shown in **Table 7**, and the abundances of these genera before and after incubation with carbon steel coupons are shown in **Figure 40**. Of these genera, SC103 and ZD0117 have not been identified in MIC communities. All the other genera, *Thiomicrospira* (Nemati et al., 2001), *Bacteroidetes_unclassidied* (Satoh et al., 2009b), *Idiomarina* (López et al., 2006), *Spirochaetes_unclassified* (Liu et al., 2017), *Chromatiales_unclassified* (Cayford et al., 2012), *Bacteroidales_unclassified* (Okoro et al., 2014), *Geotoga* (Usher et al., 2014), *Kosmotoga* (Lenhart et al., 2014), and *Lentisphaeria_unclassified* (Okoro et al., 2014) were identified previously in microbial communities associated with MIC. This observed decrease in abundance of species belonging to these genera need not relate to reduced involvement in MIC reactions and could also be due to temporal variations in the community. However, determining the temporal variations in the community in absence of carbon steel was beyond the scope of the study.

Table 7: Genera showing a statistically significant decrease in abundance (*p*-value<0.05 and fold-change<0.5) after exposure to carbon steel relative to abundance prior to exposure

Genera	**Fold-change in abundance after exposure to before exposure**
Thiomicrospira	0.48
Bacteroidetes_unclassified	0.37
Idiomarina	0.36
Spirochaetes_unclassified	0.33
Chromatiales_unclassified	0.32
Bacteroidales_unclassified	0.30
Geotoga	0.25
SC103	0.25
Kosmotoga	0.19
Lentisphaeria_unclassified	0.10
ZD0117	0.09

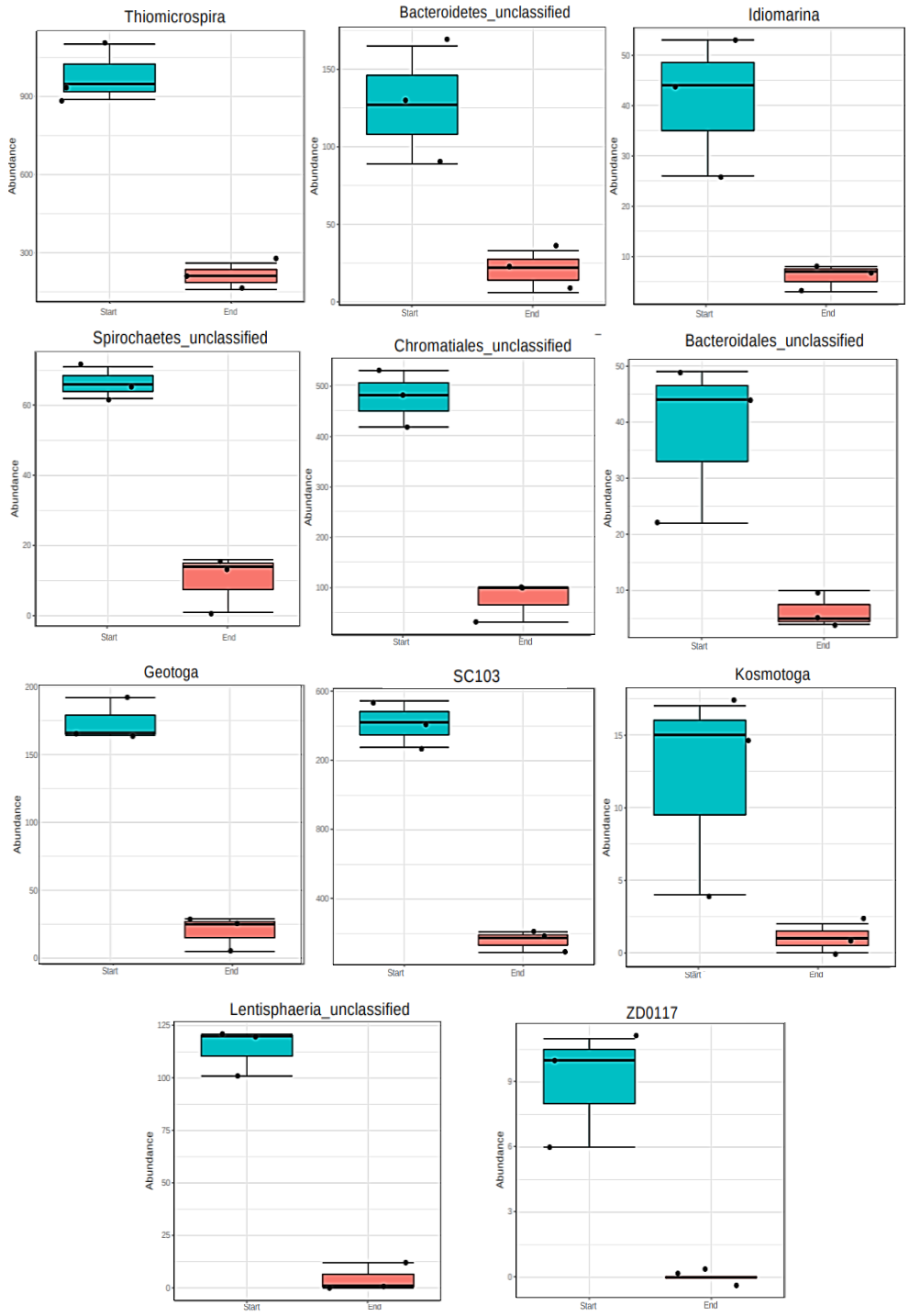

Figure 40: Genera showing statistically significant decrease in abundance (*p*-value<0.05 and fold-change<0.5) after exposure to carbon steel relative to abundance prior to exposure

Metagenome predictions of the microbial community was carried out using PICRUSt to infer alterations in the function of the microbial community upon exposure to carbon steel. Fold-changes in abundances of all genes in the community (~6900) after exposure to carbon steel coupons relative to their abundances prior to exposure were evaluated. Of these, 37% of genes increased in abundance (fold-change > 2.0) while 29% of genes decreased in abundance (fold-change < 0.5).

Specific MIC relevant metabolic pathways (**Tables 8 - 15**) were selected for analysis and fold-changes in the abundances of all genes belonging to these pathways alone were evaluated. Sixty nine genes belonging to the pathways of interest were identified with increased abundance (fold-change > 2.0) after incubation with carbon steel while 299 genes were identified with decreased abundance (fold-change < 0.5). Because a larger number of genes of interest had decreased abundance after exposure to carbon steel coupons, a fold-change threshold of 0.25 was chosen instead of 0.5. Importantly, all the genes with increased abundance (and their reactions) were different from the genes with decreased abundance.

Genes with increased abundance (fold-change > 2.0) after incubation with carbon steel and belonging to energy metabolism (**Table 8**), carbohydrate metabolism (**Table 9**), xenobiotic biodegradation and metabolism (**Table 10**), and lipid metabolism (**Table 11**) were investigated to obtain further information on the reactions they are involved in.

Table 8: PICRUSt predictions of genes and their reactions belonging to energy metabolism pathways with increased abundance (fold-change > 2.0) after incubation with carbon steel coupons compared to abundance before exposure

Pathway	Gene	Fold-change	Gene info	Reaction
Sulfur metabolism	K00380	6.90	Sulfite reductase (NADPH) flavoprotein alpha-component	hydrogen sulfide + 3 NADP+ + 3 H2O = sulfite + 3 NADPH + 3H
	K00956	4.93	Sulfate adenylyltransferase subunit 1	ATP + sulfate = diphosphate + adenylyl sulfate
	K12339	4.73	S-Sulfo-L-cysteine synthase (O-acetyl-L-serine-dependent)	O-acetyl-L-serine + thiosulfate = S-sulfo-L-cysteine + acetate
	K14155	3.60	Cystathione beta-lyase	L-cystathionine + H2O = L-homocysteine + pyruvate + NH3 (overall reaction)
	K00651	3.37	Homoserine O-succinyltransferase/ O-acetyltransferase	succinyl-CoA + L-homoserine = CoA + O-succinyl-L-homoserine
Methane metabolism	K08684	31.72	Methane monooxygenase (soluble); Methane hydroxylase	methane + NAD(P)H + H+ + O2 = methanol + NAD(P)+ + H2O
	K00436	24.48	NAD-reducing hydrogenase large subunit	H2 + NAD+ = H+ + NADH
	K13039	10.00	Sulfopyruvate decarboxylase subunit beta	3-sulfopyruvate = 2-sulfoacetaldehyde + CO2
	K13788	8.56	Phosphate acetyltransferase	acetyl-CoA + phosphate = CoA + acetyl phosphate

Table 8: Continued.

Pathway	Gene	Fold-change	Gene info	Reaction
Methane metabolism	K12234	8.55	Coenzyme F420-0:L-glutamate ligase / coenzyme F420-1:gamma-L-glutamate ligase	GTP + coenzyme F420-0 + L-glutamate = GDP + phosphate + coenzyme F420-1
	K06034	5.00	Sulfopyruvate decarboxylase subunit alpha	3-sulfopyruvate = 2-sulfoacetaldehyde + CO2
	K01595	3.26	Phosphoenol pyruvate carboxylase	phosphate + oxaloacetate = phosphoenolpyruvate + HCO3-
	K08264	2.50	Heterodisulfide reductase subunit D	CoB + CoM + methanophenazine = CoM-S-S-CoB + dihydromethano phenazine
	K01007	2.35	Pyruvate, water dikinase	ATP + pyruvate + H2O = AMP + phosphoenol pyruvate + phosphate
Nitrogen metabolism	K00370	15.95	Nitrate reductase/ nitriteoxidoreductase alpha subunit	nitrate + a quinol = nitrite + a quinone + H2O
	K00371	15.95	Nitrate reductase/ nitriteoxidoreductase beta subunit	nitrate + a quinol = nitrite + a quinone + H2O
	K01501	8.57	Nitrilase	a nitrile + 2 H2O = a carboxylate + NH3
	K07256	5.33	Taurine dehydrogenase large subunit	Taurine + H2O + 2 Ferricytochrome c <=> Sulfoacetaldehyde + Ammonia + 2 Ferrocytochrome c + 2 H+

Table 8: Continued.

Pathway	Gene	Fold-change	Gene info	Reaction
Nitrogen metabolism	K04747	4.27	Nitric oxide reductase NorF protein	2 Nitric oxide + 2 Ferrocytochrome c + 2 H+ <=> Nitrous oxide + 2 Ferricytochrome c + H2O
	K14155	3.60	Cystathione beta-lyase	L-cystathionine + H2O = L-homocysteine + pyruvate + NH3 (overall reaction)
	K04561	3.32	Nitric oxide reductase subunit B	nitrous oxide + 2 ferricytochrome c + H2O = 2 nitric oxide + 2 ferrocytochrome c + 2 H+
	K01424	2.34	L-Asparaginase	L-asparagine + H2O = L-aspartate + NH3
	K00459	2.27	Nitronate monooxygenase	ethylnitronate + O2 = acetaldehyde + nitrite + other products
	K01744	2.04	Aspartate ammonia-lyase	L-aspartate = fumarate + NH3

Table 9: PICRUSt metagenome predictions of genes and their reactions belonging to carbohydrate metabolism pathways (fold-change>2) with increased abundance after incubation with carbon steel coupons compared to abundance before exposure

Pathway	Gene	Fold-change	Gene info	Reaction
Propanoate metabolism	K01825	13.78	3-Hydroxyacyl-CoA dehydrogenase / enoyl-CoA hydratase / 3-Hydroxybutyryl-CoA epimerase / enoyl-CoA isomerase	(S)-3-hydroxyacyl-CoA + NAD+ = 3-oxoacyl-CoA + NADH + H+
	K01720	9.18	2-Methylcitrate dehydratase	(2S,3S)-2-hydroxybutane-1,2,3-tricarboxylate = (Z)-but-2-ene-1,2,3-tricarboxylate + H2O
	K13788	8.56	Phosphate acetyltransferase	acetyl-CoA + phosphate = CoA + acetyl phosphate
	K03417	8.00	Methylisocitrate lyase	(2S,3R)-3-hydroxybutane-1,2,3-tricarboxylate = succinate + pyruvate
	K00114	6.17	Alcohol dehydrogenase (cytochrome c)	a primary alcohol + 2 ferricytochrome c = an aldehyde + 2 ferrocytochrome c + 2 H+
Pyruvate metabolism	K03777	12.76	D-Lactate dehydrogenase (quinone)	(R)-lactate + a quinone = pyruvate + a quinol
	K13788	8.56	Phosphate acetyltransferase	acetyl-CoA + phosphate = CoA + acetyl phosphate
	K01571	3.65	Oxaloacetate decarboxylase, alpha subunit	oxaloacetate = pyruvate + CO2

Table 9: Continued.

Pathway	Gene	Fold-change	Gene info	Reaction
Pyruvate metabolism	K01595	3.26	Phosphoenolpyruvate carboxylase	phosphate + oxaloacetate = phosphoenolpyruvate + HCO3-
	K01007	2.35	Pyruvate, water dikinase	ATP + pyruvate + H2O = AMP + phosphoenolpyruvate + phosphate
Glycoxylate and dicarboxylate metabolism	K01458	116.94	N-Formylglutamate deformylase	N-formyl-L-glutamate + H2O = formate + L-glutamate
	K01433	6.30	Formyltetrahydrofolate deformylase	10-formyltetrahydrofolate + H2O = formate + tetrahydrofolate
	K03418	5.33	N,N-Dimethyl formamidase	N,N-dimethylformamide + H2O = dimethylamine + formate
	K01682	3.17	Aconitate hydratase 2 / 2-methylisocitrate dehydratase	citrate = isocitrate (overall reaction)
	K01569	2.61	Oxalate decarboxylase	oxalate + H+ = formate + CO2
	K00018	1.61	Glycerate dehydrogenase	D-glycerate + NAD+ = hydroxypyruvate + NADH + H+
Butanoate metabolism	K01825	13.78	3-Hydroxyacyl-CoA dehydrogenase / enoyl-CoA hydratase / 3-Hydroxybutyryl-CoA epimerase / enoyl-CoA isomerase	(S)-3-hydroxyacyl-CoA + NAD+ = 3-oxoacyl-CoA + NADH + H+

Table 9: Continued.

Pathway	Gene	Fold-change	Gene info	Reaction
Butanoate metabolism	K00248	5.37	Butyryl-CoA dehydrogenase	a short-chain acyl-CoA + electron-transfer flavoprotein = a short-chain trans-2,3-dehydroacyl-CoA + reduced electron-transfer flavoprotein
	K01640	4.79	Hydroxymethyl glutaryl-CoA lyase	(S)-3-hydroxy-3-methylglutaryl-CoA = acetyl-CoA + acetoacetate
	K00004	4.04	(R,R)-Butanediol dehydrogenase / meso-butanediol dehydrogenase / diacetyl reductase	(R,R)-butane-2,3-diol + NAD+ = (R)-acetoin + NADH + H+
Glycolysis Gluconeogenesis	K00114	6.17	Alcohol dehydrogenase (cytochrome c)	a primary alcohol + 2 ferricytochrome c = an aldehyde + 2 ferrocytochrome c + 2 H+
	K06859	2.40	Glucose-6-phosphate isomerase	D-glucose 6-phosphate = D-fructose 6-phosphate
	K03841	1.98	Fructose-1,6-bisphosphatase I	D-fructose 1,6-bisphosphate + H2O = D-fructose 6-phosphate + phosphate

Table 10: PICRUSt metagenome predictions of genes and their reactions belonging to xenobiotics biodegradation and metabolism pathways (fold-change>2) with increased abundance after incubation with carbon steel coupons compared to abundance before exposure

Pathway	Gene	Fold-change	Gene info	Reaction
Toluene degradation	K00217	3.36	Maleylacetate reductase	3-oxoadipate + NAD(P)+ = 2-maleylacetate + NAD(P)H + H+
	K07543	2.50	Benzylsuccinate CoA-transferase BbsE subunit	succinyl-CoA + (R)-2-benzylsuccinate = succinate + (R)-2-benzylsuccinyl-CoA
	K07544	2.50	Benzylsuccinate CoA-transferase BbsF subunit	succinyl-CoA + (R)-2-benzylsuccinate = succinate + (R)-2-benzylsuccinyl-CoA
	K01856	2.38	Muconate cycloisomerase	(+)-muconolactone = cis,cis-muconate
	K03381	2.28	Catechol 1,2-dioxygenase	catechol + O2 = cis,cis-muconate
Xylene degradation	K00446	4.00	Catechol 2,3-dioxygenase	Catechol + O2 = 2-hydroxymuconate-6-semialdehyde
Benzoate degradation	K01031	185.03	3-Oxoadipate CoA-transferase, alpha subunit	succinyl-CoA + 3-oxoadipate = succinate + 3-oxoadipyl-CoA
	K01032	185.03	3-Oxoadipate CoA-transferase, beta subunit	succinyl-CoA + 3-oxoadipate = succinate + 3-oxoadipyl-CoA
	K10218	50.00	4-/hydroxy-4-methyl-2-oxoglutarate aldolase	4-hydroxy-4-methyl-2-oxoglutarate = 2 pyruvate

Table 10: Continued.

Pathway	Gene	Fold-change	Gene info	Reaction
Benzoate degradation	K04098	4.27	Hydroxyquinol 1,2-dioxygenase	Hydroxyquinol + O2 = maleylacetate
	K00446	4.00	Catechol 2,3-dioxygenase	catechol + O2 = 2-hydroxymuconate-6-semialdehyde
	K04109	4.00	4-Hydroxybenzoyl-CoA reductase subunit beta	benzoyl-CoA + oxidized ferredoxin + H2O = 4-hydroxybenzoyl-CoA + reduced ferredoxin
	K00217	3.36	Maleylacetate reductase	3-oxoadipate + NAD(P)+ = 2-maleylacetate + NAD(P)H + H+
	K14333	2.80	2,3-Dihydroxybenzoate decarboxylase	2,3-dihydroxybenzoate = catechol + CO2
	K01856	2.38	Muconate cycloisomerase	(+)-muconolactone = cis,cis-muconate
	K03381	2.28	Catechol 1,2-dioxygenase	catechol + O2 = cis,cis-muconate

Table 11: PICRUSt metagenome predictions of genes and their reactions belonging to lipid metabolism pathways (fold-change>2) with increased abundance after incubation with carbon steel coupons compared to abundance before exposure

Pathway	Gene	Fold-change	Gene info	Reaction
Fatty acid biosynthesis	K11263	229.15	Acetyl-CoA/propionyl-CoA carboxylase, Biotin carboxylase, Biotin carboxyl carrier protein	ATP + acetyl-CoA + hydrogencarbonate = ADP + phosphate + malonyl-CoA
Biosynthesis of unsaturated fatty acids	K10804	3.32	Acyl-CoA thioesterase I	2-lysophosphatidylcholine + H2O = glycerophosphocholine + a carboxylate
	K00507	2.78	Stearoyl-CoA desaturase (Delta-9 desaturase)	stearoyl-CoA + 2 ferrocytochrome b5 + O2 + 2 H+ = oleoyl-CoA + 2 ferricytochrome b5 + 2 H2O

Similarly, genes with decreased abundance (fold-change < 0.25) after incubation to carbon steel coupons and belonging to energy metabolism (**Table 12**), carbohydrate metabolism (**Table 13**) xenobiotic biodegradation and metabolism (**Table 14**) ,and lipid metabolism (**Table 15**) were investigated to obtain further information on the reactions they are involved in.

Table 12: PICRUSt metagenome predictions of genes and their reactions belonging to energy metabolism pathways (fold-change<0.25) with decreased abundance after incubation with carbon steel coupons compared to abundance before exposure

Pathway	Gene	Fold-change	Gene info	Reaction
Methane metabolism	K08093	0.21	3-Hexulose-6-phosphate synthase	D-arabino-hex-3-ulose 6-phosphate = D-ribulose 5-phosphate + formaldehyde
	K00625	0.20	Phosphate acetyltransferase	acetyl-CoA + phosphate = CoA + acetyl phosphate
	K08097	0.13	Phosphosulfolactate synthase	(2R)-2-O-phospho-3-sulfolactate = phosphoenolpyruvate + sulfite
	K13831	0.12	3-Hexulose-6-phosphate synthase / 6-Phospho-3-hexuloisomerase	D-arabino-hex-3-ulose 6-phosphate = D-fructose 6-phosphate
	K00196	0.11	Anaerobic carbon-monoxide dehydrogenase iron sulfur subunit	CO + H2O + Oxidized ferredoxin <=> CO2 + Reduced ferredoxin
Nitrogen metabolism	K02594	0.16	Homocitrate synthase NifV	acetyl-CoA + H2O + 2-oxoglutarate = (2R)-2-hydroxybutane-1,2,4-tricarboxylate + CoA
	K01914	0.13	Aspartate--ammonia ligase	ATP + L-aspartate + NH3 = AMP + diphosphate + L-asparagine

Table 13: PICRUSt metagenome predictions of genes and their reactions belonging to carbohydrate metabolism pathways (fold-change<0.25) with decreased abundance after incubation with carbon steel coupons compared to abundance before exposure

Pathway	Gene	Fold-change	Gene info	Reaction
Propanoate metabolism	K00656	0.24	Formate C-acetyltransferase	acetyl-CoA + formate = CoA + pyruvate
	K00016	0.22	L-lactate dehydrogenase	S)-lactate + NAD+ = pyruvate + NADH + H+
	K00625	0.20	Phosphate acetyltransferase	acetyl-CoA + phosphate = CoA + acetyl phosphate
	K01034	0.16	Acetate CoA/acetoacetate CoA-transferase alpha subunit	acyl-CoA + acetate = a fatty acid anion + acetyl-CoA
Pyruvate metabolism	K00656	0.24	Formate C-acetyltransferase	acetyl-CoA + formate = CoA + pyruvate
	K00156	0.22	Pyruvate dehydrogenase (quinone)	pyruvate + ubiquinone + H2O = acetate + CO2 + ubiquinol
	K00016	0.22	L-Lactate dehydrogenase	(S)-lactate + NAD+ = pyruvate + NADH + H+
	K03778	0.20	D-Lactate dehydrogenase	(R)-lactate + NAD+ = pyruvate + NADH + H+

Table 13: Continued.

Pathway	Gene	Fold-change	Gene info	Reaction
Pyruvate metabolism	K00625	0.20	Phosphate acetyltransferase	acetyl-CoA + phosphate = CoA + acetyl phosphate
	K00132	0.16	Acetaldehyde Dehydrogenase (Acetylating)	acetaldehyde + CoA + NAD+ = acetyl-CoA + NADH + H+
	K04072	0.16	Acetaldehyde Dehydrogenase / Alcohol Dehydrogenase	acetaldehyde + CoA + NAD+ = acetyl-CoA + NADH + H+ / alcohol + NAD+ = aldehyde or ketone + NADH + H+
	K01596	0.15	Phosphoenolpyruvate Carboxykinase (Gtp)	GTP + oxaloacetate = GDP + phosphoenol pyruvate + CO2
Glycoxylate and dicarboxylate metabolism	K01602	0.24	Ribulose-Bisphosphate Carboxylase Small Chain	2 3-phospho-D-glycerate + 2 H+ = D-ribulose 1,5-bisphosphate + CO2 + H2O
	K00865	0.18	Glycerate 2-Kinase	ATP + D-glycerate = ADP + 2-phospho-D-glycerate

Table 13: Continued.

Pathway	Gene	Fold-change	Gene info	Reaction
Butanoate metabolism	K01641	0.25	Hydroxymethylglutaryl-Coa Synthase	acetyl-CoA + H2O + acetoacetyl- CoA = (S)-3-hydroxy-3-methylglutaryl-CoA + CoA
	K00244	0.24	Fumarate Reductase Flavoprotein Subunit	succinate + a quinone = fumarate + a quinol
	K00656	0.24	Formate C-Acetyltransferase	acetyl-CoA + formate = CoA + pyruvate
	K00634	0.19	Phosphate Butyryltransferase	butanoyl-CoA + phosphate = CoA + butanoyl phosphate
	K00929	0.18	Butyrate Kinase	ATP + butanoate = ADP +butanoyl phosphate
	K01034	0.16	Acetate Coa/Acetoacetate Coa-Transferase Alpha Subunit	acyl-CoA + acetate = a fatty acid anion + acetyl-CoA
	K00132	0.16	Acetaldehyde Dehydrogenase (Acetylating)	acetaldehyde + CoA + NAD+ = acetyl-CoA + NADH + H+
	K04072	0.16	Acetaldehyde Dehydrogenase / Alcohol Dehydrogenase	acetaldehyde + CoA + NAD+ = acetyl-CoA + NADH + H+

Table 13: Continued.

Pathway	Gene	Fold-change	Gene info	Reaction
Butanoate metabolism	K10783	0.12	Trans-2-Enoyl-Coa Reductase (Nad+)	acyl-CoA + NAD+ = transdidehydroacyl-CoA + NADH + H+
Glycolysis and Gluconeogenesis	K00844	0.25	Hexokinase	ATP + D-hexose = ADP + D-hexose 6-phosphate
	K00016	0.22	L-Lactate Dehydrogenase	(S)-lactate + NAD+ = pyruvate + NADH + H+
	K13954	0.20	Alcohol Dehydrogenase	(1) a primary alcohol + NAD+ = an aldehyde + NADH + H+
	K02779	0.18	Pts System, Glucose-Specific Iic Component	[protein]-Npi-phospho-L-histidine + D-glucose[side 1] = [protein]-L-histidine + D-glucose 6-phosphate[side 2]
	K04072	0.16	Acetaldehyde Dehydrogenase / Alcohol Dehydrogenase	acetaldehyde + CoA + NAD+ = acetyl-CoA + NADH + H+

Table 13: Continued.

Pathway	Gene	Fold-change	Gene info	Reaction
Glycolysis and Gluconeogenesis	K01596	0.15	Phosphoenolpyruvate Carboxykinase (Gtp)	GTP + oxaloacetate = GDP + phosphoenolpyruvate + CO2
	K00918	0.12	Adp-Dependent Phosphofructokinase/Glucokinase	ADP + D-fructose 6-phosphate = AMP + D-fructose 1,6-bisphosphate

Table 14: PICRUSt metagenome predictions of genes and their reactions belonging to xenobiotics biodegradation and metabolism pathways (fold-change<0.25) with decreased abundance after incubation with carbon steel coupons compared to abundance before exposure

Pathway	Gene	Fold-change	Gene info	Reaction
Toluene degradation	K00244	0.24	Fumarate Reductase Flavoprotein Subunit	succinate + a quinone = fumarate + a quinol
Xylene degradation	K00132	0.16	Acetaldehyde Dehydrogenase (Acetylating)	acetaldehyde + CoA + NAD+ = acetyl-CoA + NADH + H+
	K04072	0.16	Acetaldehyde Dehydrogenase / Alcohol Dehydrogenase	acetaldehyde + CoA + NAD+ = acetyl-CoA + NADH + H+
Benzoate degradation	K00132	0.16	Acetaldehyde Dehydrogenase (Acetylating)	acetaldehyde + CoA + NAD+ = acetyl-CoA + NADH + H+
	K04072	0.16	Acetaldehyde Dehydrogenase / Alcohol Dehydrogenase	acetaldehyde + CoA + NAD+ = acetyl-CoA + NADH + H+
	K01826	0.14	5-Carboxymethyl-2-Hydroxymuconate Isomerase	5-carboxymethyl-2-hydroxymuconate = (3E,5R)-5-carboxy-2-oxohept-3-enedioate

Table 15: PICRUSt metagenome predictions of genes and their reactions belonging to carbohydrate metabolism pathways (fold-change<0.25) with decreased abundance after incubation with carbon steel coupons compared to abundance before exposure

Pathway	Gene	Fold-change	Gene info	Reaction
Fatty acid biosynthesis	K03921	0.13	Acyl-[acyl-carrier-protein] desaturase	stearoyl-[acyl-carrier protein] + 2 reduced ferredoxin [iron-sulfur] cluster + O2 + 2 H+ = oleoyl-[acyl-carrier protein] + 2 oxidized ferredoxin [iron-sulfur] cluster + 2 H2O
Biosynthesis of unsaturated fatty acids	K03921	0.13	Acyl-[acyl-carrier-protein] desaturase	stearoyl-[acyl-carrier protein] + 2 reduced ferredoxin [iron-sulfur] cluster + O2 + 2 H+ = oleoyl-[acyl-carrier protein] + 2 oxidized ferredoxin [iron-sulfur] cluster + 2 H2O

Metabolomic analysis

Principal component analysis of the metabolites detected from HILIC negative-ion mode (**Figure 41**) and reverse-phase positive-ion mode analysis (**Figure 42**) were performed. The separation between metabolites obtained from produced water before and after incubation with carbon steel coupons was larger compared to that observed between autoclaved produced water before and after incubation in both modes of analyses. This indicates that more pronounced alterations in the abundance of metabolites were observed with produced water compared to autoclaved produced water. In addition, the metabolites extracted from the metal coupon surface were significantly different from the produced water, both without and with exposure to the metal coupon. This suggests that the biochemical reactions and the subsequent reaction products in the produced water (i.e., in the bulk or suspension phase) and on the coupon surface (i.e., biofilm) are different.

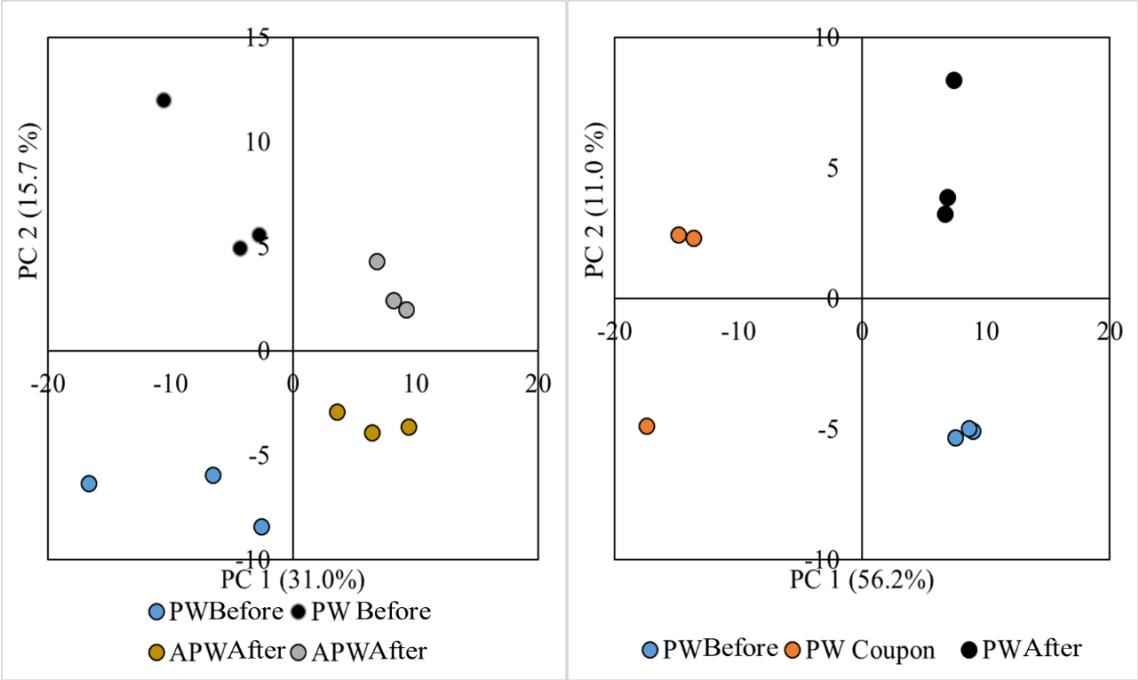

Figure 41: Principal component analysis of metabolites detected with HILIC negative-mode of analysis. PW – Produced water and APW – Autoclaved produced water. APW Before and PW Before represent metabolites extracted from produced water before incubation with carbon steel coupons. PW After and APW After represent metabolites extracted from produced water after incubation. PW Coupon represents the metabolites extracted from the metal coupons exposed to produced water.

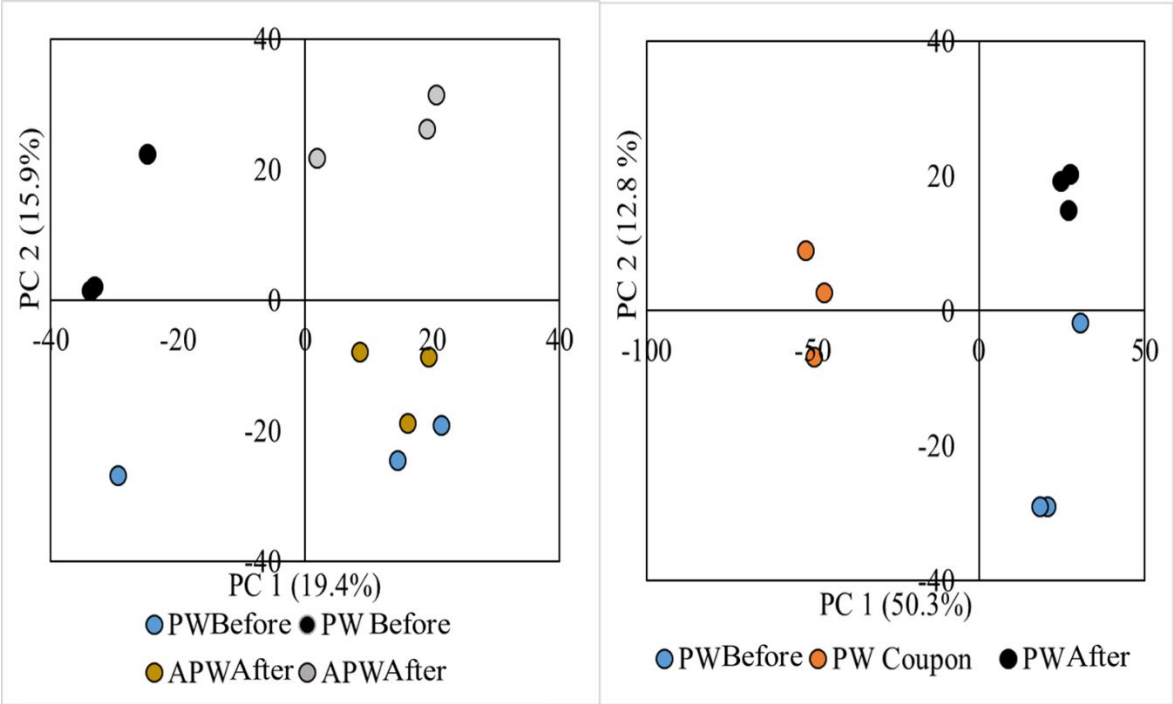

Figure 42: Principal component analysis of metabolites detected in reverse-phase positive mode of analysis. APW Before and PW Before represent metabolites extracted from produced water before incubation with carbon steel coupons. PW After and APW After represent metabolites extracted from produced water after incubation. PW Coupon represents the metabolites extracted from the metal coupons exposed to produced water.

Differential abundance analysis was used to identify metabolites that significantly contribute to MIC. Metabolites that were significantly altered in abundance in autoclaved produced water (i.e., those arising from abiotic corrosion reactions) were eliminated from the list of metabolites observed with produced water to generate a list of metabolites that could be ascribed to biochemical reactions **(Table 16)**. Several of these putatively identified metabolites such as carboxylic acids and derivatives (cinnamic acid and nicotinic acid), fatty acids and derivatives (octadecanoic acid), amino acids and derivatives (phenyl alanine, proline, phenyl alanine, and tryptamine) have been previously associated with MIC reactions (Beale et al., 2010; Beale et al., 2012b; Bonifay et al., 2017).

A larger number of metabolites (putatively identified as lauric acid, toluic acid, nonanoic acid, palmitoleic acid, decanoic acid, cinnamyl alcohol, and cinnamaldehyde) were significantly abundant on the carbon steel coupon surface compared to the bulk produced water after exposure to carbon steel coupons (**Table 17**). Among these, nonanoic acid and decanoic acid (Beale et al., 2013; Beale et al., 2012b) have been formerly identified to be associated with MIC. These metabolites potentially represent products from the reactions occurring specifically in biofilms on the metal surface as opposed to those taking place in the bulk phase.

Table 16: Metabolites significantly increased in abundance (*p*-value < 0.05 and fold-change > 2.0) in produced water after exposure to carbon steel coupons compared to abundance prior to exposure and contributing to MIC reactions

(15Z)-9,12,13-Trihydroxy-15-octadecenoic acid	Cinnamic acid
(1S,2R,5S)-2-Isopropyl-5-methylcyclohexyl 3-oxobutanoate	Deschloro-N-ethyl-ketamine
(3aR,5R,5aS,8aS,8bR)-2,2,5,7,7-Pentamethyltetrahydro-3aH-bis[1,3]dioxolo[4,5-b:4',5'-d]pyran	Dioxohongdenafil
2,4-Xylidine	Encainide
2,6-Dimethyl-γ-pyrone	Ethyl lactate
2-Amino-5-nitrobenzophenone	Fluroxene
2-C-methylerythritol 4-phosphate	Gabapentin
2'-Deoxyadenosine	Gamfexine
2-Hydroxyphenylalanine	Imagabalin
2-Methoxyestrone	Lignocaine
4-Acetyl-4-phenylpiperidine	L-Phenylalanine
4-Hydroxy-5-(phenyl)-valeric acid-O-sulphate	L-Proline
4'-Nitro-4-biphenylcarboxylic acid	L-Tryptophan
5,6,7-Trimethoxy-2H-chromen-2-one	N-Acetyl-L-phenylalanine
5-Methoxytryptophol	Oxadixyl
6-Hydroxynicotinic acid	Piracetam
6-Methylquinoline	Sinapyl alcohol
Aceclidine	Styrene
Acetophenone	Tetrafluorophosphonium
Amphetamine	Tryptamine

Table 17: Metabolites significantly increased in abundance (*p*-value<0.05 and fold-change>2) on carbon steel coupons immersed produced water compared to bulk produced water after incubation with coupons

(−)-trans-Methyl dihydrojasmonate	3a,6,6,9a-tetramethylperhydronaphtho[2,1-b]furan	Diatrizoic acid	N-formylkynurenine
(+)-Aspicilin	3-Allylcyclohexene	Dibenzoylmethane	Nonanoic acid
(+/-)-2 Hydroxy glutaric acid	3-Methylsalicylic acid	Dibutyl phenylphosphonate	Palmitoleic acid
(+/-)-Methoprene	4-Trimethylammonio-3-(undecanoyloxy) butanoate	Diethylcyclopropan-1,1-dicarboxylate	Panthenol
(2E)-4-Hydroxy-2-nonenal	4-Acetamido-2-amino-6-nitrotoluene	Diethylpyrocarbonate	PEG n5
(3beta,24xi)-Stigmastan-3-yl 4-O-beta-D-glucopyranosyl-beta-D-glucopyranoside	4'-Methoxy-3-morpholino-propiophenone	Dimethyl sebacate	PEG n6
(3E)-3-(Hydroxymethyl)-2-oxo-5-[(1S,8aS)-5,5,8a-trimethyl-2-methylenedecahydro-1-naphthalenyl]-3-pentenoic acid	4-Methoxy cinnamaldehyde	Dimetofrine	PEG n7
(3-Oxo-2-pentylcyclopentyl)acetic acid	4-Toluic acid	Dimorpholamine	Penicillin A
(3S)-3-{(Z)-[(3S)-3-{(Z)-[(3R)-3-Amino-1-hydroxy-4-methylpentylidene]amino}-1-hydroxybutylidene]amino}-5-methylhexanoic acid	5,5-Dimethyl-4-(3-oxobutyl)dihydro-2(3H)-furanone	DL-Tryptophan	Perfluoro-1-butanesulfonic acid (PFBS)

Table 17: Continued.

(3S,4R)-3-(1-hydroxyhexyl)-4-(hydroxymethyl)oxolan-2-one	5-Hydroxy-DL-tryptophan	Ethyl 2-amino-4-(2-furyl)-3-thiophenecarboxylate	Pivagabine
(3S,6S)-3-(4-Hydroxybenzyl)-6-(hydroxymethyl)-2,5-piperazinedione	5-Methoxy benzimidazole	Ethyl 2-oxocyclohexane carboxylate	Poly THF n5
(4-Amino-2,2,5,5-tetramethyl-2,5-dihydro-1H-imidazol-1-yl)oxidanyl	5-methyl benzimidazole	Fluoro[(1E)-1-hexen-1-yl]dimethylsilane	Psoralidin
(4S)-4-[(2E)-2-Octenoyloxy]-4-(trimethylammonio) butanoate	6(1H)-Purinone, 2,3-dihydro-3,7-dimethyl-1-(2-hydroxy-3-(4-(2-hydroxyethyl)piperazinyl)propyl)-	Fluoromethyl methyl disulfide	p-Xylene
(9aR,9bS)-9a-Hydroxy-6,9-dimethyl-3-methylene-3,3a,4,5,9a,9b-hexahydroazuleno[4,5-b]furan-2,7-dione	6,7,8-Triphenyl-2,3-dihydro[1,2,4]triazolo[4,3-b]pyridazin-3-one	g-Aminobutyryl-lysine	Roxane
(9E)-9-Octadecenedioic acid	6-[(1Z)-1-Propen-1-yl]-2,3,4,5-tetrahydropyridine	Guanadrel	Ruscopine
(E)-Dacarbazine	6-Ketoprostaglandin F1α	Hexose	Sebacic acid
(E)-Ferulic acid	9-(3-Methyl-5-pentyl-2-furyl)nonanoic acid	Hydrogen {6-[tris(2-aminoethyl)ammonio]hexyl}phosphonate	Sedanolide
1-(Phenylsulfonyl)-4-piperidinecarboxylic acid	9-Oxo-10(E),12(E)-octadecadienoic acid	Hydroxy amphetamine	Sulcatone
1,2-Cyclohexanediol	Actinonin	Hymecromone	trans,trans-2,4-Heptadienal

Table 17: Continued.

1-[(Cyclopentylmethyl)sulfonyl]-3-{[(2-phenylethyl)carbamoyl]amino}-2-propanyl dihydrogen phosphate	Alizapride	Inversine	Traumatic Acid
1-[1-(1-Benzothiophen-2-yl)ethyl]urea	Asarone	Kinoprene	Triethylene glycol monobutyl ether
10-HDA	Asparagine	Lauric acid	Trigonelline
10-Nitrolinoleate	Atagabalin	Lysylvaline	Trimethoprim
15-Acetyl deoxynivalenol	Azelaic acid	Methyl 2-octynoate	Trolox
16-Hydroxy hexadecanoic acid	Benzoic acid	Methyl 9-oxononanoate	Tryptoline
2-(2-Ethoxyethoxy) ethanol	Bis(2-methyl-2-propanyl) (4-acetamido-1,2-cyclohexanediyl)bis carbamate	Methylmalonic acid	Tyramine
2,6-di-tert-Butylphenol	Cafestol	Methyprylon	Valeric acid
2-Ethyl-2-phenylmalonamide	Calpeptin	Miglustat	Zileuton
2-Ethylhexanoic acid	Capuride	Myristic acid	Zonisamide
2-Methoxynaphthalene	Cinnamaldehyde	N(3)-(4-Methoxy fumaroyl)-2,3-di aminopropionic acid	Zopiclone
3-(1H-Indol-3-yl)-N-methylpropanamide	Cinnamyl alcohol	N~6~-Hydroxy-N~2~,N~2~,N~4~,N~4~-tetramethyl-1,3,5-triazine-2,4,6-triamine	α-Eleostearic acid
3-(4-Methoxy phenyl)-5-[(4-nitrophenoxy) methyl]-4,5-dihydroisoxazole	Decanoic acid	N1,N12-Diacetylspermine	

It was observed that very few metabolites significantly decreased in abundance in produced water after exposure to carbon steel relative to abundance before exposure (**Table 18**). In contrast, a large number of metabolites on the carbon steel coupons significantly decreased in abundance compared to their abundance in bulk produced water after incubation with coupons (**Table 19**).

Table 18: Metabolites significantly decreased in abundance (*p*-value<0.05 and fold-change<2) in produced water after exposure to carbon steel coupons compared to their abundance prior to exposure and contributing to MIC reactions

1-[1-(1-Benzothiophen-2-yl)ethyl]urea
2,7,8-Trioxa-1-phosphabicyclo[3.2.1]octane 1-sulfide
2-Amino-9,10-epoxy-8-oxodecanoic acid
2-sec-Butoxy-4-methyl-1,3,2-dioxaphospholane 2-sulfide
4-(Dimethylsulfonio)-2-hydroxybutanoate
Dinitrilodisilane
D-Pantothenic acid
Nitrobenzene

Table 19: Metabolites significantly decreased in abundance (*p*-value<0.05 and fold-change<2) on carbon steel coupons immersed produced water compared to bulk produced water after incubation with coupons

(−)-(alpha)-Kainic Acid	Alprenolol	g-Butyrobetaine	n-Hexanamide
(-)-Lupinine	Altretamine	Glycine anhydride	Nicotinamide
(-)-Nupharamine	Aminolevulinic acid	Guaiazulene	Nicotinic acid
(+/-)-Camphoric acid	Amphetamine	Guvacine	Nipecotic acid
(+/-)-Metanephrine	Anhydroecgonine methyl ester	Heptaminol	Nisoxetine
(2,7-Dimethyloctahydro-1H-cyclopenta[c]pyridin-4-yl)methanol	Anisindione	Hexobarbital	N-lauroylglycine
(2E)-4-Hydroxy-2-nonenal	Anthranilic acid	Histamine	N-Methyl anthranilamide
(2R)-2-Piperazine carboxylic acid	a-Pyrrolidino hexanophenone	Hydroquinone	N-Methyl hexanamide
(8E)-11,13-Dihydroxy-4-methyl-4,5,6,7-tetrahydro-2H-3-benzoxacyclododecine-2,10(1H)-dione	Arecoline	Isoxaben	N-Methyl pyrrolidone
(Hydroxyethyl)methacrylate	Atagabalin	Jasmonic acid	Norfenefrine
(S)-2-Hydroxypropyl phosphonic acid	Benzoic acid	Ketoprofen	Norlidocaine
1,2-Dichloropropane	Benzyl formate	L-(+)-Leucine	Oxepanone

Table 19: Continued.

1,5-Dihydro-1-pyrenol	beta-D-Ethyl glucuronide	L-dihydroanticapsin	Oxprenolol
10-Nitrolinoleate	Bethanidine	Levonorgestrel	Oxymatrine
15-Acetyldeoxy nivalenol	Biotin	Levulinic acid	Oxy phencyclimine
1-Methyl-2,3,4,9-tetrahydro-1H-beta-carboline-3-carboxylic acid	Butenylcarnitine	L-Proline	P,P-Bis(1-aziridinyl)-N-methyl-N-phenyl phosphinic amide
1-Methyl nicotinamide	Cannabinol	L-Pyroglutamic acid	Paracetamol
2-(Diethylamino) ethanol	Caprolactam	Lycocernuine	Phenacetin
2,2-Dichloro-1,1-ethanediol	Caproylglycine	MDMA	Phenyl ethanolamine
2,2'-Iminodipropan-1-ol	Capryloylglycine	Mebicar	Phenyliso cyanate
2-Amino-4-{6-[(3-methyl-2-buten-1-yl)amino]-3H-purin-3-yl}butanoic acid	carbocromen	Melagatran	Piracetam
2-Aminonicotinic acid	Ciclopirox	Melamine	Pivagabine
2-Ethyl-2-oxazoline	Cyclo(leucylprolyl)	Meperidine	Pregabalin
2-Hexenoylcarnitine	Cycloheximide	Metalaxyl	Pseudo pelletierine
2-Methoxy-5-methylaniline	Debrisoquine	Methcathinone	Pyridoxal

Table 19: Continued.

2-n-Butyl-4-ethyl-5-methyloxazole	Dichloromethane	Methyprylon	Pyridoxamine
3-(2,6-Dioxocyclohexyl) propanenitrile	Dicloralurea	Metirosine	Pyridoxine
3,5-di-tert-Butyl-4-hydroxy benzaldehyde	Didemethyl isoproturon	Metoprolol	Resorufin
3,8-Dimethyl-7-decen-1-yl dihydrogen phosphate	Diethanolamine	Mexiletine	Sedamine
3-Hydroxynonanoic acid	Dihydrothymine	N-(1-Allylcyclohexyl)-N-phenethylamine	Stachydrine
3-Hydroxysebacic acid	DL-Carnitine	N-2-Oxotetrahydro-3-furanylhexanamide	Sunepitron
3-Methoxy-4-(3-methyl-2-buten-1-yl)-5-[(E)-2-phenylvinyl] phenol	DL-Lysine	N-(4-Acetylphenyl)methanesulfonamide	Tebutam
4-[(4-Bromobenzyl)oxy]-3,5-diiodobenzoic acid	DL-Stachydrine	N-(tert-Butoxycarbonyl)-L-leucine	Tetramethyl urea
4-Methoxyaniline	Ecgonine	N,N'-Didecyl-P-phenylphosphonothioic diamide	Tramadol
4-Morpholinylacetic acid	Ecgonine methyl ester	N,N-Diisopropyl ethylamine(DIPEA)	Tranexamic acid

Table 19: Continued.

4-Oxo-4-[(3-oxo-2-decanyl)amino] butanoic acid	Ethephon	N-[(S)-(+)-1-Ethoxycarbonyl-3-phenylpropyl]-L-alanine	trans-3-Hydroxy cotinine
4-Phenylbutyric acid	Ethyl [(methylsulfonyl)oxy] acetate	N'1,N'3-Bis[(2,2-dimethylpropanoyl) oxy]-5-methyl benzene-1,3-di carboximidamide	Triethanol amine
5,6-Dihydrophenanthridin-6-one	Ethyl acetate	N-Acetyldopamine	Trihomo methionine
5-Indolol	Ethyl N-[(2-isopropyl-5-methylcyclohexyl) carbonyl]glycinate	N-Acetyl-L-leucine	Triisopropanolamine cyclic borate
5-Methoxy tryptophol	Exalamide	N-Acetylvaline	Tris(bromomethyl)phosphine oxide
6-Diazonio[1,2,4] triazolo[1,5-a]pyrimidin-7-olate	Favan-3-ol	Neostigmine	Tropinone
6-hydroxypseudo oxynicotine	Gabapentin	N-Heptanoylhomo serine lactone	Valyl-4-hydroxyproline
7,14,16-Trihydroxy-3-methyl-3,4,5,6,7,8,9,10,11,12-decahydro-1H-2-benzoxacyclotetradecin-1-one	Gaboxadol	N-Hexahydro[1,3]thiazolo[3,4-a]pyridin-3-ylidene-1,3-benzodioxol-5-amine	Venlafaxine N-Oxide
Afegostat	Vigabatrin		

Correlation between metagenomic and metabolomic data

The genes and reactions with increased fold-change identified from PICRUSt analysis **(Table 8- 11**) and the putatively identified metabolites with increased fold-change (**Table 16 & Table 17**) were compared to determine the extent of overlap. These comparison data show that several putatively identified metabolites like methyl disulfide and dibenzoylmethane (energy metabolism pathways), ethyl lactate and panthenol (carbohydrate metabolism pathways), benzoic acid, toluic acid, and cinnamic acid (xenobiotic metabolism and degradation pathways), and fatty acid derivatives decanoic acid, nonanoic acid, and lauric acid (lipid metabolism pathways) were also predicted by the PICRUSt analysis. This independent validation suggests that these metabolites may be key participants in MIC reactions and could potentially be markers for MIC detection if identified in multiple studies.

5.4 Summary

The goals of this study were to identify plausible "metabolite markers" characteristic to MIC and correlate the functional capability of the microbial community to the observed markers of corrosion. Carbon steel coupons exposed to produced water from west Texas oil field showed a 5-fold higher corrosion rate with MIC compared to that observed with abiotic corrosion. Metagenomic analysis of the produced water before and after incubation with carbon steel coupons showed clear temporal separation. Differential analysis revealed that 14 genera significantly increased in abundance over two-fold while

11 genera significantly decreased in abundance during exposure with carbon steel coupons. Most of these genera were reported to be associated with MIC in prior studies. Metagenome predictions of the community indicated the increased abundance of genes involved with energy metabolism, carbohydrate metabolism, xenobiotic metabolism and degradation and lipid metabolism pathways.

Principal component analysis (PCA) of the metabolites before and after incubation with carbon steel coupons revealed larger separation between metabolites associated with MIC compared with abiotic corrosion compounds. PCA also showed that the metabolites in the bulk produced water differed from the metabolites on the metal coupon suggesting that different reactions were occurring on the metal surface and the bulk phase. Several of the significantly abundant metabolites that were putatively identified as carboxylic acids and derivatives (cinnamic acid, toluic acid, and nicotinic acid), fatty acids and derivatives (lauric acid, octadecanoic acid, and nonanoic acid), amino acids and derivatives (phenyl alanine, proline, and tryptamine) were previously associated with MIC. Comparison of the metagenome functional predictions to metabolite profiles identified common metabolites belonging to energy metabolism, carbohydrate metabolism pathways, xenobiotic metabolism and degradation, and lipid metabolism pathways, and suggest the significance of these metabolites in MIC.

6. CONCLUSIONS AND FUTURE DIRECTIONS

6.1 Conclusions

A novel microfluidic flow model, M-MIC1, was developed for investigating biocide efficacy against co-culture biofilms causing MIC. This model was tested using two common biocides (glutaraldehyde and THPS) against mono-culture and co-culture biofilms (*V. natriegens* and *S. oneidensis*) grown for short and long periods of time (12 h and 36 h). Single-species biofilms and co-culture biofilms grown for 36 h exhibited significantly higher resistance to both glutaraldehyde and THPS than biofilms grown for 12 h even though the biofilm thickness remained the same. Single species biofilms of *S. oneidensis* and co-culture biofilms were significantly more resistant to biocide treatment (both glutaraldehyde and THPS) than single-species biofilms of *V. natriegens* grown for 12 h and 36 h. THPS was significantly more effective in reducing biofilm viability than glutaraldehyde for *V. natriegens* and co-culture biofilms grown for 12 h and co-culture biofilms grown for 36 h. Our results show that the M-MIC 1 model can be adapted to investigate MIC using inoculum from MIC impacted field location in addition to using model organisms.

A second microfluidic-flow model, M-MIC2, was developed for MIC studies by integrating biofilm imaging and impedance spectroscopy measurements. The preliminary prototype of the system was fabricated using aluminum and investigated with co-culture biofilms of *V. natriegens* and *S. oneidensis*. Due to passivation of the system with aluminum oxides and electrical shorting between the electrodes, a second prototype was

developed with titanium as the counter electrode and carbon steel as the working electrode. This system was characterized by performing studies with sterile LB media, single-species biofilms, and co-culture biofilms. No significant changes in EIS spectra were observed with sterile LB media, *V. natriegens* biofilms and co-culture biofilms even when considerable changes to biofilm biomass were detected. *S. oneidensis* biofilms indicated a correlation between changes in the EIS spectra in the mid-frequency region (1-100 Hz) to increased biofilm biomass. However, the time at which this was observed varied between different experimental runs and is likely due to inconsistencies in the roughness and uniformity of the deposited metal. Preliminary static experiments with sterile LB media showed only minor variations with time in the EIS spectra. Static studies with *S. oneidensis* biofilms indicated a gradual change in the mid-frequency and high-frequency regions of Bode plot with increasing biofilm biomass and thickness. This suggests that M-MIC2 can be used to simultaneously monitor biofilm growth dynamics and impedance changes and subsequently develop correlations between them.

To characterize the changes in the microbial community composition and metabolites produced in MIC, we exposed carbon steel coupons to produced water from Texas oilfield. Higher corrosion rates in the produced water system compared to abiotic corrosion rates suggests the manifestation of MIC. 16S rRNA sequencing showed increases in the abundance of specific genera (*Rhodobacteraceae, Deltaproteobacteria*, *Nitratireductor, Desulfobacteraceace,* and *Desulfovibrio*) and PICRUSt functional prediction suggested an increase in the abundance of certain genes in energy metabolism, carbohydrate metabolism pathways, xenobiotic metabolism and degradation, and lipid

metabolism pathways. Untargeted metabolomic profiling showed an increase in the abundance of carboxylic acids, fatty acids and derivatives, and amino acids and derivatives, relative to abiotic controls. Good consistency was observed between the functional predictions and metabolite measurements, which suggests that these molecules may be playing a significant role in MIC.

6.2 Future directions

Developing new microfluidic device prototypes for MIC studies

The current M-MIC1 model comprises of a single flow channel in which biocide efficacy can be evaluated by monitoring biofilms on carbon steel. The M-MIC2 device comprises of a single flow channel with two metal electrodes coated on the glass slide that is bonded to the flow channel and facilitates an integrated measurement of biofilm physiology and electrochemical impedance. While both these models are useful for MIC studies, there are several ways these microfluidic flow models can be further improved. Some of these possibilities are discussed below.

a) High-throughput microfluidic flow model to compare biocide efficacies

M-MIC1 can be modified in to a high-throughput flow model to enable comparison of biocide efficacies. **Figure 43** depicts the PDMS layer of the microfluidic channel with a single cell inlet splitting into three microchambers for biofilm establishment and growth. This model can be used for comparing three different biocides that can be introduced

through three separate inlets. While **Figure 43** shows three parallel chambers, ~ 10 parallel microchambers can be realistically fabricated so that multiple biocides can be compared. The glass slide can be coated with carbon steel such that the microchambers overlay with coated carbon steel. This flow model enables comparison of efficacies of different biocides on microbial control required for MIC mitigation.

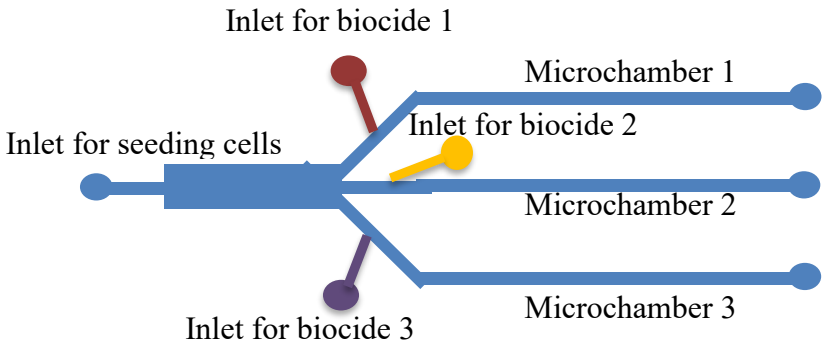

Figure 43: Schematic top-view of a high-throughput microfluidic flow model to compare biocide efficacies

b) Microfluidic flow models for investigating the susceptibility of different materials to MIC

The M-MIC1 and M-MIC2 devices can also be modified by replacing carbon steel with other metals or alloys like iron, copper, stainless steel, and other grades of carbon steel. These flow models can be used to compare the susceptibility of various materials to MIC initiating from field waters as well as laboratory grown biofilms. These studies can

be performed to establish microbial attachment, biofilm growth dynamics, electrochemical behavior, and material degradation for various materials. Such studies can be performed in the design stages of equipment in process systems to determine the best material for construction.

c) Combinatorial microfluidic flow model for determining biocide dosage

One major improvement of the M-MIC1 model could be to increase the throughput for determining the minimal inhibitory concentration of a biocide at different concentrations or combinations of biocides against specific laboratory grown co-culture biofilms. Previous work from our laboratory (Kim et al., 2012) described the development of a microfluidic biofilm model for high-throughput studies. This device can be modified with carbon steel (or any other metal of interest) deposition onto the glass slide so that corrosion of carbon steel can be investigated along with biofilm formation. The device developed by Kim et al has three layers, namely the glass slide, bottom PDMS layer comprising eight microchambers and top PDMS layer containing microvalves for controlling flow. Both the top and bottom PDMS layers have diffusive mixers that can be used for generating concentration gradients of soluble mediators. The bottom layer can be used for generating concentration gradients of the biocide and to flow microbial growth media through the microchambers while the top layer can be used to seed cells into the microchambers. This device can facilitate investigation of appropriate biocide dosages on the biofilms developed in the microchambers, as well as for mitigating carbon steel corrosion under the conditions tested. Furthermore, this high-throughput flow model can

be used to test the concentration-dependent interactions between biocide active ingredients and biocide enhancers, as well as the compatibility between biocides and other chemicals (such as corrosion inhibitors and paraffin removers) used in microbial mitigation.

d) Modifying M-MIC2 to obtain consistent and stable impedance measurements

The M-MIC2 device was fabricated by depositing a ~200 nm layer of carbon steel and titanium on the glass surface. Increasing the metal layer deposition thickness can avoiding the concerns with inconsistencies in the variations of EIS spectra and minor changes in EIS spectra that cannot be correlated to biofilm biomass and thickness. Different metal thickness ranges 500 nm-50 μm can be tested to determine the optimal thickness at which these issues are addressed. The increased metal thickness can be achieved by performing longer time electron beam evaporation and sputtering for titanium and carbon steel respectively.

e) Modifying M-MIC2 to develop a three-electrode system

The M-MIC2 device uses a two-electrode system comprising the working electrode, carbon steel and counter and pseudo-reference electrode, titanium. This two-electrode system measures both voltage and current across the working and counter electrodes. However, the counter electrode's potential can drift with time based on the current. Although this system has high resistance and the use of microelectrodes minimizes the changes in the counter electrode's potential, the counter electrode cannot always be reliably used to measure potential difference (Bard et al., 1980). A proposed alternative is

to use a three-electrode system that measures voltage across working and reference electrodes and current across working and counter electrodes. Thus, the M-MIC2 can be improved by incorporating a third reference electrode into the system. A schematic of the suggested design of the three-electrode microfluidic flow model is depicted in **Figure 44**. Shinwari et al. describes several ways reference microelectrodes can be fabricated or printed (Shinwari et al., 2010). Due to the simplicity associated with its assembly and ease of use, silver/silver-chloride reference microelectrode can be used for this system. Dong et al. describes the screen printing of silver/silver-chloride paste on polyester substrates as a simple and inexpensive method for fabricating silver/silver-chloride reference microelectrodes (Dong et al., 2007). This screen-printing method can be extended for fabricating the reference microelectrode on glass as part of M-MIC2 assembly.

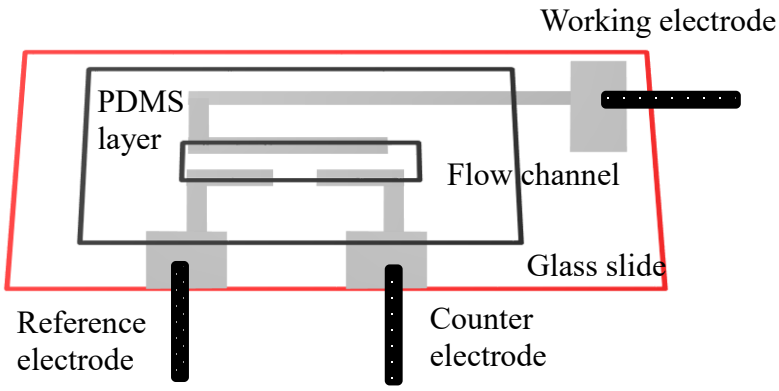

Figure 44: Schematic of the three-electrode M-MIC flow model

Multi-variate association analysis between microbial metabolites and environmental conditions

Our work (**Chapter 5**) demonstrates the potential for integrating metagenomic and metabolomic for laboratory MIC studies. While this analysis was carried out for produced water from one location (West Texas oil fields), similar analysis can be performed for samples collected from various MIC impacted field locations. The identified metabolites and strains from the different locations can be compared, along with metadata such as the geographical location, operating conditions, fluids composition, and other important factors to enable better understanding of underlying MIC phenomena. A multivariate statistical framework such as MaAsLin (multivariate association with linear models; (Morgan et al., 2012) can be used to find associations between the microbial community abundance, metabolites, and the environmental conditions.

REFERENCES

31205(NACE), 2006. Selection, Evaluation and Application of Biocides in the Oil and Gas Industry. National Association of Corrosion Engineers International, Houston, Texas.

Abram, F., 2015. Systems-based approaches to unravel multi-species microbial community functioning. Computational and structural biotechnology journal 13, 24-32.

Adam, B., Baillie, G.S., Douglas, L.J., 2002. Mixed species biofilms of Candida albicans and Staphylococcus epidermidis. Journal of medical microbiology 51, 344-349.

Adams, D.L., 2010. Microbiologically influenced corrosion of electrical-submersible-pumping-system components associated with acid-producing bacteria and sulfate-reducing bacteria: case histories, SPE Latin American and Caribbean Petroleum Engineering Conference. Society of Petroleum Engineers, Lima, Peru.

Alabbas, F.M., 2017. MIC case histories in oil, gas, and associated operations, In: Skovhus, T.L., Enning, D., Lee, J.S. (Eds.), Microbiologically Influenced Corrosion in the Upstream Oil and Gas Industry. CRC Press.

Alexander, M., 1965. Most-probable-number method for microbial populations. Methods of Soil Analysis. Part 2. Chemical and Microbiological Properties, 1467-1472.

Allen, J., Davey, H.M., Broadhurst, D., Heald, J.K., Rowland, J.J., Oliver, S.G., Kell, D.B., 2003. High-throughput classification of yeast mutants for functional genomics using metabolic footprinting. Nature Biotechnology 21.

Almstrand, R., Pinto, A.J., Figueroa, L.A., Sharp, J.O., 2016. Draft genome sequence of a novel Desulfobacteraceae member from a sulfate-reducing bioreactor metagenome. Genome announcements 4, e01540-01515.

Amann, R., Fuchs, B.M., 2008. Single-cell identification in microbial communities by improved fluorescence in situ hybridization techniques. Nature Reviews Microbiology 6, 339.

Amann, R.I., Ludwig, W., Schleifer, K.H., 1995. Phylogenetic identification and in situ detection of individual microbial cells without cultivation. Microbiological Reviews 59, 143-169.

Antony, P., Chongdar, S., Kumar, P., Raman, R., 2007. Corrosion of 2205 duplex stainless steel in chloride medium containing sulfate-reducing bacteria. Electrochimica Acta 52, 3985-3994.

Arps, P.J., Earthman, J.C., Xu, L.-c., Syrett, B.C., Green, R., Wood, T., Mansfeld, F.B., 2003. Field evaluation of corrosion control using regenerative biofilms (CCURB), CORROSION 2003. NACE International.

Aßhauer, K.P., Wemheuer, B., Daniel, R., Meinicke, P., 2015. Tax4Fun: predicting functional profiles from metagenomic 16S rRNA data. Bioinformatics 31, 2882-2884.

Aziz, F.A., Suzuki, K., Ohtaki, A., Sagegami, K., Hirai, H., Seno, J., Mizuno, N., Inuzuka, Y., Saito, Y., Tashiro, Y., 2015. Interspecies interactions are an integral determinant of microbial community dynamics. Frontiers in Microbiology 6, 1148.

Baker, G.C., Smith, J.J., Cowan, D.A., 2003. Review and re-analysis of domain-specific 16S primers. J Microbiol Methods 55, 541-555.

Ballantyne, B., Jordan, S.L., 2004. Biocides. Pesticide Toxicology and International Regulation 1, 365.

Bard, A.J., Faulkner, L.R., Leddy, J., Zoski, C.G., 1980. Electrochemical methods: fundamentals and applications. wiley New York.

Beale, D.J., Barratt, R., Marlow, D.R., Dunn, M.S., Palombo, E.A., Morrison, P.D., Key, C., 2013. Application of metabolomics to understanding biofilms in water distribution systems: a pilot study. Biofouling 29, 283-294.

Beale, D.J., Dunn, M., Marney, D., Marlow, D., 2012a. Metabolomic footprinting and MIC within water supply networks. Corrosion and Materials 37, 69-77.

Beale, D.J., Dunn, M.S., Marney, D., 2010. Application of GC–MS metabolic profiling to ‘blue-green water’ from microbial influenced corrosion in copper pipes. Corrosion Science 52, 3140-3145.

Beale, D.J., Dunn, M.S., Morrison, P.D., Porter, N.A., Marlow, D.R., 2012b. Characterisation of bulk water samples from copper pipes undergoing microbially influenced corrosion by diagnostic metabolomic profiling. Corrosion Science 55, 272-279.

Beale, D.J., Morrison, P.D., Key, C., Palombo, E.A., 2014. Metabolic profiling of biofilm bacteria known to cause microbial influenced corrosion. Water Science and Technology 69, 1-8.

Becker, S., Kortz, L., Helmschrodt, C., Thiery, J., Ceglarek, U., 2012. LC–MS-based metabolomics in the clinical laboratory. Journal of Chromatography B 883, 68-75.

Beech, I.B., Sunner, J., 2004. Biocorrosion: towards understanding interactions between biofilms and metals. Curr Opin Biotechnol 15, 181-186.

Beech, I.B., Sunner, J., 2007. Sulphate-reducing bacteria and their role in corrosion of ferrous materials. Sulphate-Reducing Bacteria–Environmental and Engineered Systems.

Benbouzid-Rollet, N.D., Conte, M., Guezennec, J., Prieur, D., 1991. Monitoring of a Vibrio natriegens and Desulfovibrio vulgaris marine aerobic biofilm on a stainless steel surface in a laboratory tubular flow system. Journal of Applied Bacteriology 71, 244-251.

Bernstein, J.A., Khodursky, A.B., Lin, P.-H., Lin-Chao, S., Cohen, S.N., 2002. Global analysis of mRNA decay and abundance in Escherichia coli at single-gene resolution using two-color fluorescent DNA microarrays. Proceedings of the National Academy of Sciences of the United States of America 99, 9697-9702.

Berry, D., Xi, C., Raskin, L., 2006. Microbial ecology of drinking water distribution systems. Curr Opin Biotechnol 17, 297-302.

Bhola, R., Bhola, S.M., Mishra, B., Olson, D.L., 2010a. Microbiologically influenced corrosion and its mitigation: A review. Material Science Research India 7, 407-412.

Bhola, R., Bhola, S.M., Mishra, B., Olson, D.L., 2010b. Microbiologically Influenced Corrosion and Its Mitigation: A Review. Mater. Sci. Res. India 7, 407-412.

Biesbroek, G., Sanders, E.A., Roeselers, G., Wang, X., Caspers, M.P., Trzciński, K., Bogaert, D., Keijser, B.J., 2012. Deep sequencing analyses of low density microbial communities: working at the boundary of accurate microbiota detection. PLOS One 7, e32942.

Bonifay, V., Wawrik, B., Sunner, J., Snodgrass, E.C., Aydin, E., Duncan, K.E., Callaghan, A.V., Oldham, A., Liengen, T., Beech, I., 2017. Metabolomic and metagenomic analysis of two crude oil production pipelines experiencing differential rates of corrosion. Frontiers in Microbiology 8, 99.

Borenstein, S.W., 1991. Microbiologically influenced corrosion of austenitic stainless steel weldments.

Borriello, G., Werner, E., Roe, F., Kim, A.M., Ehrlich, G.D., Stewart, P.S., 2004. Oxygen limitation contributes to antibiotic tolerance of Pseudomonas aeruginosa in biofilms. Antimicrobial Agents and Chemotheraphy 48, 2659-2664.

Boschker, H., Nold, S., Wellsbury, P., Bos, D., De Graaf, W., Pel, R., Parkes, R.J., Cappenberg, T., 1998. Direct linking of microbial populations to specific biogeochemical processes by 13C-labelling of biomarkers. Nature 392, 801-805.

Brauer, J.I., Makama, Z., Bonifay, V., Aydin, E., Kaufman, E.D., Beech, I.B., Sunner, J., 2015. Mass spectrometric metabolomic imaging of biofilms on corroding steel surfaces using laser ablation and solvent capture by aspiration. Biointerphases 10, 019003.

Bryan, E., Veale, M.A., Talbot, R.E., Cooper, K.G., Matthews, N.S., 1995. Biocidal compositions and treatments. Google Patents.

Bryant, R.D., Laishley, E.J., 1990. The role of hydrogenase in anaerobic biocorrosion. Canadian Journal of Microbiology 36, 259-264.

Caffrey, S.M., 2010. Which microbial communities are present? Sequence-based metagenomics, Applied Microbiology and Molecular Biology in Oilfield Systems. Springer, pp. 63-76.

Capdeville, B., Rols, J.L., 1992. Introduction to Biofilms in Water and Wastewater Treatment, In: Melo, L.F., Bott, T.R., Fletcher, M., Capdeville, B. (Eds.), Biofilms — Science and Technology. Springer Netherlands, Dordrecht, pp. 13-20.

Castaneda, H., Benetton, X.D., 2008. SRB-biofilm influence in active corrosion sites formed at the steel-electrolyte interface when exposed to artificial seawater conditions. Corrosion Science 50, 1169-1183.

Cayford, B.I., Dennis, P.G., Tyson, G.W., Bond, P.L., 2012. Microbial communities involved in the corrosion of concrete sewer infrastructure, 14th International Symposium on Microbial Ecology (ISME14).

Chakravorty, S., Helb, D., Burday, M., Connell, N., Alland, D., 2007. A detailed analysis of 16S ribosomal RNA gene segments for the diagnosis of pathogenic bacteria. J Microbiol Methods 69, 330-339.

Chen, E., Chen, R., 1984. Monitoring microbial corrosion in large oilfield water systems. Journal of Petroleum Technology 36, 1,171-171,176.

Cheng, S., Tian, J., Chen, S., Lei, Y., Chang, X., Liu, T., Yin, Y., 2009. Microbially influenced corrosion of stainless steel by marine bacterium Vibrio natriegens:Corrosion behavior. Materials Science and Engineering: C 29, 751-755.

Chin, C.D., Laksanasopin, T., Cheung, Y.K., Steinmiller, D., Linder, V., Parsa, H., Wang, J., Moore, H., Rouse, R., Umviligihozo, G., 2011. Microfluidics-based diagnostics of infectious diseases in the developing world. Nature medicine 17, 1015-1019.

Costerton, J.W., Cheng, K.J., Geesey, G.G., Ladd, T.I., Nickel, J.C., Dasgupta, M., Marrie, T.J., 1987a. Bacterial biofilms in nature and disease. Annu Rev Microbiol 41, 435-464.

Costerton, J.W., Cheng, K.J., Geesey, G.G., Ladd, T.I., Nickel, J.C., Dasgupta, M., Marrie, T.J., 1987b. Bacterial biofilms in nature and disease. Annual Reviews in Microbiology 41, 435-464.

Costerton, J.W., Lewandowski, Z., Caldwell, D.E., Korber, D.R., Lappin-Scott, H.M., 1995. Microbial biofilms. Annual Reviews in Microbiology 49, 711-745.

Costerton, J.W., Stewart, P.S., Greenberg, E.P., 1999. Bacterial biofilms: a common cause of persistent infections. Science 284, 1318-1322.

Dang, H., Chen, R., Wang, L., Shao, S., Dai, L., Ye, Y., Guo, L., Huang, G., Klotz, M.G., 2011. Molecular characterization of putative biocorroding microbiota with a novel niche detection of Epsilon- and Zetaproteobacteria in Pacific Ocean coastal seawaters. Environmental Microbiology 13, 3059-3074.

Dang, H., Lovell, C.R., 2016. Microbial surface colonization and biofilm development in marine environments. Microbiology and molecular biology reviews 80, 91-138.

Dass, C., 2006. Hyphenated separation techniques, Fundamentals of Contemporary Mass Spectrometry. John Wiley & Sons, Inc., pp. 151-194.

De Beer, D., Stoodley, P., Lewandowski, Z., 1996. Liquid flow and mass transport in heterogeneous biofilms. Water Res 30, 2761-2765.

de Beer, D., Stoodley, P., Roe, F., Lewandowski, Z., 1994. Effects of biofilm structures on oxygen distribution and mass transport. Biotechnology and Bioengineering 43, 1131-1138.

De Hoffmann, E., 2000. Mass spectrometry. Kirk-Othmer Encyclopedia of Chemical Technology.

de Paula, R.M., Keasler, V.V., Bennett, B., Clark, J.C., Cloud, R., 2014. On-site evaluation of microbiologically induced corrosion and the effects of continuous low dosage corrosion inhibitor application, CORROSION 2014. NACE International, San Antonio, Texas, USA.

de Romero, M., De Rincon, O., Ocando, L., 2009. Cathodic protection efficiency in the presence of SRB: State of the art, CORROSION 2009. NACE International.

De Windt, W., Boon, N., Siciliano, S.D., Verstraete, W., 2003. Cell density related H2 consumption in relation to anoxic Fe (0) corrosion and precipitation of corrosion products by Shewanella oneidensis MR-1. Environmental Microbiology 5, 1192-1202.

Dettmer, K., Aronov, P.A., Hammock, B.D., 2007. Mass spectrometry-based metabolomics. Mass Spectrometry Reviews 26, 51-78.

Dexter, S., Duquette, D., Siebert, O., Videla, H., 1991. Use and limitations of electrochemical techniques for investigating microbiological corrosion. Corrosion 47, 308-318.

Dhariwal, A., Chong, J., Habib, S., King, I.L., Agellon, L.B., Xia, J., 2017. MicrobiomeAnalyst: a web-based tool for comprehensive statistical, visual and meta-analysis of microbiome data. Nucleic Acids Research 45, W180-W188.

Dittrich, P.S., Manz, A., 2006. Lab-on-a-chip: microfluidics in drug discovery. Nature Reviews Drug Discovery 5, 210-218.

Dong, H., Li, C.-M., Zhang, Y.-F., Cao, X.-D., Gan, Y., 2007. Screen-printed microfluidic device for electrochemical immunoassay. Lab on a Chip 7, 1752-1758.

Duan, J., Wu, S., Zhang, X., Huang, G., Du, M., Hou, B., 2008. Corrosion of carbon steel influenced by anaerobic biofilm in natural seawater. Electrochimica Acta 54, 22-28.

Dudley, E., Yousef, M., Wang, Y., Griffiths, W., 2010. Targeted metabolomics and mass spectrometry. Advances in Protein Chemistry and Structural Biology 80, 45-83.

Duncan, K.E., Gieg, L.M., Parisi, V.A., Tanner, R.S., Tringe, S.G., Bristow, J., Suflita, J.M., 2009. Biocorrosive thermophilic microbial communities in Alaskan North Slope oil facilities. Environmental Science and Technology 43, 7977-7984.

Dunn, A.K., Millikan, D.S., Adin, D.M., Bose, J.L., Stabb, E.V., 2006. New rfp- and pES213-derived tools for analyzing symbiotic Vibrio fischeri reveal patterns of infection and lux expression in situ. Appl Environ Microbiol 72, 802-810.

Dunn, W.B., Ellis, D.I., 2005. Metabolomics: current analytical platforms and methodologies. TrAC-Trends in Analytical Chemistry 24, 285-294.

Dunn, W.B., Erban, A., Weber, R.J., Creek, D.J., Brown, M., Breitling, R., Hankemeier, T., Goodacre, R., Neumann, S., Kopka, J., 2013. Mass appeal: metabolite identification in mass spectrometry-focused untargeted metabolomics. Metabolomics 9, 44-66.

Eashwar, M., Subramanian, G., Palanichamy, S., Rajagopal, G., Madhu, S., Kamaraj, P., 2009. Cathodic behaviour of stainless steel in coastal Indian seawater: calcareous deposits overwhelm biofilms. Biofouling 25, 191-201.

Eckert, R.B., 2015. Emphasis on biofilms can improve mitigation of microbiologically influenced corrosion in oil and gas industry. Corrosion Engineering, Science and Technology 50, 163-168.

Eckert, R.B., Amend, B., 2017. MIC and materials selection, In: Skovhus, T.L., Enning, D., Lee, J.S. (Eds.), Microbiologically Influenced Corrosion in the Upstream Oil and Gas Industry. CRC Press.

Eckert, R.B., Skovhus, T.L., 2018. Advances in the application of molecular microbiological methods in the oil and gas industry and links to microbiologically influenced corrosion. International Biodeterioration & Biodegradation 126, 169-176.

Edmonds, P., Cooney, J.J., 1967. Identification of microorganisms isolated from jet fuel systems. Appl Microbiol 15, 411-416.

Elhariry, H., Gherbawy, Y., El-Deeb, B., Altalhi, A., 2012. Molecular Identification and Biofilm-Forming Ability of Culturable Aquatic Bacteria In Microbial Biofilms Formed in Drinking Water Distribution Networks. Geomicrobiology Journal 29, 561-569.

Elifantz, H., Horn, G., Ayon, M., Cohen, Y., Minz, D., 2013. Rhodobacteraceae are the key members of the microbial community of the initial biofilm formed in Eastern Mediterranean coastal seawater. FEMS microbiology ecology 85, 348-357.

Enning, D., Garrelfs, J., 2014. Corrosion of iron by sulfate-reducing bacteria: new views of an old problem. Appl Environ Microbiol 80, 1226-1236.

Enning, D., Smith, R., Stolle, J., 2016a. Evaluating the efficacy of weekly THPS and glutaraldehyde batch treatment to control severe microbial corrosion in a simulated seawater injection system, CORROSION 2016. NACE International.

Enning, D., Smith, R., Stolle, J., 2016b. Evaluating the Efficacy of Weekly THPS and Glutaraldehyde Batch Treatment to Control Severe Microbial Corrosion in a Simulated Seawater Injection System. NACE International.

Enning, D., Venzlaff, H., Garrelfs, J., Dinh, H.T., Meyer, V., Mayrhofer, K., Hassel, A.W., Stratmann, M., Widdel, F., 2012. Marine sulfate-reducing bacteria cause serious corrosion of iron under electroconductive biogenic mineral crust. Environmental Microbiology 14, 1772-1787.

Enos, D., Taylor, S., 1996. Influence of sulfate-reducing bacteria on alloy 625 and austenitic stainless steel weldments. Corrosion 52, 831-842.

Evans, U.R., 1969. Mechanism of rusting. Corrosion Science 9, 813-821.

Faúndez, G., Troncoso, M., Navarrete, P., Figueroa, G., 2004. Antimicrobial activity of copper surfaces against suspensions of Salmonella enterica and Campylobacter jejuni. BMC Microbiol 4, 19.

Figeys, D., Pinto, D., 2000. Lab-on-a-chip: a revolution in biological and medical sciences. ACS Publications.

Flemming, H.-C., Wingender, J., 2010. The biofilm matrix. Nat Rev Micro 8, 623-633.

Flemming, H.C., 1994. Microbial material destruction Basics : Economic - Technical Overview. Materials and Corrosion 45, 5-9.

Gardner, L., 2005. The use of stainless steel in structures. Progress in Structural Engineering and Materials 7, 45-55.

Gaylarde, C., Beech, I., 1988. Molecular basis of bacterial adhesion to metals. Microbial Corrosion-1 1, 20.

Geissler, B., De Paula, R., Keller-Schultz, C., Lilley, J., Keasler, V., 2014a. Data mining to prevent microbiologically influenced corrosion?, CORROSION 2014. NACE International.

Geissler, B., De Paula, R., Keller-Schultz, C., Lilley, J., Keasler, V., 2014b. Data mining to prevent microbiologically influenced corrosion?, CORROSION 2014. NACE International.

Gerchakov, S., Little, B., Wagner, P., 1986. Probing microbiologically induced corrosion. Corrosion 42, 689-692.

Gomez-Alvarez, V., Revetta, R.P., Santo Domingo, J.W., 2012. Metagenome analyses of corroded concrete wastewater pipe biofilms reveal a complex microbial system. BMC Microbiol 12, 122.

Gowda, G.N., Zhang, S., Gu, H., Asiago, V., Shanaiah, N., Raftery, D., 2008. Metabolomics-based methods for early disease diagnostics. Expert Review of Molecular Diagnostics 8, 617-633.

Griffiths, W.J., Koal, T., Wang, Y., Kohl, M., Enot, D.P., Deigner, H.P., 2010. Targeted metabolomics for biomarker discovery. Angewandte Chemie International Edition 49, 5426-5445.

Grobe, K.J., Zahller, J., Stewart, P.S., 2002. Role of dose concentration in biocide efficacy against Pseudomonas aeruginosa biofilms. Journal of Industrial Microbiology & Biotechnology 29, 10-15.

Guijas, C., Montenegro-Burke, J.R., Domingo-Almenara, X., Palermo, A., Warth, B., Hermann, G., Koellensperger, G., Huan, T., Uritboonthai, W., Aisporna, A.E., 2018. METLIN: a technology platform for identifying knowns and unknowns. Analytical Chemistry 90, 3156-3164.

Hall-Stoodley, L., Costerton, J.W., Stoodley, P., 2004. Bacterial biofilms: from the Natural environment to infectious diseases. Nat Rev Micro 2, 95-108.

Hamilton, W.A., 1983. Sulphate-reducing bacteria and the offshore oil industry. Trends in Biotechnology 1, 36-40.

Hardy, J., 1981. The enumeration, isolation and characterization of sulphate-reducing bacteria from North Sea waters. Journal of Applied Bacteriology 51, 505-516.

Hashimoto, K., 2002. 2002 WR Whitney Award Lecture: In pursuit of new corrosion-resistant alloys. Corrosion 58, 715-722.

He, Z., Gentry, T.J., Schadt, C.W., Wu, L., Liebich, J., Chong, S.C., Huang, Z., Wu, W., Gu, B., Jardine, P., Criddle, C., Zhou, J., 2007. GeoChip: a comprehensive microarray for investigating biogeochemical, ecological and environmental processes. ISME J 1, 67-77.

Herb, S., Stair, J.O., Ringelberg, D.B., White, D.C., Flemming, H.-C., 1995. Characterization of biofilms on corroded concrete surfaces in drinking water reservoirs. Water Science and Technology 32, 141-147.

Herrera, L.K., Videla, H.A., 2009. Role of iron-reducing bacteria in corrosion and protection of carbon steel. International Biodeterioration & Biodegradation 63, 891-895.

Heydorn, A., Nielsen, A.T., Hentzer, M., Sternberg, C., Givskov, M., Ersbøll, B.K., Molin, S., 2000. Quantification of biofilm structures by the novel computer program comstat. Microbiology 146, 2395-2407.

Holmkvist, L., Østergaard, J.J., Skovhus, T.L., 2010. Which Microbial Communities Are Present? Using Fluorescence In Situ Hybridisation (FISH): Microscopic Techniques for Enumeration of Troublesome Microorganisms in Oil and Fuel Samples, Applied Microbiology and Molecular Biology in Oilfield Systems. Springer, pp. 55-61.

Hong, S.H., Hegde, M., Kim, J., Wang, X., Jayaraman, A., Wood, T.K., 2012a. Synthetic quorum-sensing circuit to control consortial biofilm formation and dispersal in a microfluidic device. Nature Communications 3, 613.

Hong, S.H., Hegde, M., Kim, J., Wang, X., Jayaraman, A., Wood, T.K., 2012b. Synthetic quorum-sensing circuit to control consortial biofilm formation and dispersal in a microfluidic device. Nat Commun 3, 613.

Huttunen-Saarivirta, E., Rajala, P., Bomberg, M., Carpén, L., 2017. Corrosion of copper in oxygen-deficient groundwater with and without deep bedrock micro-organisms: Characterisation of microbial communities and surface processes. Applied Surface Science 396, 1044-1057.

Ilhan-Sungur, E., Cansever, N., Cotuk, A., 2007. Microbial corrosion of galvanized steel by a freshwater strain of sulphate reducing bacteria (Desulfovibrio sp.). Corrosion Science 49, 1097-1109.

Iverson, W.P., 1987. Microbial corrosion of metals. Adv. Appl. Microbiol. 32, 1-35.

Jan-Roblero, J., Romero, J.M., Amaya, M., Le Borgne, S., 2004. Phylogenetic characterization of a corrosive consortium isolated from a sour gas pipeline. Appl Microbiol Biotechnol 64, 862-867.

Javaherdashti, R., 2008a. Microbiologically influenced corrosion (MIC). Microbiologically Influenced Corrosion: An Engineering Insight, 29-71.

Javaherdashti, R., 2008b. Microbiologically influenced corrosion (MIC): an engineering insight. Springer, Perth, Australia.

Javaherdashti, R., 2017. How Does a System Become Vulnerable to MIC?, Microbiologically Influenced Corrosion. Springer, pp. 81-97.

Jayaraman, A., Cheng, E., Earthman, J., Wood, T., 1997a. Importance of biofilm formation for corrosion inhibition of SAE 1018 steel by axenic aerobic biofilms. Journal of Industrial Microbiology and Biotechnology 18, 396-401.

Jayaraman, A., Cheng, E.T., Earthman, J.C., Wood, T.K., 1997b. Axenic aerobic biofilms inhibit corrosion of SAE 1018 steel through oxygen depletion. Applied Microbiology and Biotechnology 48, 11-17.

Jayaraman, A., Cheng, E.T., Earthman, J.C., Wood, T.K., 1997c. Axenic aerobic biofilms inhibit corrosion of SAE 1018 steel through oxygen depletion. Appl Microbiol Biotechnol 48, 11-17.

Jayaraman, A., Earthman, J., Wood, T., 1997d. Corrosion inhibition by aerobic biofilms on SAE 1018 steel. Applied Microbiology and Biotechnology 47, 62-68.

Jayaraman, A., Hallock, P., Carson, R., Lee, C.-C., Mansfeld, F., Wood, T., 1999. Inhibiting sulfate-reducing bacteria in biofilms on steel with antimicrobial peptides generated in situ. Applied Microbiology and Biotechnology 52, 267-275.

Jayaraman, A., Sun, A.K., Wood, T.K., 1998. Characterization of axenic Pseudomonas fragi and Escherichia coli biofilms that inhibit corrosion of SAE 1018 steel. J Appl Microbiol 84, 485-492.

Jin, U.H., Lee, S.O., Sridharan, G., Lee, K., Davidson, L.A., Jayaraman, A., Chapkin, R.S., Alaniz, R., Safe, S., 2014. Microbiome-derived tryptophan metabolites and their aryl hydrocarbon receptor-dependent agonist and antagonist activities. Mol Pharmacol 85, 777-788.

Jones, D.A., 1996. Principles and Prevention of Corrosion, 2nd. Ed. Upper Saddle River, NY: Prentice Hall, 168-198.

Jonsson, P., Gullberg, J., Nordström, A., Kusano, M., Kowalczyk, M., Sjöström, M., Moritz, T., 2004. A strategy for identifying differences in large series of metabolomic samples analyzed by GC/MS. Analytical Chemistry 76, 1738-1745.

Kaplan, J.B., 2010. Biofilm Dispersal: Mechanisms, Clinical Implications, and Potential Therapeutic Uses. Journal of Dental Research 89, 205-218.

Karatan, E., Watnick, P., 2009. Signals, regulatory networks, and materials that build and break bacterial biofilms. Microbiol Mol Biol Rev 73, 310-347.

Kell, D.B., Young, M., 2000. Bacterial dormancy and culturability: the role of autocrine growth factors: Commentary. Current Opinion in Microbiology 3, 238-243.

Kelly, R.G., Scully, J.R., Shoesmith, D., Buchheit, R.G., 2002. Electrochemical techniques in corrosion science and engineering. CRC Press.

Keren, I., Kaldalu, N., Spoering, A., Wang, Y., Lewis, K., 2004. Persister cells and tolerance to antimicrobials. FEMS Microbiology Letters 230, 13-18.

Kim, J., Hegde, M., Jayaraman, A., 2010. Co-culture of epithelial cells and bacteria for investigating host-pathogen interactions. Lab Chip 10, 43-50.

Kim, J., Hegde, M., Kim, S.H., Wood, T.K., Jayaraman, A., 2012. A microfluidic device for high throughput bacterial biofilm studies. Lab Chip 12, 1157-1163.

King, R.A., 2007. Microbiologically induced corrosion in the oil industry and the impact of mitigation programmes, Symp. Microbiol. Induced Corrosion., Extrin, Perth, WA.

Kip, N., van Veen, J.A., 2015. The dual role of microbes in corrosion. ISME J 9, 542-551.

Koch G, V.J., Thompson N, Moghissi O, Gould M, Payer J, 2016. NACE International IMPACT (International Measures of Prevention, Application, and Economics of Corrosion Technologies) Study.

Koch, G.H., Brongers, M.P., Thompson, N.G., Virmani, Y.P., Payer, J.H., 2002. Corrosion cost and preventive strategies in the United States.

Kolari, M., Mattila, K., Mikkola, R., Salkinoja-Salonen, M.S., 1998. Community structure of biofilms on ennobled stainless steel in Baltic Sea water. Journal of Industrial Microbiology and Biotechnology 21, 261-274.

Kotu, S.P., Erbay, C., Sobahi, N., Han, A., Mannan, S., Jayaraman, A., 2016. Integration of electrochemical impedance spectroscopy and microfluidics for investigating microbially influenced corrosion using co-culture biofilms, CORROSION 2016. NACE International, Vancouver, Canada.

Kotu, S.P., Jayaraman, A., Mannan, S., Han, A., 2018. M-MIC: Microfluidic microbiologically influenced corrosion model. Texas A&M University.

Kuczynski, J., Stombaugh, J., Walters, W.A., González, A., Caporaso, J.G., Knight, R., 2012. Using QIIME to Analyze 16S rRNA Gene Sequences from Microbial Communities. Current Protocols in Microbiology Chapter 1, Unit 1E 5.

Kumar, C.G., Anand, S.K., 1998. Significance of microbial biofilms in food industry: a review. International Journal of Food Microbiology 42, 9-27.

Kus, E., Nealson, K., Mansfeld, F., 2006. Corrosion Protection due to Bacteria/Metal Interactions, Meeting Abstracts. The Electrochemical Society, pp. 865-865.

Kushner, S.R., 2002. mRNA decay in Escherichia coli comes of age. Journal of Bacteriology 184, 4658-4665.

Landoulsi, J., Cooksey, K., Dupres, V., 2011. Review–interactions between diatoms and stainless steel: focus on biofouling and biocorrosion. Biofouling 27, 1105-1124.

Langille, M.G., Zaneveld, J., Caporaso, J.G., McDonald, D., Knights, D., Reyes, J.A., Clemente, J.C., Burkepile, D.E., Thurber, R.L.V., Knight, R., 2013a. Predictive

functional profiling of microbial communities using 16S rRNA marker gene sequences. Nature Biotechnology 31, 814.

Langille, M.G.I., Zaneveld, J., Caporaso, J.G., McDonald, D., Knights, D., Reyes, J.A., Clemente, J.C., Burkepile, D.E., Vega Thurber, R.L., Knight, R., Beiko, R.G., Huttenhower, C., 2013b. Predictive functional profiling of microbial communities using 16S rRNA marker gene sequences. Nature biotechnology 31, 814.

Lanneluc, I., Langumier, M., Sabot, R., Jeannin, M., Refait, P., Sablé, S., 2015. On the bacterial communities associated with the corrosion product layer during the early stages of marine corrosion of carbon steel. International Biodeterioration & Biodegradation 99, 55-65.

Larsen, J., Rasmussen, K., Pedersen, H., Sørensen, K., Lundgaard, T., Skovhus, T.L., 2010. Consortia of MIC bacteria and archaea causing pitting corrosion in top side oil production facilities, CORROSION 2010. NACE International.

Lawrence, J.R., Korber, D.R., Hoyle, B.D., Costerton, J.W., Caldwell, D.E., 1991. Optical sectioning of microbial biofilms. J Bacteriol 173, 6558-6567.

Leary, D.H., Li, R.W., Hamdan, L.J., Hervey, W.J., Lebedev, N., Wang, Z., Deschamps, J.R., Kusterbeck, A.W., Vora, G.J., 2014. Integrated metagenomic and metaproteomic analyses of marine biofilm communities. Biofouling 30, 1211-1223.

Lee, J.-H., Kaplan, J.B., Lee, W.Y., 2008. Microfluidic devices for studying growth and detachment of Staphylococcus epidermidis biofilms. Biomedical microdevices 10, 489-498.

Lee, M.-H.P., Caffrey, S.M., Voordouw, J.K., Voordouw, G., 2010. Effects of biocides on gene expression in the sulfate-reducing bacterium Desulfovibrio vulgaris Hildenborough. Appl Microbiol Biotechnol 87, 1109-1118.

Lee, W., Lewandowski, Z., Nielsen, P.H., Hamilton, W.A., 1995. Role of sulfate-reducing bacteria in corrosion of mild steel: A review. Biofouling 8, 165-194.

Lenhart, T.R., Duncan, K.E., Beech, I.B., Sunner, J.A., Smith, W., Bonifay, V., Biri, B., Suflita, J.M., 2014. Identification and characterization of microbial biofilm communities associated with corroded oil pipeline surfaces. Biofouling 30, 823-835.

Li, K., Whitfield, M., Van Vliet, K.J., 2013. Beating the bugs: roles of microbial biofilms in corrosion. Corrosion Reviews 31, 73-84.

Li, X., Duan, J., Xiao, H., Li, Y., Liu, H., Guan, F., Zhai, X., 2017. Analysis of Bacterial Community Composition of Corroded Steel Immersed in Sanya and Xiamen Seawaters in China via Method of Illumina MiSeq Sequencing. Frontiers in Microbiology 8, 1737.

Lin, C.Y., Viant, M.R., Tjeerdema, R.S., 2006. Metabolomics: methodologies and applications in the environmental sciences. Journal of Pesticide Science 31, 245-251.

Lin, S.-Y., Hameed, A., Liu, Y.-C., Hsu, Y.-H., Lai, W.-A., Shen, F.-T., Young, L.-S., Tsai, C.-F., Young, C.-C., 2013a. Aureimonas ferruginea sp. nov. and Aureimonas rubiginis sp. nov., two siderophore-producing bacteria isolated from rusty iron plates. International journal of systematic and evolutionary microbiology 63, 2430-2435.

Lin, W., Yu, Z., Chen, X., Liu, R., Zhang, H., 2013b. Molecular characterization of natural biofilms from household taps with different materials: PVC, stainless steel, and cast iron in drinking water distribution system. Appl Microbiol Biotechnol 97, 8393-8401.

Little, B., Ray, R., Pope, R., 2000. Relationship between corrosion and the biological sulfur cycle: a review. Corrosion 56, 433-443.

Little, B., Wagner, P., Mansfeld, F., 1992. An overview of microbiologically influenced corrosion. Electrochimica Acta 37, 2185-2194.

Little, B., Wagner, P., Ray, R., McNeil, M., 1990. Microbiologically influenced corrosion in copper and nickel seawater piping systems. NAVAL OCEANOGRAPHIC AND ATMOSPHERIC RESEARCH LAB STENNIS SPACE CENTER MS.

Little, B.J., Lee, J.S., 2006. Impact of Alloying Elements to Susceptibility of Microbiologically Influenced Corrosion, In: Little, B.J., Lee, J.S. (Eds.), Microbiologically Influenced Corrosion, pp. 127-146.

Little, B.J., Lee, J.S., 2009. Microbiologically influenced corrosion. Wiley Online Library.

Little, B.J., Lee, J.S., 2014. Microbiologically influenced corrosion: an update. International Materials Reviews 59, 384-393.

Little, B.J., Lee, J.S., Ray, R., 2006. Diagnosing microbiologically influenced corrosion: a state-of-the-art review. Corrosion 62, 1006-1017.

Little, J.L., 1999. Artifacts in trimethylsilyl derivatization reactions and ways to avoid them. Journal of Chromatography A 844, 1-22.

Littmann, E., 1975. Oilfield bactericide parameters as measured by ATP analysis, SPE Oilfield Chemistry Symposium. Society of Petroleum Engineers.

Liu, G., Bakker, G., Li, S., Vreeburg, J., Verberk, J., Medema, G., Liu, W., Van Dijk, J., 2014. Pyrosequencing reveals bacterial communities in unchlorinated drinking water distribution system: an integral study of bulk water, suspended solids, loose deposits, and pipe wall biofilm. Environmental science & technology 48, 5467-5476.

Liu, T., Cheng, Y.F., Sharma, M., Voordouw, G., 2017. Effect of fluid flow on biofilm formation and microbiologically influenced corrosion of pipelines in oilfield produced water. Journal of Petroleum Science and Engineering 156, 451-459.

Lock, M.A., Wallace, R.R., Costerton, J.W., Ventullo, R.M., Charlton, S.E., 1984. River epilithon: Toward a structural-functional model. Oikos 42, 10-22.

Lomans, B.P., de Paula, R., Geissler, B., Kuijvenhoven, C.A., Tsesmetzis, N., 2016. Proposal of Improved Biomonitoring Standard for Purpose of Microbiologically Influenced Corrosion Risk Assessment, SPE International Oilfield Corrosion Conference and Exhibition. Society of Petroleum Engineers.

Lopes, F.A., Morin, P., Oliveira, R., Melo, L.F., 2006a. Interaction of Desulfovibrio desulfuricans biofilms with stainless steel surface and its impact on bacterial metabolism. Journal of Applied Microbiology 101, 1087-1095.

Lopes, F.A., Morin, P., Oliveira, R., Melo, L.F., 2006b. Interaction of Desulfovibrio desulfuricans biofilms with stainless steel surface and its impact on bacterial metabolism. J Appl Microbiol 101, 1087-1095.

López, M.A., Díaz de la Serna, F.J.Z., Jan-Roblero, J., Romero, J.M., Hernández-Rodríguez, C., 2006. Phylogenetic analysis of a biofilm bacterial population in a water pipeline in the Gulf of Mexico. FEMS microbiology ecology 58, 145-154.

Lücker, S., Steger, D., Kjeldsen, K.U., MacGregor, B.J., Wagner, M., Loy, A., 2007. Improved 16S rRNA-targeted probe set for analysis of sulfate-reducing bacteria by fluorescence in situ hybridization. J Microbiol Methods 69, 523-528.

Ludwig, W., Klenk, H.-P., 2005. Overview: a phylogenetic backbone and taxonomic framework for procaryotic systematics, Bergey's manual® of systematic bacteriology. Springer, pp. 49-66.

Maharjan, R.P., Ferenci, T., 2003. Global metabolite analysis: the influence of extraction methodology on metabolome profiles of Escherichia coli. Analytical Biochemistry 313, 145-154.

Maillard, J.Y., 2002. Bacterial target sites for biocide action. J Appl Microbiol 92, 16S-27S.

Mamas, M., Dunn, W.B., Neyses, L., Goodacre, R., 2011. The role of metabolites and metabolomics in clinically applicable biomarkers of disease. Archives of toxicology 85, 5-17.

Mand, J., Park, H.S., Jack, T.R., Voordouw, G., 2014. The role of acetogens in microbially influenced corrosion of steel. Frontiers in Microbiology 5, 268.

Mansfeld, F., Little, B., 1991. A technical review of electrochemical techniques applied to microbiologically influenced corrosion. Corrosion Science 32, 247-272.

Mata, A., Fleischman, A.J., Roy, S., 2005. Characterization of polydimethylsiloxane (PDMS) properties for biomedical micro/nanosystems. Biomedical microdevices 7, 281-293.

McLeod, E.S., Dawood, Z., MacDonald, R., Oosthuizen, M.C., Graf, J., Steyn, P.L., Brözel, V.S., 1998. Isolation and identification of sulphite- and iron reducing, hydrogenase positive facultative anaerobes from cooling water systems. Systematic and Applied Microbiology 21, 297-305.

McLeod, E.S., MacDonald, R., Brozel, V.S., 2002. Distribution of Shewanella putrefaciens and Desulfovibrio vulgaris in sulphidogenic biofilms of industrial cooling water systems determined by fluorescent in situ hybridisation. Water Sa 28, 123-128.

Miller, J., Tieler, A., 1971a. Microbial corrosion of buried and immersed metal, In: Purkiss, B., Miller, J. (Eds.), Microbial Aspects of Metallurgy. Medical and Technical Publishing Co. Etd., Aylesbury. England, pp. 61-105.

Miller, J., Tieler, A., 1971b. Microbial corrosion of buried and immersed metal, Microbial Aspects or Metallurgy. Medical and Technical Publishing Co. Etd.; Aylesbury. England., pp. 61-105.

Miller, S.R., Strong, A.L., Jones, K.L., Ungerer, M.C., 2009. Bar-coded pyrosequencing reveals shared bacterial community properties along the temperature gradients of two alkaline hot springs in Yellowstone National Park. Appl Environ Microbiol 75, 4565-4572.

Morgan, X.C., Tickle, T.L., Sokol, H., Gevers, D., Devaney, K.L., Ward, D.V., Reyes, J.A., Shah, S.A., LeLeiko, N., Snapper, S.B., 2012. Dysfunction of the intestinal microbiome in inflammatory bowel disease and treatment. Genome biology 13, R79.

Mori, K., Tsurumaru, H., Harayama, S., 2010. Iron corrosion activity of anaerobic hydrogen-consuming microorganisms isolated from oil facilities. Journal of bioscience and bioengineering 110, 426-430.

Morris, B.E., Van Der Kraan, G.M., 2017. Application of Biocides and Chemical Treatments to Both Combat Microorganisms and Reduce (Bio)Corrosion, In: Skovhus, T.L., Enning, D., Lee, J.S. (Eds.), Microbiologically Influenced Corrosion in the Upstream Oil and Gas Industry. CRC Press.

Muyzer, G., Marty, F., 2014. Molecular methods in microbiologically influenced corrosion research, monitoring and control, In: Skovhus, S.M.C.T.L. (Ed.), Applications of Molecular Microbiological Methods. Caister Academic Press, United Kingdom.

Myers, H.C., 1947. The role of algae in corrosion. Journal (American Water Works Association) 39, 322-324.

NACE, 2006. Selection, evaluation and application of biocides in the oil and gas industry, NACE 31205. National Association of Corrosion Engineers International, Houston, TX.

Nemati, M., Jenneman, G.E., Voordouw, G., 2001. Impact of nitrate-mediated microbial control of souring in oil reservoirs on the extent of corrosion. Biotechnology progress 17, 852-859.

Nivens, D., Nichols, P., Henson, J., Geesey, G., White, D., 1986. Reversible acceleration of the corrosion of AISI 304 stainless steel exposed to seawater induced by growth and secretions of the marine bacterium Vibrio natriegens. Corrosion 42, 204-210.

Nyamundanda, G., Brennan, L., Gormley, I.C., 2010. Probabilistic principal component analysis for metabolomic data. BMC bioinformatics 11, 571.

Okabe, S., Odagiri, M., Ito, T., Satoh, H., 2007a. Succession of sulfur-oxidizing bacteria in the microbial community on corroding concrete in sewer systems. Appl Environ Microbiol 73, 971-980.

Okabe, S., Odagiri, M., Ito, T., Satoh, H., 2007b. Succession of sulfur-oxidizing bacteria in the microbial community on corroding concrete in sewer systems. Appl Environ Microbiol 73, 971-980.

Okoro, C., Ekun, O.A., Nwume, M.I., Lin, J., 2016. Molecular analysis of microbial community structures in Nigerian oil production and processing facilities in order to access souring corrosion and methanogenesis. Corrosion Science 103, 242-254.

Okoro, C., Smith, S., Chiejina, L., Lumactud, R., An, D., Park, H.S., Voordouw, J., Lomans, B.P., Voordouw, G., 2014. Comparison of microbial communities involved in souring and corrosion in offshore and onshore oil production facilities in Nigeria. Journal of Industrial Microbiology and Biotechnology 41, 665-678.

Papavinasam, S., 2011. Corrosion inhibitors. Uhlig's Corrosion Handbook, 1021-1032.

Park, H.S., Chatterjee, I., Dong, X., Wang, S.H., Sensen, C.W., Caffrey, S.M., Jack, T.R., Boivin, J., Voordouw, G., 2011. Effect of sodium bisulfite injection on the microbial community composition in a brackish-water-transporting pipeline. Appl Environ Microbiol 77, 6908-6917.

Patti, G.J., 2011. Separation strategies for untargeted metabolomics. Journal of Separation Science 34, 3460-3469.

Patti, G.J., Yanes, O., Siuzdak, G., 2012. Innovation: metabolomics: the apogee of the omics trilogy. Nature Reviews Molecular Cell Biology 13, 263-269.

Pedersen, A., Hermansson, M., 1991. Inhibition of metal corrosion by bacteria. Biofouling 3, 1-11.

Perez, N., 2004. Electrochemistry and corrosion science. Springer.

Potter, H., Heller, R., 2003. Transfection by Electroporation. Current protocols in molecular biology / edited by Frederick M. Ausubel ... [et al.] CHAPTER, Unit-9.3.

Pournia, M., Bahador, N., Salekdeh, G.H., 2018. Microbial Diversity of Long-Duration Gas Injection Oil Reservoir Based on Next Generation Sequencing in South of Iran. Nature Environment and Pollution Technology 17, 413-420.

Price, C., 1993. Fluorescence in situ hybridization. Blood Reviews 7, 127-134.

Quarini, J., Shire, S., 2007. A review of fluid-driven pipeline pigs and their applications. Proceedings of the Institution of Mechanical Engineers, Part E: Journal of Process Mechanical Engineering 221, 1-10.

Rajasekar, A., Anandkumar, B., Maruthamuthu, S., Ting, Y.-P., Rahman, P.K., 2010a. Characterization of corrosive bacterial consortia isolated from petroleum-product-transporting pipelines. Applied Microbiology and Biotechnology 85, 1175-1188.

Rajasekar, A., Anandkumar, B., Maruthamuthu, S., Ting, Y.P., Rahman, P.K., 2010b. Characterization of corrosive bacterial consortia isolated from petroleum-product-transporting pipelines. Appl Microbiol Biotechnol 85, 1175-1188.

Rao, T., Sairam, T., Viswanathan, B., Nair, K., 2000. Carbon steel corrosion by iron oxidising and sulphate reducing bacteria in a freshwater cooling system. Corrosion Science 42, 1417-1431.

Rauch, M., Graef, H., Rozenzhak, S., Jones, S., Bleckmann, C., Kruger, R., Naik, R., Stone, M., 2006. Characterization of microbial contamination in United States Air Force aviation fuel tanks. Journal of Industrial Microbiology and Biotechnology 33, 29-36.

Roux, A., Lison, D., Junot, C., Heilier, J.-F., 2011. Applications of liquid chromatography coupled to mass spectrometry-based metabolomics in clinical chemistry and toxicology: a review. Clinical Biochemistry 44, 119-135.

Rowe, G., Sweet, M., Beebee, T., 2017. An introduction to molecular ecology. Oxford University Press.

Russell, A., 2003a. Similarities and differences in the responses of microorganisms to biocides. Journal of Antimicrobial Chemotherapy 52, 750-763.

Russell, A.D., 2003b. Biocide use and antibiotic resistance: the relevance of laboratory findings to clinical and environmental situations. The Lancet Infectious Diseases 3, 794-803.

Salerno, J., Little, B., Lee, J., Hamdan, L.J., 2018. Exposure to crude oil and chemical dispersant may impact marine microbial biofilm composition and steel corrosion. Frontiers in Marine Science 5.

Salvarezza, R., Videla, H., 1984. Microbiological Corrosion in Fuel Storage Tanks. I.--Anodic Behavior. Acta Cient. Venez. 35, 244-247.

Satoh, H., Odagiri, M., Ito, T., Okabe, S., 2009a. Microbial community structures and in situ sulfate-reducing and sulfur-oxidizing activities in biofilms developed on mortar specimens in a corroded sewer system. Water Res 43, 4729-4739.

Satoh, H., Odagiri, M., Ito, T., Okabe, S., 2009b. Microbial community structures and in situ sulfate-reducing and sulfur-oxidizing activities in biofilms developed on mortar specimens in a corroded sewer system. Water Res 43, 4729-4739.

Sawabe, T., Fukui, Y., Stabb, E.V., 2006. Simple conjugation and outgrowth procedures for tagging vibrios with GFP, and factors affecting the stable expression of the gfp tag. Lett Appl Microbiol 43, 514-522.

Scalbert, A., Brennan, L., Fiehn, O., Hankemeier, T., Kristal, B.S., van Ommen, B., Pujos-Guillot, E., Verheij, E., Wishart, D., Wopereis, S., 2009. Mass-spectrometry-based metabolomics: limitations and recommendations for future progress with particular focus on nutrition research. Metabolomics 5, 435.

Schäfer, K., 1994. Analysis of short chain fatty acids from different intestinal samples. I: by packed column gas chromatography. Chromatographia 39, 706-712.

Schloss, P.D., Westcott, S.L., Ryabin, T., Hall, J.R., Hartmann, M., Hollister, E.B., Lesniewski, R.A., Oakley, B.B., Parks, D.H., Robinson, C.J., 2009. Introducing mothur: open-source, platform-independent, community-supported software for describing and comparing microbial communities. Appl Environ Microbiol 75, 7537-7541.

Schutz, R.W., 1991. A case for titanium's resistance to microbiologically influenced corrosion.

Scott, P., Davies, M., Goldie, J., 1991. Ranking alloys for susceptibility to MIC; A preliminary report on high-Mo alloys. Materials Performance;(United States) 30.

Sekirov, I., Russell, S.L., Antunes, L.C.M., Finlay, B.B., 2010. Gut microbiota in health and disease. Physiological Reviews 90, 859-904.

Semple, K., Westlake, D., 1987. Characterization of iron-reducing Alteromonas putrefaciens strains from oil field fluids. Canadian journal of microbiology 33, 366-371.

Shinwari, M.W., Zhitomirsky, D., Deen, I.A., Selvaganapathy, P.R., Deen, M.J., Landheer, D., 2010. Microfabricated reference electrodes and their biosensing applications. Sensors 10, 1679-1715.

Situma, C., Hashimoto, M., Soper, S.A., 2006. Merging microfluidics with microarray-based bioassays. Biomolecular engineering 23, 213-231.

Skovhus, T.L., 2014. Biocide testing using single and multispecies biofilms, In: Dobretsov, S., Williams, D.N., Thomason, J.C. (Eds.), Biofouling methods. John Wiley & Sons.

Skovhus, T.L., Eckert, R.B., 2014. Practical aspects of MIC detection, monitoring and management in the oil and gas industry, CORROSION 2014. NACE International.

Skovhus, T.L., Eckert, R.B., Rodrigues, E., 2017. Management and control of microbiologically influenced corrosion (MIC) in the oil and gas industry—Overview and a North Sea case study. Journal of Biotechnology 256, 31-45.

Smart, J., Smith, G., 1992. Pigging and chemical treatment for oil and gas pipelines. Materials Performance;(United States) 31.

Sørensen, K.B., Skovhus, T.L., Larsen, J., 2010. How many microorganisms are present? Techniques for enumerating microorganisms in oilfields, Applied Microbiology and Molecular Biology in Oilfield Systems. Springer, pp. 85-91.

Sowards, J.W., Mansfield, E., 2014. Corrosion of copper and steel alloys in a simulated underground storage-tank sump environment containing acid-producing bacteria. Corrosion Science 87, 460-471.

Sridharan, G.V., Choi, K., Klemashevich, C., Wu, C., Prabakaran, D., Pan, L.B., Steinmeyer, S., Mueller, C., Yousofshahi, M., Alaniz, R.C., Lee, K., Jayaraman, A.,

2014. Prediction and quantification of bioactive microbiota metabolites in the mouse gut. Nature Communications 5, 5492.

Standard, A., 2017. G1-03, Standard Practice for preparing, cleaning, and evaluating corrosion test specimens, Annual Book of ASTM Standards, pp. 17-25.

Stevenson, B.S., Drilling, H.S., Lawson, P.A., Duncan, K.E., Parisi, V.A., Suflita, J.M., 2011. Microbial communities in bulk fluids and biofilms of an oil facility have similar composition but different structure. Environmental Microbiology 13, 1078-1090.

Stewart, P.S., 2003. Diffusion in biofilms. Journal of Bacteriology 185, 1485-1491.

Stipanicev, M., Turcu, F., Esnault, L., Rosas, O., Basseguy, R., Sztyler, M., Beech, I.B., 2014. Corrosion of carbon steel by bacteria from North Sea offshore seawater injection systems: laboratory investigation. Bioelectrochemistry 97, 76-88.

Suflita, J.M., Aktas, D.F., Oldham, A.L., Perez-Ibarra, B.M., Duncan, K., 2012. Molecular tools to track bacteria responsible for fuel deterioration and microbiologically influenced corrosion. Biofouling 28, 1003-1010.

Sule, N., Pasupuleti, S., Kohli, N., Menon, R., Dangott, L.J., Manson, M.D., Jayaraman, A., 2017. The norepinephrine metabolite 3, 4-dihydroxymandelic acid is produced by the commensal microbiota and promotes chemotaxis and virulence gene expression in enterohemorrhagic Escherichia coli. Infection and Immunity 85, e00431-00417.

Sun, H., Shi, B., Bai, Y., Wang, D., 2014. Bacterial community of biofilms developed under different water supply conditions in a distribution system. Science of the Total Environment 472, 99-107.

Tang, J., 2011. Microbial metabolomics. Current Genomics 12, 391-403.

Telang, A.J., Ebert, S., Foght, J.M., Westlake, D., Jenneman, G.E., Gevertz, D., Voordouw, G., 1997. Effect of nitrate injection on the microbial community in an oil field as monitored by reverse sample genome probing. Appl Environ Microbiol 63, 1785-1793.

Teng, F., Guan, Y.T., Zhu, W.P., 2008. Effect of biofilm on cast iron pipe corrosion in drinking water distribution system: corrosion scales characterization and microbial community structure investigation. Corrosion Science 50, 2816-2823.

Theodoridis, G.A., Gika, H.G., Want, E.J., Wilson, I.D., 2012. Liquid chromatography–mass spectrometry based global metabolite profiling: a review. Analytica chimica acta 711, 7-16.

Thormann, K.M., Saville, R.M., Shukla, S., Pelletier, D.A., Spormann, A.M., 2004. Initial phases of biofilm formation in Shewanella oneidensis MR-1. Journal of Bacteriology 186, 8096-8104.

Tidwell, T.J., De Paula, R., Broussard, Z., Keasler, V., 2016. A Comprehensive Approach to Diagnosing a Solution for a South Texas Production System with Severe MIC. NACE International.

Tidwell, T.J., de Paula, R.M., Nilsen, G.P., Keasler, V.V., 2015. Visualization and Quantification of Biofilm Removal for the Mitigation of MIC, CORROSION 2015. NACE International.

TM0194, N., 2014. Field Monitoring of Bacterial Growth in Oil and Gas Systems. NACE International.

TM0212, N., 2018. Detection, Testing, and Evaluation of Microbiologically Influenced Corrosion on Internal Surfaces of Pipelines. NACE International.

Usher, K., Kaksonen, A., MacLeod, I., 2014. Marine rust tubercles harbour iron corroding archaea and sulphate reducing bacteria. Corrosion Science 83, 189-197.

van der Kraan, G.M., De Ridder, M., Lomans, B.P., Muyzer, G., 2010. Sampling and nucleic extraction procedures from oil reservoir samples, Applied Microbiology and Molecular Biology in Oilfield Systems. Springer, pp. 7-16.

Vert, M., Hellwich, K.-H., Hess, M., Hodge, P., Kubisa, P., Rinaudo, M., Schué, F., 2012. Terminology for biorelated polymers and applications (IUPAC Recommendations 2012). Pure and Applied Chemistry 84, 377-410.

Videla, H.A., 1996. Manual of biocorrosion. CRC Press.

Videla, H.A., 2001. Microbially induced corrosion: an updated overview. International Biodeterioration and Biodegradation 48, 176-201.

Videla, H.A., 2002. Prevention and control of biocorrosion. International Biodeterioration & Biodegradation 49, 259-270.

Videla, H.A., Herrera, L.K., 2009. Understanding microbial inhibition of corrosion. A comprehensive overview. International Biodeterioration & Biodegradation 63, 896-900.

Vinaixa, M., Schymanski, E.L., Neumann, S., Navarro, M., Salek, R.M., Yanes, O., 2016. Mass spectral databases for LC/MS-and GC/MS-based metabolomics: state of the field and future prospects. TrAC-Trends in Analytical Chemistry 78, 23-35.

Vincke, E., Boon, N., Verstraete, W., 2001. Analysis of the microbial communities on corroded concrete sewer pipes–a case study. Appl Microbiol Biotechnol 57, 776-785.

Voordouw, G., Shen, Y., Harrington, C.S., Telang, A.J., Jack, T.R., Westlake, D.W., 1993. Quantitative reverse sample genome probing of microbial communities and its application to oil field production waters. Appl Environ Microbiol 59, 4101-4114.

Vorregaard, M., 2008. Comstat2-a modern 3D image analysis environment for biofilms.

Wagner, P., Little, B., 1993. Impact of alloying on microbiologically influenced corrosion. A review. Materials Performance 32, 65-68.

Wang, J., 2000. Survey and summary: from DNA biosensors to gene chips. Nucleic Acids Research 28, 3011-3016.

Wang, Y., Liu, S., Hu, Y., Li, P., Wan, J.-B., 2015. Current state of the art of mass spectrometry-based metabolomics studies–a review focusing on wide coverage, high throughput and easy identification. Rsc Advances 5, 78728-78737.

Whitby, C., Skovhus, T.L., 2011. Applied microbiology and molecular biology in oilfield systems. Springer.

White, D., Nivens, D., Nichols, P., Mikell, A., Kerger, B., Henson, J., Geesey, G., Clarke, C., 1986. Role of aerobic bacteria and their extracellular polymers in the facilitation of corrosion: use of Fourier transforming infrared spectroscopy and ‘signature’phospholipid fatty acid analysis. Biologically induced corrosion, 233-243.

White, R.A., Blainey, P.C., Fan, H.C., Quake, S.R., 2009. Digital PCR provides sensitive and absolute calibration for high throughput sequencing. BMC Genomics 10, 116.

Whitesides, G.M., 2006. The origins and the future of microfluidics. Nature 442, 368-373.

Williams, J., 2002. Microfluidics system for single molecule DNA sequencing, U.S. Patent Application 10/228,729.

Williams, J.D., 1990. Understanding antibacterial action and resistance. Journal of Hospital Infection 16, 188.

Williams, T.M., Schultz, C.M., 2015. Effect of Environmental Parameters on the Stability and Performance of Oil and Gas Biocides, SPE International Symposium on Oilfield Chemistry. Society of Petroleum Engineers.

Wilson, S.L., Jack, T.R., 2017. MIC mitigation: Coatings and cathodic protection, In: Skovhus, T.L., Enning, D., Lee, J.S. (Eds.), Microbiologically Influenced Corrosion in the Upstream Oil and Gas Industry. CRC Press.

Wintermute, E.H., Silver, P.A., 2010. Emergent cooperation in microbial metabolism. Molecular Systems Biology 6, 407.

Wishart, D.S., Feunang, Y.D., Marcu, A., Guo, A.C., Liang, K., Vázquez-Fresno, R., Sajed, T., Johnson, D., Li, C., Karu, N., 2017. HMDB 4.0: the human metabolome database for 2018. Nucleic Acids Research 46, D608-D617.

Wuchter, C., Banning, E., Mincer, T., Drenzek, N.J., Coolen, M.J., 2013. Microbial diversity and methanogenic activity of Antrim Shale formation waters from recently fractured wells. Frontiers in Microbiology 4, 367.

Wunch, K.G., Penkala, J.E., 2010. DNA microarray for quantitative detection of microbial processes in the oilfield, United States.

Xu, C., Zhang, Y., Cheng, G., Zhu, W., 2007. Localized corrosion behavior of 316L stainless steel in the presence of sulfate-reducing and iron-oxidizing bacteria. Material Science and Engineering: A 443, 235-241.

Xu, D., Li, Y., Song, F., Gu, T., 2013. Laboratory investigation of microbiologically influenced corrosion of C1018 carbon steel by nitrate reducing bacterium Bacillus licheniformis. Corrosion Science 77, 385-390.

Yanes, O., Tautenhahn, R., Patti, G.J., Siuzdak, G., 2011. Expanding coverage of the metabolome for global metabolite profiling. Analytical Chemistry 83, 2152-2161.

Yin, B., Williams, T., Koehler, T., Morris, B., Manna, K., 2018. Targeted microbial control for hydrocarbon reservoir: Identify new biocide offerings for souring control using thermophile testing capabilities. International Biodeterioration & Biodegradation 126, 204-207.

Yin, Y.S., Cheng, S., Lau, K.T., Chen, S.G., Liu, T., 2008a. The Influence of the Marine Bacterium Vibrio Natriegens Growth on Metallic Corrosion as Studied by Microscope Technologies. Advanced Materials Research 47-50, 169-172.

Yin, Y.S., Cheng, S., Lau, K.T., Chen, S.G., Liu, T., 2008b. The Influence of the Marine Bacterium Vibrio Natriegens Growth on Metallic Corrosion as Studied by Microscope Technologies, Advanced Materials Research. Trans Tech Publ, pp. 169-172.

Yin, Y.S., Cheng, S., Lau, K.T., Chen, S.G., Liu, T., 2008c. The influence of the marine bacterium Vibrio natriegens growth on metallic corrosion as studied by microscope technologies. Advanced Materials Research 47, 169-172.

Zhang, P., Xu, D., Li, Y., Yang, K., Gu, T., 2015. Electron mediators accelerate the microbiologically influenced corrosion of 304 stainless steel by the Desulfovibrio vulgaris biofilm. Bioelectrochemistry 101, 14-21.

Zhang, T., Fang, H., Ko, B., 2003. Methanogen population in a marine biofilm corrosive to mild steel. Appl Microbiol Biotechnol 63, 101-106.

Zhang, T., Watson, D.G., 2015. A short review of applications of liquid chromatography mass spectrometry based metabolomics techniques to the analysis of human urine. Analyst 140, 2907-2915.

Zhang, W., Culley, D.E., Nie, L., Scholten, J.C., 2007. Comparative transcriptome analysis of Desulfovibrio vulgaris grown in planktonic culture and mature biofilm on a steel surface. Appl Microbiol Biotechnol 76, 447-457.

Zhou, F., Mbadinga, S.M., Liu, J.-F., Gu, J.-D., Mu, B.-Z., 2013. Evaluation of microbial community composition in thermophilic methane-producing incubation of production water from a high-temperature oil reservoir. Environmental Technology 34, 2681-2689.

Zhu, X., Kilbane, J., II, Ayala, A., Modi, H., 2005. Application of quantitative, real-time PCR in monitoring microbiologically influenced corrosion (MIC) in gas pipelines, CORROSION 2005. NACE International.

Zuñiga, C., Zaramela, L., Zengler, K., 2017. Elucidation of complexity and prediction of interactions in microbial communities. Microbial Biotechnology 10, 1500-1522.

Zuo, R., Wood, T.K., 2004. Inhibiting mild steel corrosion from sulfate-reducing and iron-oxidizing bacteria using gramicidin-S-producing biofilms. Appl Microbiol Biotechnol 65, 747-753.